The *s* process: Nuclear physics, stellar models, and observations

F. Käppeler*

Karlsruhe Institute of Technology, Campus Nord, Institut für Kernphysik, 76021 Karlsruhe, Germany

R. Gallino†

Dipartimento di Fisica Generale, Università di Torino I-10125 Torino, Italy, and INAF-Osservatorio Astronomico di Teramo, I-64100 Teramo, Italy

S. Bisterzo‡

Dipartimento di Fisica Generale, Università di Torino, I-10125 Torino, Italy

Wako Aoki§

National Astronomical Observatory, Mitaka, Tokyo 181-8588, Japan

(Received 9 April 2010; published 1 April 2011)

Nucleosynthesis in the *s* process takes place in the He-burning layers of low-mass asymptotic giant branch (AGB) stars and during the He- and C-burning phases of massive stars. The *s* process contributes about half of the element abundances between Cu and Bi in solar system material. Depending on stellar mass and metallicity the resulting *s*-abundance patterns exhibit characteristic features, which provide comprehensive information for our understanding of the stellar life cycle and for the chemical evolution of galaxies. The rapidly growing body of detailed abundance observations, in particular, for AGB and post-AGB stars, for objects in binary systems, and for the very faint metal-poor population represents exciting challenges and constraints for stellar model calculations. Based on updated and improved nuclear physics data for the *s*-process reaction network, current models are aiming at an *ab initio* solution for the stellar physics related to convection and mixing processes. Progress in the intimately related areas of observations, nuclear and atomic physics, and stellar modeling is reviewed and the corresponding interplay is illustrated by the general abundance patterns of the elements beyond iron and by the effect of sensitive branching points along the *s*-process path. The strong variations of the *s*-process efficiency with metallicity bear also interesting consequences for galactic chemical evolution.

DOI: 10.1103/RevModPhys.83.157 PACS numbers: 26.20.Kn, 97.10.Cv, 97.10.Tk

CONTENTS

I. Introduction 158
II. Nuclear Physics 159
A. Measurement of neutron-capture rates 159
1. Pulsed neutron sources 159
2. Time-of-flight methods 160
3. Data acquisition and analysis techniques 162
4. Activations 163
5. Studies on radioactive isotopes 164
B. Cross-section calculations 166
1. Statistical model 166
2. Maxwellian averaged cross sections 166
3. Stellar enhancement factors 166
C. β decay under stellar conditions 167
D. Status and prospects 167
1. Compilations of stellar (n, γ) cross sections and further requirements 167
2. Measurements on rare and unstable samples 168
III. *s*-Process Models 170
A. Classical approach 170
B. Massive stars 171
C. AGB stars 171
D. Theoretical AGB results 173
E. The main *s* component and the role of a galactic chemical evolution model 176
IV. Observational Constraints 177
A. Stellar abundances 177
1. AGB, post-AGB, and planetary nebulae 178
2. Binary systems affected by mass transfer 178
B. Abundance patterns of heavy elements 179
1. Overall abundance patterns covering three magic neutron numbers 179
2. Detailed abundance patterns: CEMP-*s* and -*s*/*r* stars 180
C. Branchings 181
1. ^{85}Kr branch 181
2. ^{151}Sm branch 181
D. Stellar evolution 182
E. Contribution to the Galactic chemical evolution 182
1. *s*-process contributions to Galactic field stars 183
2. Globular clusters and galaxies in the local group 185
V. Summary 186

*franz.kaeppeler@kit.edu
†gallino@ph.unito.it
‡bisterzo@ph.unito.it
§aoki.wako@nao.ac.jp

I. INTRODUCTION

Neutron-capture nucleosynthesis during stellar He burning contributes about half of the elemental abundances between Fe and Bi. Substantial progress in the quantitative description of this slow neutron-capture (*s*) process has been achieved by an interdisciplinary approach involving improved nuclear physics input, advanced stellar model codes, and a wealth of data from astronomical observations and from the analysis of circumstellar dust grains. These three topics and their mutual connections are briefly described, before each topic is addressed in detail in Secs. II, III, and IV. In the final section the synergies between the main topics are outlined with particular emphasis on the open quests and future prospects of this field.

The phenomenological picture of the classical *s* process was formulated about 50 years ago in the seminal papers of Burbidge *et al.* (1957) (hereafter referred to as B^2FH) and of Cameron (1957), where the entire *s*-process panorama was already sketched in its essential parts. These ideas were worked out in the following decades by Clayton *et al.* (1961), Seeger *et al.* (1965), Clayton and Rassbach (1967), and Clayton and Ward (1974). The distinction of a slow and a rapid (*s* and *r*) neutron-capture process follows from the isotopic pattern in the chart of nuclides (Fig. 1), which shows that the *s* process follows the stability valley because the neutron-capture time scale is slower than that for β decay. The neutron-rich isotopes outside the *s* path are ascribed to the *r* process, which occurs under explosive conditions, presumably in supernovae. The decay of the reaction products from the *r*-process path on the far neutron-rich side of the stability valley forms the *r*-only isotopes. It also contributes to most of the other isotopes, except for those which are shielded by stable isobars. The corresponding ensembles of *s*- and *r*-only isotopes are important for the separation of the respective abundance distributions. The subset of stable isotopes on the proton-rich side are ascribed to the *p* process, which is likely to occur also in supernova explosions (Arnould and Goriely, 2003). With a few exceptions, the *p* abundances are much smaller than the *s* and *r* components.

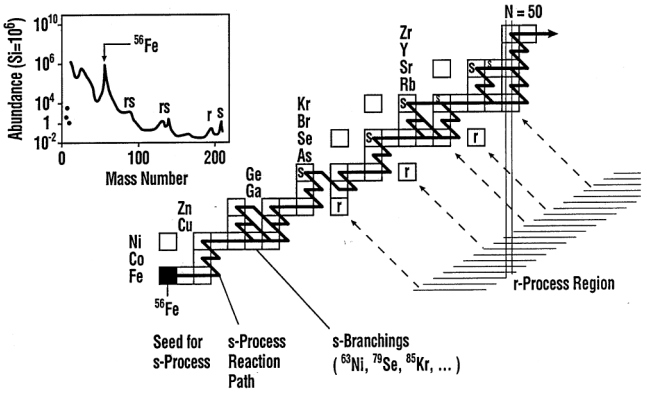

FIG. 1. Illustration of the neutron-capture processes responsible for the formation of the nuclei between iron and the actinides. The observed abundance distribution in the inset shows characteristic twin peaks. These result from the nuclear properties where the *s*- and *r*-reaction paths encounter magic neutron numbers. Note that a *p* process has to be invoked for producing the proton-rich nuclei that are not reached by neutron-capture reactions. For details see discussion in text.

The decisive role of nuclear physics for a quantitative model of the *s* process was clearly expressed already by B^2FH. In spite of the fact that neither the neutron source reactions nor the neutron-capture cross sections in the astrophysically relevant energy range were known apart from some scattered and uncertain information, all essential features had been inferred from this meager information: The product of the stellar (n, γ) cross sections and of the resulting *s* abundances $\langle\sigma\rangle N_s$, which represents the reaction flow, was found to be a smooth function of mass number *A*. From the composite slope of this function, the two different *s* processes had already been postulated. The steep decline between $A \approx 63$ and 100 was interpreted as the result of an *s*-process site with not enough neutrons available per ^{56}Fe seed to build the nuclei to their saturation abundances. In the mass region beyond $A \approx 100$, the much smaller slope suggested that steady flow was achieved and that all of these nuclei reached their saturation abundances. It was concluded that "two different processes might have occurred in two different red-giant stars (B^2FH)."

In the 1990s, however, improvements in the accuracy of the nuclear input data revealed that the classical *s* process suffered from inconsistencies in the description of the abundance signatures in *s*-process branchings. Because such patterns are particularly sensitive to neutron density and temperature, this implied that these parameters were not constant in time as assumed in the formulation of the classical model (Käppeler, 1999).

A few years before, stellar models of the He-burning stages of stellar evolution started to provide an increasingly realistic picture of *s*-process nucleosynthesis. The prospects of this approach were clearly superior to that of the classical model because it could be directly linked to astronomical observations.

A first generation of models (Gallino *et al.*, 1988; Hollowell and Iben, 1988) was soon replaced by scenarios related to core He (Heger, 2006; Chieffi and Limongi, 2006) and shell C burning (Raiteri *et al.*, 1991, 1993; Limongi *et al.*, 2000) in massive stars for the weak *s* process, on the one hand, and to thermally pulsing low-mass asymptotic giant branch (AGB) stars (Straniero *et al.*, 1995; Gallino *et al.*, 1998; Arlandini *et al.*, 1999) for the main *s* process, on the other hand. The current status of AGB evolution includes phenomena such as hot bottom burning, the *ab initio* treatment of third dredge up, and related mixing processes as well as the effect of metallicity and initial stellar mass (Herwig, 2005). The latter aspects are particularly important for the discussion of the *s*-process component in galactic chemical evolution (Travaglio *et al.*, 2004).

The success of the stellar models could be impressively verified by comparison with the solar *s* component and with a large body of data obtained from analyses of presolar material in the form of refractive dust grains of circumstellar origin (Zinner, 1998).

With respect to the origin of the heavy elements, observations of *s*-process abundances in AGB stars began in 1952 with the discovery of Tc lines in red-giant stars of spectral type S by Merrill (1952). Ever since, spectral observations of peculiar red giants turned out to be a prolific source of *s*-process information for the He-burning stage of stellar

evolution (Gustafsson, 1989). Spectroscopy of astronomical objects has made spectacular progress over the last decades by the deployment of new telescopes on the ground and in space and by the impressive increase in computing power that led to enormous improvement in the modeling of stellar atmospheres and in synthetic spectrum calculations (Asplund, 2005). Our understanding of stellar and galactic evolution has been promoted accordingly, e.g., via refined studies along the AGB (Lambert, 1991; Lambert *et al.*, 1995; Herwig, 2005). Separation of the *s* and *r* components in solar material through careful evaluation of the *s* abundances (Arlandini *et al.*, 1999) provided the key for the abundance distributions in the oldest, very metal-poor stars in the Universe (Sneden *et al.*, 1998; Cayrel *et al.*, 2001; Cowan and Sneden, 2006), which were found to scale with the solar *r*-process distribution (Beers and Christlieb, 2005). The composition of planetary nebulae (Péquignot and Baluteau, 1994) and circumstellar envelopes (Habing, 1996) could be investigated by IR observations, while the composition of interstellar matter (Savage and Sembach, 1996) is inferred from UV absorption line diagnostics. At higher energies, x-ray (Fürst *et al.*, 1997) and γ-ray astronomy (Diehl, 1998) has produced exciting new vistas of explosive nucleosynthesis (Clayton *et al.*, 1992; Dupraz *et al.*, 1997).

The three aspects of *s*-process research are addressed in the following sections with an attempt to illustrate their mutual connections.

II. NUCLEAR PHYSICS

The discussion of the nuclear part concentrates on the neutron-capture reactions and β-decay rates needed to calculate the *s* abundances between Cu and Bi. For a summary of the charged-particle reactions, which are of key importance for energy and neutron production at the various *s*-process sites and for further stellar evolution, see the compiled data of the NACRE Collaboration (Angulo *et al.*, 1999) and of Iliadis *et al.* (2001) as well as recent work on ^{12}C (Plag *et al.*, 2005; Assunção *et al.*, 2006) and on the two major neutron source reactions ^{13}C$(\alpha, n)^{16}$O (Heil *et al.*, 2008a) and ^{22}Ne$(\alpha, n)^{25}$Mg (Jaeger *et al.*, 2001).

In their discussion of the *s*-abundance characteristics, B^{2}FH noted that more detailed conclusions were impeded by the lack of reliable neutron-capture cross sections and emphasized that "unambiguous results would be obtained by measuring the total absorption cross sections. It is our view that such measurements would serve as a crucial test of the validity of the *s* process."

The importance of a complete set of experimental data for the reliable description of the $\langle\sigma\rangle N_s$ curve is shown in Fig. 2, which corresponds to the situation obtained by the time of the cross-section compilation of Bao *et al.* (2000), when experimentally determined cross sections were available for the majority of the involved isotopes.

Apart from the clear separation of the two *s*-process components, Fig. 2 also shows the pronounced effect of *s*-process branchings, which could not be addressed by B^{2}FH simply because the data at the time were far too uncertain to reveal their signatures in the $\langle\sigma\rangle N_s$ curve. These branchings are the result of the competition between neutron capture and β decay at unstable isotopes in the half-life range from a few weeks to a few years. For the same reason, the effect of stellar temperature on the β-decay half-lives also had not been anticipated. ^{79}Se represents such an example, where the drastically reduced stellar half-life gives rise to a pronounced branching that can be characterized by the strongly different $\langle\sigma\rangle N_s$ values of the *s*-only isotopes ^{80}Kr and ^{82}Kr (Klay and Käppeler, 1988).

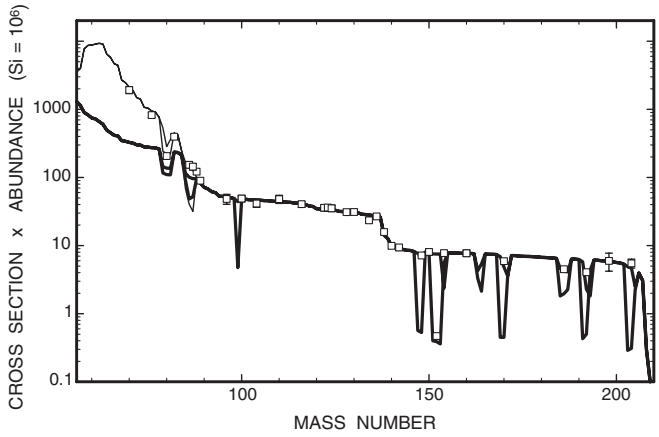

FIG. 2. The characteristic product of cross section times *s*-process abundance $\langle\sigma\rangle N_s$ plotted as a function of mass number. The thick solid line represents the main component obtained by means of the classical model, and the thin line corresponds to the weak component in massive stars (see text). Symbols denote the empirical products for the *s*-only nuclei. Some important branchings of the neutron-capture chain are indicated as well.

This section on the nuclear physics of the *s* process starts with a summary of current techniques for the experimental determination of stellar neutron-capture rates (Sec. II.A), followed by the theoretical aspects, which have to be considered in the process from laboratory measurements to stellar applications (Sec. II.B). The problems related to the often dramatic enhancement of β-decay rates under stellar conditions are discussed in Sec. II.C. The status of stellar (n, γ) rates and further improvements by new experimental facilities and advanced techniques are addressed in Sec. II.D.

A. Measurement of neutron-capture rates

1. Pulsed neutron sources

The laboratory neutron sources used in nuclear astrophysics measurements cover a variety of facilities, which differ in many aspects. The discussion presented here is focused on the main concepts and, therefore, does not include rarely used options such as filtered reactor beams (Bradley *et al.*, 1979) and radioactive sources (Knoll, 1979).

At small accelerators, neutrons are produced by nuclear reactions, such as the ^{7}Li$(p, n)^7$Be reaction, with the possibility of tailoring the neutron spectrum exactly to the stellar energy range between 0.3 and $\approx$ 500 keV. In many cases, the limited source strength can be compensated by low backgrounds and the use of comparably short neutron flight paths (Wisshak and Käppeler, 1981; Nagai *et al.*, 1991; Jaag and Käppeler, 1996b). Operated in direct current (DC) mode this type of accelerator can also be used for the simulation of

stellar neutron spectra, which are important in applications of the activation technique (see Sec. II.A.4).

Much higher intensities can be achieved via (γ, n) reactions at electron linear accelerators, such as GELINA at Geel, Belgium, and ORELA at Oak Ridge, Tennessee, by bombarding heavy metal targets with electron beams of typically 50 to 100 MeV. These so-called white neutron sources provide continuous neutron spectra over an energy range from thermal to some tens of MeV. Measurements at these facilities need to be carried out at larger neutron flight paths because of the strong γ flash from the impact of the electron beam. In turn, the longer flight paths provide the possibility to study the resolved resonance region with high resolution [see, for example, Koehler *et al.* (1996)].

Spallation reactions induced by energetic particle beams constitute the most prolific pulsed sources of fast neutrons suited for time-of-flight (TOF) measurements. Presently, two such spallation sources are in operation, LANSCE at Los Alamos (Lisowski *et al.*, 1990) and the n_TOF facility at CERN (Abbondanno *et al.*, 2003). The main advantage of these facilities is the superb efficiency for neutron production due to the high primary proton beam energies of 800 MeV and 20 GeV at LANSCE and n_TOF, respectively. At n_TOF, for example, 300 neutrons are produced per incident proton, which makes this facility the most luminous white neutron source presently available.

Because of their excellent efficiency, spallation sources can be operated at rather low repetition rates while still maintaining high average intensities. The situation at LANSCE is characterized by a comparably short flight path of 20 m, a time resolution of 250 ns, and a repetition rate of 50 Hz, similar to the performance of the SNS at Oak Ridge (ORNL) (Spallation Neutron Source, 2004) and at J-PARC in Japan (Japan Proton Accelerator Complex, 2004). The n_TOF facility at CERN represents a complementary approach aiming at higher resolution (185 m flight path, 7 ns pulse width) and even lower repetition rates of typically 0.4 Hz (Abbondanno *et al.*, 2003).

The astrophysics options at various white neutron sources have been compared by Koehler (2001) with respect to measurements on radioactive samples. As expected, spallation sources are unique for their superior peak neutron fluxes in the astrophysically relevant keV region. However, only the n_TOF facility exhibits a neutron energy resolution comparable to that of electron linear accelerators.

2. Time-of-flight methods

The aim of the energy-differential TOF methods is to measure the neutron-capture cross sections over a sufficiently large neutron energy range where Maxwellian averaged cross sections (MACS) can be determined from these data for any stellar temperature of interest. Recent developments and improvements in pulsed neutron sources and detection techniques have led to (n, γ) cross-section measurements with improved accuracy, in many cases with uncertainties of a few percent. This progress is essential for obtaining the *s* abundances accurately enough to infer the physical conditions at the stellar site by analysis of the abundance patterns of *s*-process branchings either in solar material or in presolar grains.

a. Total absorption calorimeters

The energy sum of the γ-ray cascade emitted in the decay of the compound nucleus corresponds to the binding energy of the captured neutron. Therefore, this neutron separation energy represents the best signature of a capture event. Hence, 4π detectors with an efficiency close to 100% are the most direct way to unambiguously identify (n, γ) reactions and to determine capture cross sections. This calorimetric approach started with the use of large liquid scintillator tanks, which are meanwhile replaced by arrays of BaF_2 crystals because of their superior resolution in γ-ray energy and their correspondingly lower backgrounds. A detector of this type consisting of 42 modules was developed at Karlsruhe (Wisshak *et al.*, 1990) and is also in use at the n_TOF facility at CERN (Heil *et al.*, 2001). In this design the BaF_2 crystals are shaped as truncated pyramids, forming a fullerene-type geometry where each module covers the same solid angle with respect to the sample. A somewhat simpler approach was chosen at ORNL (Guber *et al.*, 1997) and at FZ Rossendorf (Klug *et al.*, 2007), where cylindrical BaF_2 arrays have been constructed with hexagonal crystals.

Recent examples of accurate cross-section measurements made with the Karlsruhe 4π detector comprise the unstable branch-point isotope ^{151}Sm (Wisshak *et al.*, 2006c) and the Lu and Hf isotopes (Wisshak *et al.*, 2006a, 2006b). These results are essential for constraining the temperature at the *s*-process site via the branchings at $A = 151$, 175, and 179.

A higher segmentation of such a 4π detector is an advantage for separating true capture events from backgrounds and for handling the data rates in measurements on radioactive samples. The state of the art in this respect is the DANCE array with 162 BaF_2 modules that is operated at the LANSCE facility in Los Alamos (Reifarth *et al.*, 2004).

The high efficiency of 4π arrays in combination with intense pulsed neutron sources provides the possibility for measurements on very small samples. In general, this is important for any samples, where only small quantities are available, and, in particular, for radioactive isotopes, where the background from the activity of the sample needs to be kept to a minimum. An illustrative example for the first aspect is the keV (n, γ) cross section of ^{180}Ta where the sample consisted of 6.7 mg of ^{180}Ta immersed in 145 mg of ^{181}Ta (Wisshak *et al.*, 2004). Even smaller samples of about 200–400 μg have recently been used in the DANCE array to determine the keV (n, γ) cross sections of actinide samples (Esch *et al.*, 2008; Jandel *et al.*, 2008). A detailed survey for future measurements of neutron-capture cross sections on radioactive isotopes with special emphasis on branching points along the *s*-process path is given by Couture and Reifarth (2007).

The main problem in using 4π arrays arises from their response to neutrons scattered in the sample. Although the scintillator is selected to consist of nuclei with small (n, γ) cross sections, about 10% of the scattered neutrons are captured in the scintillator. The resulting background can be attenuated by an absorber shell around the sample, preferentially consisting of ^{6}LiH (Reifarth *et al.*, 2004b) or a ^{6}Li containing compound (Heil *et al.*, 2001). Such an absorber is not required in the setup at Karlsruhe if the neutron spectrum is limited to energies below 225 keV, which allows one to

separate the background from sample scattered neutrons via TOF.

This type of background becomes crucial in measurements on neutron-magic nuclei and on light isotopes, where neutron scattering dominates the rather weak capture by orders of magnitude. Therefore, large detector arrays are less suited for these isotopes, which are of fundamental importance because they act as bottlenecks in the *s*-process path or as potential neutron poisons.

The potential of a 4π BaF_2 array was extensively used at Karlsruhe for determination of accurate MACS values for an almost complete set of lanthanide isotopes between ^{141}Pr (Voss *et al.*, 1999) and ^{176}Lu (Wisshak *et al.*, 2006b) including all *s*-only nuclei.[1] The group of the lanthanide isotopes are particularly suited for a precise test of *s*-process nucleosynthesis concepts, because the relative abundances of the lanthanides are very well known (Asplund *et al.*, 2009) so that the *s*-process reaction chain and the associated branchings can be consistently followed. In fact, the failure of the classical *s* process and the success of the stellar *s* process in thermally pulsing low-mass AGB stars (Arlandini *et al.*, 1999) was possible after accurate cross sections for the Nd isotopes and, in particular, for the *s*-only nucleus ^{142}Nd became available (Wisshak *et al.*, 1998) (see Sec. III. A).

Comprehensive measurements were also performed at Karlsruhe for the long isotope chains of Cd (Wisshak *et al.*, 2002), Sn (Wisshak *et al.*, 1996), Te (Wisshak *et al.*, 1992), and Ba (Voss *et al.*, 1994) to provide detailed information for studying the full mass range of the main *s*-process component with well-defined MACS data. Reliable cross sections are also instrumental for defining the strength of the branchings in the reaction path, where the specific abundance patterns yield constraints for important parameters of the stellar plasma, i.e., neutron density, temperature, pressure, and mixing phenomena. Such examples are the branchings at $A = 122/123$, 128, and 147/148, which represent sensitive tests for the quasiequilibrium of the *s*-process reaction flow (Wisshak *et al.*, 1992) and for details of the stellar *s*-process conditions, i.e., for the convective velocities (Reifarth *et al.*, 2004a) and the neutron density (Wisshak *et al.*, 1993) during He shell flashes in thermally pulsing low-mass AGB stars. Complementary information on the *s*-process temperature can be obtained from the branchings at ^{151}Sm (Abbondanno *et al.*, 2004a; Marrone *et al.*, 2006a; Wisshak *et al.*, 2006c) and at ^{175}Lu (Wisshak *et al.*, 2006a, 2006b). These important aspects of the *s*-abundance distribution are the subject of Secs. III C and IV.C.

b. Detectors with low neutron sensitivity

Originally, the neutron sensitivity problem led to the development of Moxon-Rae-type detectors (Moxon and Rae, 1963). The idea was to design a γ-ray detector with an efficiency proportional to the energy deposited. With this feature, the probability for detecting a capture event becomes

$$\varepsilon_{\mathrm{casc}} = \sum_{i=1}^{m} \varepsilon_i(E_\gamma^i) = \sum_{i=1}^{m} kE_\gamma^i = kE_\gamma^{\mathrm{tot}}, \tag{1}$$

independent of the cascade multiplicity m and of the γ energies. To avoid systematic uncertainties, the efficiency of Moxon-Rae detectors had to be small enough so that no more than one γ ray was detected per cascade.

In order to improve the overall efficiency, the principle of Moxon-Rae detectors was generalized by introducing the pulse height weighting technique (PHWT) (Rau, 1963; Macklin *et al.*, 1967), where the proportionality between deposited energy and γ-ray efficiency is achieved *a posteriori* by an off-line weighting function applied to the detector signals.

The PHWT technique was first used in experiments with C_6F_6 liquid scintillators. Although smaller than for scintillators containing hydrogen, the neutron sensitivity of C_6F_6 detectors gave rise to large systematic uncertainties as shown by Koehler *et al.* (2000) and Guber *et al.* (2005)a, (2005)b. This problem was reduced in a second generation of detectors, which are based on deuterated benzene (C_6D_6) because of the smaller capture cross section of deuterium. Further improvement was achieved by minimizing the construction materials and by replacing aluminum and steel by graphite or carbon fiber, resulting in a solution, where the background due to scattered neutrons is practically negligible (Plag *et al.*, 2003).

The accuracy of the PHWT has been an issue for a long time. When the technique was proposed, the uncertainties introduced by the weighting function (WF) were about 20% in some particular cases (Macklin, 1987). Dedicated measurements and Monte Carlo (MC) calculations (Corvi *et al.*, 1988; Perey *et al.*, 1988) have led to gradually improved WFs. With present advanced MC codes, realistic detector response functions and WFs can be determined by means of precise and detailed computer models of the experimental setup (Koehler *et al.*, 1996; Tain *et al.*, 2002; Abbondanno *et al.*, 2004b; Borella *et al.*, 2005). A dedicated set of measurements at the n_TOF facility confirmed that WFs obtained by such refined simulations allow one to determine neutron-capture cross sections with a systematic accuracy of better than 2% (Abbondanno *et al.*, 2004b).

Recent applications of the improved PHWT technique with optimized C_6D_6 detectors are the measurements of (n, γ) cross sections on isotopes at or near magic neutron numbers, which are characterized by small capture-to-scattering ratios. Examples for such measurements are the studies of the n_TOF Collaboration on ^{209}Bi (Domingo-Pardo *et al.*, 2006a) and on a sequence of stable Pb isotopes (Domingo-Pardo *et al.*, 2006b, 2007a, 2007b). Several of the involved resonances show the effect of neutron sensitivity as shown in Fig. 3 for two cases in the ^{209}Bi cross section, where the resonance yields obtained from previous data are clearly overestimated.

Other neutron-magic isotopes, which were recently studied with improved accuracy, are ^{139}La (Terlizzi *et al.*, 2007) and ^{90}Zr (Tagliente *et al.*, 2008). The importance of ^{139}La results from the fact that it is abundantly produced by the *s* process (e.g., 70% of solar La). Because La is easily detectable by stellar spectroscopy, it can be used as an indicator for the

[1] http://www.kadonis.org.

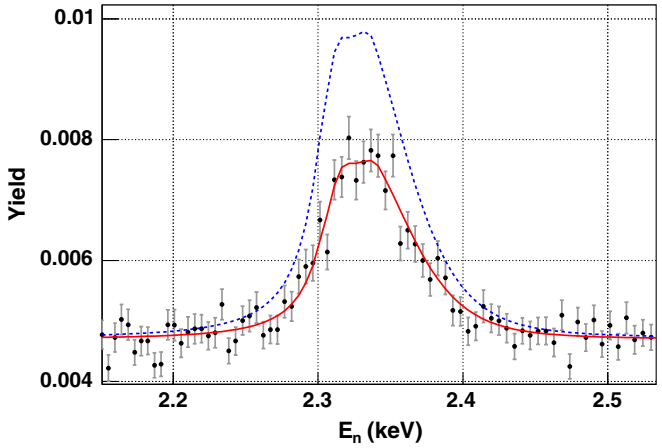

FIG. 3 (color online). *R*-matrix analysis of the second resonance in bismuth. The dashed line corresponds to the yield calculated with the resonance parameters from the ENDF/B-VI.8 evaluation which exhibits the effect of neutron sensitivity in previous data.

onset of the *s* process in low-metallicity stars, which were formed early in galactic history. It is interesting to note that the ^{139}La cross section was accurately confirmed by independent activation measurements (O'Brien *et al.*, 2003; Winckler *et al.*, 2006). The position of ^{90}Zr in the *s*-process reaction chain is located exactly at the matching point between the mass regions dominated by the weak and main *s* process. Therefore, this isotope assumes a key role among the isotopes with $N = 50$. As in the Bi and Pb isotopes, the new data are significantly smaller than measured previously due to neutron sensitivity problems in the past.

The potential of TOF measurements is given in Table I at the example of the important pairs of *s*-only isotopes, which can be used to define branching ratios

$$B = \frac{\langle\sigma\rangle_p N_p}{\langle\sigma\rangle_f N_f},$$

where $\langle\sigma\rangle_p$ denotes the MACS of the partially bypassed isotope and N_p its isotopic abundance. The corresponding values for the heavier isotope, which experiences the full reaction flow, are indicated by the index f. One such pair are the isotopes ^{80}Kr and ^{82}Kr, which characterize the branching at ^{79}Se as shown in Fig. 1. Pairs of *s*-only isotopes are particularly valuable because these branchings can be evaluated without interference by the uncertainties related to elemental abundance values. For this reason, the MACS of these isotopes have been determined with the highest possible accuracy. The uncertainties of the respective branching ratios in the last column of Table I refer to only the MACS uncertainties, although isotopic abundance ratios exhibit also non-negligible uncertainties (Rosman and Taylor, 1998). For example, a 6% uncertainty has been attributed to the abundance ratio of ^{122}Te and ^{124}Te. The quoted values, which include small corrections due to minor deviations from reaction flow equilibrium (Arlandini *et al.*, 1999), were estimated via the classical approach. Note that weak branchings can only be analyzed with confidence if the MACS are accurately known as in the case of the ^{148,150}Sm pair.

3. Data acquisition and analysis techniques

Modern electronic techniques have led to substantial improvements in data acquisition and analysis. At the front end, flash analog-to-digital converters (FADCs) provide the fastest and safest way to record the complete information contained in the analog detector output by digitizing the entire waveform of the signals. This has the obvious advantage of the raw data being preserved for repeated and refined off-line analysis, which allows for the efficient identification and correction of baseline shifts, pileup, and noise, resulting in a rigorous assessment of systematic uncertainties. Specifically designed pulse shape analysis algorithms can be used for evaluating the relevant signal parameters, i.e., time information, amplitude, area, and shape, for each type of detector. In case these algorithms are improved at some point, one can always return to the original information and repeat the analysis of a particular experiment.

Another advantage is that accidental errors due to the failure of an electronic module are minimized, simply because there is much less electronics needed to run an experiment. It is sufficient, for example, to connect the anode signal of a photomultiplier tube with an FADC channel, which is then read by a computer.

These features were recently used in (n, γ) studies with 4π BaF_2 arrays, where flexible algorithms have been employed to reduce background events in the scintillator via n/γ identification (Marrone *et al.*, 2006b) and to suppress the intrinsic α background in BaF_2 crystals (Reifarth *et al.*, 2004b).

A good example is the data acquisition system at n_TOF (Abbondanno *et al.*, 2005), which is based on 8-bit FADC modules, with sampling rates up to 2 GHz and 8 or 16 Mbytes memory. The low repetition rate of ~0.4 Hz leaves enough time to digitize and store all the raw FADC information accumulated during each neutron bunch and for all detectors employed. Although peak rates of 8 Mbytes are reached per burst and per detector due to the very high instantaneous neutron flux, the data acquisition system works practically dead-time free, except for a narrow interval of 15–20 ns that is needed to separate two consecutive signals unambiguously.

TABLE I. MACS results at $kT = 30$ keV for elements with a pair of *s*-only isotopes. [Data are from KADONiS, Dillmann *et al.*, (2005); see Sec. II.D].

s-only isotopes	Maxwellian averaged cross section (mb)		Abundance ratio (Rosman and Taylor, 1998)	Branching ratio
^{80,82}Kr	267 ± 14	90 ± 6	2.28/11.58	0.61 ± 0.05
^{122,124}Te	295 ± 3	155 ± 2	2.55/4.74	1.06 ± 0.02
^{128,130}Xe	262.5 ± 3.7	132.0 ± 2.1	1.92/4.08	0.96 ± 0.02
^{134,136}Ba	176.0 ± 5.6	61.2 ± 2.0	2.417/7.854	0.94 ± 0.04
^{148,150}Sm	241 ± 2	422 ± 4	11.24/7.38	0.88 ± 0.01

The use of FADCs in TOF measurements at facilities with repetition rates above about 1 kHz is hampered by rapidly increasing dead times caused by the transfer of a large amount of data to the storage medium, a problem that is presently studied by the EFNUDAT Collaboration (Plag, 2009).

The main drawback of a FADC-based acquisition system is the large amount of accumulated data, which demands large storage capabilities and high data transfer rates. While this difficulty can be mitigated by applying a zero suppression algorithm on the fly (Abbondanno *et al.*, 2005), the enormous improvement in computing power and the capacity of storage media was essential for the handling and analysis of terabytes of data taken with FADC systems.

Another general aspect of data analysis techniques is the increasing importance of Monte Carlo simulations, which are becoming standard tools for the planning of measurements and for analyzing experimental data. The efficient application of the GEANT (Agostinelli *et al.*, 2003) and MCNP (Brown *et al.*, 2007) software packages has also been favored by the recent advances in computing power.

4. Activations

Activation in a quasistellar neutron spectrum provides a completely different approach for the determination of stellar (n, γ) rates. Apart from the fact that the method is restricted to cases where neutron-capture produces an unstable nucleus, it has a number of appealing features.

- It was found that stellar neutron spectra can be well approximated in the laboratory so that MACS measurements can be directly performed by irradiation and subsequent determination of the induced activity.
- Technically, the method is comparably simple and can be performed at small electrostatic accelerators with standard equipment for γ spectroscopy.
- The sensitivity is orders of magnitude better than for TOF experiments because the accelerator can be operated in DC mode and because the sample can be placed directly at the neutron production target in the highest possible neutron flux. This feature opens the possibility for measurements on sub-μg samples and on rare isotopes, an important advantage if one deals with radioactive materials.
- In most cases the induced activity can be measured via the γ decay of the product nucleus. This implies favorable signal-to-background ratios and unambiguous identification of the reaction products. The excellent selectivity achieved in this way can often be used to study more than one reaction in a single irradiation, by using either elemental samples of natural composition or suited chemical compounds.

In an astrophysical environment with temperature T, interacting particles are quickly thermalized by collisions in the stellar plasma. The neutron energy distribution corresponds to a Maxwell-Boltzmann spectrum,

$$\Phi = dN/dE_n \sim \sqrt{E_n}\exp(-E_n/kT).$$

So far experimental neutron spectra, which simulate the energy dependence of the product $v\Phi \sim E_n \exp(-E_n/kT)$, have been produced by three reactions. The ^{7}Li$(p, n)^7$Be reaction allows one to simulate the spectrum for a thermal energy of $kT = 25$ keV (Beer and Käppeler, 1980; Ratynski and Käppeler, 1988) very close to the 23 keV effective thermal energy in He shell flashes of low-mass AGB stars, where neutrons are produced via the ^{22}Ne$(\alpha, n)^{25}$Mg reaction. More recently, the ^{18}O$(p, n)^{18}$F reaction has been shown to provide a spectrum for $kT = 5$ keV (Heil *et al.*, 2005), which is well suited for *s*-process studies of the main neutron source in these stars, the ^{13}C$(\alpha, n)^{16}$O reaction that operates at 8 keV thermal energy.

While these two quasistellar spectra allow one to determine the MACS necessary for studies of the main *s* component, the weak component associated with massive stars is characterized by higher temperatures, i.e., 26 keV thermal energy during core He burning and about 90 keV in the shell C-burning phase. The situation during core He burning is again well described by the ^{7}Li$(p, n)^7$Be reaction, but the high temperatures during shell C burning are only roughly represented by means of the ^{3}H$(p, n)^3$He reaction, which provides a spectrum for $kT = 52$ keV (Käppeler *et al.*, 1987). In this case, the measured MACS have to be extrapolated by statistical model calculations.

Because the proton energies for producing these quasistellar spectra are only slightly higher than the reaction thresholds, all neutrons are emitted in forward direction. In this way, the samples are exposed to the full spectrum and backgrounds from scattered neutrons are negligible. With a proton beam current of 100 μA on target, neutron intensities of the order of 10^9, 10^8, and 10^5 s^{-1} can be achieved for the (p, n) reactions on ^{7}Li, ^{3}H, and ^{18}O with present electrostatic accelerators. Future developments, however, will provide much higher beam currents and correspondingly higher neutron fluxes (see Sec. II.A.4).

Already at present the neutron intensities for activation measurements exceed the fluxes obtainable in TOF measurements by orders of magnitude. For example, the highest neutron flux reached at an experimental TOF setup is 5×10^5 s^{-1} at the DANCE array in Los Alamos. Accordingly, activation represents the most sensitive method for (n, γ) measurements in the astrophysically relevant energy range. This feature is unique for the possibility to measure the MACS of neutron poisons, abundant light isotopes with very small cross sections, as well as for the use of extremely small sample masses.

The latter aspect is most important for the determination of MACS of unstable isotopes, which are needed for investigating unstable nuclei of relevance for *s*-process branchings. In most cases TOF measurements on unstable branch-point isotopes are challenged by the background due to the sample activity (Sec. II.A.4). Illustrative examples in this respect are the successful measurements of the MACS of ^{60}Fe (Uberseder *et al.*, 2009) and ^{147}Pm (Reifarth *et al.*, 2003). In the first case, the sample (Schumann *et al.*, 2010) consisted of 1.4×10^{16} atoms or 1.4 μg and the activation was complicated by the 6 min half-life of ^{61}Fe, which required 47 repeated irradiations, and by the small capture cross section of 5.7 mb. Note that the number of atoms and the cross-section result are reduced by a factor of 1.75 compared to the original paper (Uberseder *et al.*, 2009), because of a new precise half-life determination for ^{60}Fe (Rugel *et al.*, 2009).

The second experiment was performed with an even smaller sample of only 28 ng or 1.1×10^{14} atoms in order to keep the ^{147}Pm activity ($t_{1/2} = 2.6$ yr) at a reasonable value. In this case, the small sample mass could be used because the half-life of ^{148}Pm and the cross section were conveniently large.

Another advantage of the activation method is that it is insensitive to the reaction mechanism. In particular, it includes the contributions from direct capture, where the neutron is captured directly into a bound state. The direct capture component, which contributes substantially to the (n, γ) cross sections of light nuclei, is extremely difficult to determine in TOF measurements [for an exception see the specialized setup used by Igashira *et al.* (1995)].

Apart from measurements on unstable isotopes as discussed below, the excellent sensitivity of the activation technique has been extensively used for the determination of cross sections with non-negligible direct capture components, for the determination of partial cross sections with the population of isomeric states, and for the measurement of small cross sections in general.

Prominent examples of the latter type are the series of measurements between Fe and Sr, which are related to the reaction flow of the weak component (Rugel *et al.*, 2007; Heil *et al.*, 2008a, 2008b; Marganiec *et al.*, 2009). These data were consistently smaller than previous TOF results, which evidently suffered from an underestimated neutron sensitivity. Figure 4 shows that these changes gave rise to strong propagation effects in the abundance distribution. These effects originate to a large part from the high-temperature phase during shell C burning that operates at $kT = 90$ keV. In order to reduce the uncertainties in the extrapolation from the measured MACS at 25 keV, complementary TOF measurements on the stable Fe and Ni isotopes are under way at CERN.

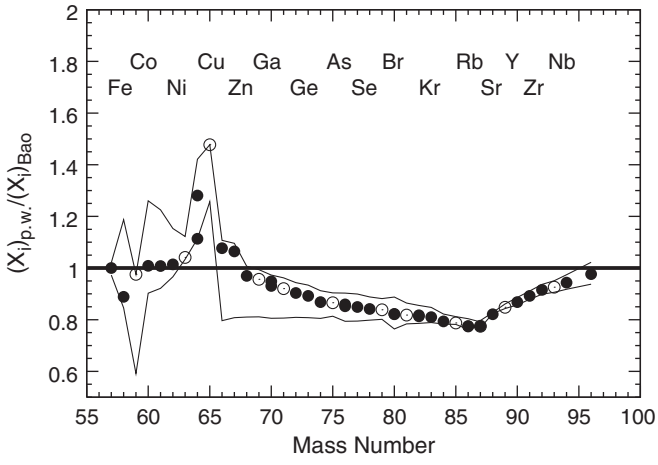

FIG. 4. Nucleosynthesis yields between Fe and Nb showing the final *s*-process yields after shell C burning for a $25M_\odot$ star with solar metallicity. To illustrate the combined effect of new cross sections for ^{58}Fe, ^{59}Co, ^{64}Ni, and ^{63,65}Cu the yield is plotted relative to the case obtained with the previous cross sections of Bao *et al.* (2000). Even and odd Z elements are distinguished by black and open symbols, respectively. The thin lines demonstrate the uncertainties stemming from the extrapolation of the measured cross sections to higher and lower energies.

For some branchings the population of long-lived isomers plays an important role (Ward, 1977). In most cases the respective partial cross sections feeding the isomers have to be determined in activation measurements because this information is difficult to obtain via the TOF technique. Important isomers are those in ^{176}Lu and ^{180}Ta, for example. The isomer in ^{176}Lu at 123 keV is the key for the interpretation of the mother-to-daughter ratio of the *s*-only isotopes ^{176}Lu and ^{176}Hf as an *s*-process thermometer for the He shell flashes in low-mass AGB stars (Klay *et al.*, 1991; Doll *et al.*, 1999). At temperatures above about 150 MK the initial population probabilities of isomer ($t_{1/2} = 3.68$ h) and ground state ($t_{1/2} = 37.5$ Gyr) (Wisshak *et al.*, 2006b; M. Heil *et al.*, 2008c) are altered by a delicate interplay between neutron density and temperature, depending on subtle details in the nuclear structure of ^{176}Lu (Mohr *et al.*, 2009). The case of ^{180}Ta is of interest because this is the only isotope in nature which is (almost) stable in its isomeric state. Again, the survival of ^{180}Ta^m depends on the (n, γ) cross section (Wisshak *et al.*, 2001; Käppeler *et al.*, 2004; Wisshak *et al.*, 2004) and on the effect of the high temperatures at the *s*-process site (Belic *et al.*, 1999, 2002) in depopulating the isomer to the ground state.

A few years ago, the potential of the activation technique was considerably extended by counting the activation products directly via accelerator mass spectrometry (AMS) instead of measuring the induced activity (see Sec. II.D.2).

The complementarity between TOF and activation measurements is given in Table II for examples between Fe and Au. Overall, there is good agreement between the results obtained with both methods. As far as the related uncertainties are concerned, one could be tempted to assume that the small, resonance-dominated cross sections of the Fe group and at magic neutron numbers are more accurately determined by activation, whereas the smooth cross sections of the heavier nuclei are generally better determined in TOF experiments. However, there is no general rule as indicated by the cases of ^{88}Sr and ^{197}Au, but the quality of the data depends on individual details of the respective experiments.

5. Studies on radioactive isotopes

Although many cross sections of the stable isotopes are still rather uncertain and need to be improved, a major challenge of future experiments is to extend such measurements to the largely unexplored subset of unstable branch-point nuclei.

The concept of *s*-process branchings was formulated by Ward *et al.* (1976) to obtain information on *average* *s*-process neutron densities and temperatures. With the advent of quantitative stellar models the abundance patterns of the branchings were understood to represent sensitive tests for the time dependence of these parameters during the various *s*-process episodes in thermally pulsing low-mass AGB stars (Gallino *et al.*, 1998; Arlandini *et al.*, 1999) and in massive stars (Raiteri *et al.*, 1991a).

Branchings in the *s* path occur whenever $\lambda_n \approx \lambda_\beta$. The β-decay rate is $\lambda_\beta = \ln 2/t_{1/2}$, whereas the neutron-capture rate $\lambda_n = n_n \langle \sigma v \rangle v_T$ is the product of neutron density, MACS, and mean thermal velocity. Depending on neutron density and on the MACS of the unstable branch-point

TABLE II. Recent MACS results at $kT = 30$ keV obtained via TOF techniques and with the activation method. [Data are from KADONiS, Dillmann *et al.* (2005); see Sec. II.D].

Target isotope	Maxwellian averaged cross section (mb) TOF technique		Activation method	
^{58}Fe	12.1 ± 1.1	Käppeler *et al.* (1983)	13.5 ± 0.7	Heil *et al.* (2008b)
^{59}Co	38 ± 3	Spencer and Macklin (1976)	39.6 ± 2.7	Heil *et al.* (2008b)
^{62}Ni	25.8 ± 3.7	Alpizar-Vicente *et al.* (2008)	20.2 ± 2.1	Nassar *et al.* (2005); Dillmann *et al.* (2009)
	37.0 ± 3.2	Tomyo *et al.* (2005)	23.4 ± 4.6	Dillmann *et al.* (2010)
^{87}Rb	15.5 ± 1.5	Jaag and Käppeler (1996a)	15.8 ± 0.9	Heil *et al.* (2008a)
^{88}Sr	6.01 ± 0.17	Koehler *et al.* (2000); (2001)	6.13 ± 0.18	F. Käppeler *et al.* (1990)
^{89}Y	21 ± 3	de L. Musgrove *et al.* (1978)	19.0 ± 0.6	F. Käppeler *et al.* (1990)
^{139}La	32.4 ± 3.1	Terlizzi *et al.* (2007)	31.6 ± 0.8	O'Brien *et al.* (2003)
^{146}Nd	91.2 ± 1.0	Wisshak *et al.* (1998)	87.1 ± 4.0	Toukan *et al.* (1995)
^{148}Nd	146.6 ± 1.9	Wisshak *et al.* (1998)	152 ± 9	Toukan *et al.* (1995)
^{176}Lu	1639 ± 14	Wisshak *et al.* (2006b)	1599 ± 85*	Beer and Käppeler (1980)
^{180}Hf	156.5 ± 1.9	Wisshak *et al.* (2006a)	168 ± 9	Beer *et al.* (1982)
^{197}Au	588 ± 20	Macklin *et al.* (1975); Macklin (1982a)	592 ± 9	Ratynski and Käppeler (1988)

isotope, the stellar half-lives of branch-point nuclei may range between several days and several years. In addition, stellar half-lives can be strongly enhanced compared to the corresponding terrestrial values as discussed in Sec. II.C.

The branch-point isotope ^{79}Se in Fig. 1 represents such a case, where the decay is accelerated by thermal population of a short-lived excited state. In contrast, the other two branch points shown in Fig. 1, ^{63}Ni and ^{85}Kr, are not or only weakly altered by temperature effects. All three branch points fall in the mass range of the weak component associated with massive stars.

Measurements of the MACS for the branch points of the weak component are hampered by the high specific activity of ^{85}Kr and by the lack of sample material in the case of ^{79}Se. Only for ^{63}Ni has a TOF measurement recently been performed with the DANCE detector at Los Alamos using a mildly enriched nickel sample containing 11% ^{63}Ni (Couture, 2009).

For the main component experimental information can be obtained for some important branch-point isotopes. With one exception these measurements were performed via the activation technique, where the activity problem was relaxed because the high sensitivity of the method allows one to use μg or even sub-μg samples. Results were reported for ^{135}Cs (Patronis *et al.*, 2004), ^{147}Pm (Reifarth *et al.*, 2003), ^{163}Ho (Jaag and Käppeler, 1996b), ^{155}Eu (Jaag and Käppeler, 1995), and ^{182}Hf (Vockenhuber *et al.*, 2007). As noted before, the data obtained via activation usually represent the respective MACS values at $kT = 25$ keV and have to be extrapolated to higher and lower temperatures by means of theoretical data (see Sec. II.B).

TOF measurements on branch-point isotopes of the main component have been reported for the quasistable nuclei ^{99}Tc (Macklin, 1982b; Winters and Macklin, 1987), ^{107}Pd (Macklin, 1985), and ^{129}I (Macklin, 1983). To date ^{151}Sm is the only branch point with a half-life shorter than 100 yr, where the (n, γ) cross section has been studied by means of the TOF technique over a wide energy range. Combination of the accurate and comprehensive data measured at Karlsruhe (Wisshak *et al.*, 2006c) and CERN (Abbondanno *et al.*, 2004a) provided a full set of MACS values for ^{151}Sm.

The measurement of the ^{14}C$(n, \gamma)^{15}$C cross section (Reifarth *et al.*, 2008) was of interest because this reaction determines whether the neutron balance of the *s* process can be affected by neutron induced CNO cycles (Wiescher *et al.*, 1999). It contributes to the reaction flow in neutrino driven wind scenarios of the *r* process (Terasawa *et al.*, 2001) and is important for validating the (n, γ) cross sections calculated via detailed balance from the inverse Coulomb dissociation reaction (Wiescher *et al.*, 1990; Timofeyuk *et al.*, 2006).

The possibility of complementing (n, γ) experiments by studies of the inverse (γ, n) reactions has been invoked by Sonnabend *et al.* (2003) and Mohr *et al.* (2004) for the branch-point isotope ^{185}W. Other examples of (γ, n) measurements refer to applications in the *p* process rather than in the *s* process (Vogt *et al.*, 2001; Sonnabend *et al.*, 2004, 2005).

Another indirect approach for obtaining information on (n, γ) cross sections of unstable nuclei is the surrogate method (Escher *et al.*, 2005; Dietrich and Escher, 2007), which uses the assumption that the reaction of interest proceeds via the formation of a compound nucleus and that formation and decay of the compound state can be separated, provided that both steps are independent of each other. In many cases, the formation cross section can be calculated reasonably well by using optical potentials, but theoretical decay probabilities are often quite uncertain. In the surrogate approach the compound nucleus is produced via an alternative direct reaction and its decay probability is then measured. There are several challenges of the surrogate method, in particular, the "J population mismatch," which means that in the desired reaction different compound states might be populated: the difficulty to convert the experimental observables into decay probabilities, the role of preequilibrium reactions, where the intermediate configuration decays before a compound nucleus is formed, and the role of projectile breakup, which may disturb the proper identification of the surrogate reaction (Forssén *et al.*, 2005). A recent example for the application of this method is the work of Boyer *et al.* (2006).

Although the indirect approaches rely in essential parts on theory and are therefore limited in accuracy, they often

provide valuable information, which is impossible to obtain otherwise.

B. Cross-section calculations

As pointed out in the previous sections, measurements cannot be performed at all energies and for all relevant isotopes. In addition, the reaction rates in a stellar environment require estimation of reaction processes for nuclei in their excited states, which are impossible to measure under laboratory conditions. Therefore, a close collaboration between experiment and theory remains crucial for establishing the complete nuclear physics input for *s*-process studies. On the other hand, experimental information is also mandatory for guiding and testing developments in theory in the region of unstable nuclei, a necessary step toward quantitative models of explosive nucleosynthesis.

1. Statistical model

The key approach for the calculation of stellar *s*-process reaction rates is based on the Hauser-Feshbach statistical model (HFSM), which was formulated over 30 years ago (Moldauer, 1975). The model relies essentially on two basic assumptions, the validity of the compound nucleus reaction mechanism and a statistical distribution of nuclear excited states. With these assumptions, the reaction cross section (e.g., for neutron capture) can be written in terms of model parameters such as the energy-dependent neutron transmission functions $T_{n,ls}$ and the γ-ray transmission functions $T_{\gamma,J}$. The general expression reads

$$\sigma_{n,\gamma}(E_n) = \frac{\pi}{k_n^2} \sum_{J,\pi} g_J \frac{\sum_{ls} T_{n,ls} T_{\gamma,J}}{\sum_{ls} T_{n,ls} + \sum_{ls} T_{n',ls} + T_{\gamma,J}} W_{\gamma,J}, \quad (2)$$

where E_n is the incident neutron energy, k_n is the wave number, $s = 1/2$ is the intrinsic spin of the incident particle, and l is the orbital angular momentum of neutron and nucleus. The $g_J = (2J+1)(2s+1)^{-1}(2I+1)^{-1}$ is a statistical weight factor for target nuclei of spin I and compound states of total angular momentum J compatible with spin and parity conservation laws. The width fluctuation factor W_γ takes different statistical properties of the γ-decay channel and of the competing neutron elastic (n, n) and inelastic (n, n') channels into account. The various HFSM approaches differ by the particular nuclear structure and deexcitation models adopted for calculating the nuclear quantities in Eq. (2).

Examples of widely used HFSM approaches for applications in nuclear astrophysics are those of Holmes *et al.* (1976), Harris (1981), and the latest NON-SMOKER (Rauscher, 2001), MOST (Goriely, 1998), and TALYS (Koning *et al.*, 2005) versions. Most of the quoted references also include HFSM computer codes for calculation of reaction cross sections. A repository of parameters and systematics of nuclear structure quantities can be found in the "RIPL" initiative (Belgya *et al.*, 2005). Additional model codes have been used for individual reaction rate calculations.

2. Maxwellian averaged cross sections

The neutron spectrum typical of the various *s*-process sites is described by a Maxwell-Boltzmann distribution, because neutrons are quickly thermalized in the dense stellar plasma. The effective stellar reaction cross sections are therefore obtained by averaging the experimental data over that spectrum. The resulting MACS

$$\langle \sigma \rangle_{kT} = \frac{2}{\sqrt{\pi}} \frac{\int_0^\infty \sigma(E_n) E_n e^{-E_n/kT} dE_n}{\int_0^\infty E_n e^{-E_n/kT} dE_n} \quad (3)$$

are commonly compared for a thermal energy of $kT = 30$ keV, but for realistic *s*-process scenarios a range of thermal energies has to be considered, from about 8 keV in the ^{13}C pocket of thermally pulsing low-mass AGB stars to about 90 keV during carbon shell burning in massive stars. To cover this full range, energy-differential cross sections $\sigma(E_n)$ are needed in the energy region $0.1 \leq E_n \leq 500$ keV. Whenever experimental data are available for only part of this range, cross-section calculations are required for filling these gaps. Correspondingly, calculated cross sections are needed to extrapolate the results from activation measurements to the entire temperature range of the various *s*-process sites [see Heil *et al.* (2008)b].

As a service to the community a complete set of MACS data is available from the continuously updated compilation described in Sec. II.D.1.

3. Stellar enhancement factors

Apart from the need of cross-section calculations for filling the gaps in experimental data, theory is indispensable for adapting the experimental data to the stellar environment. With respect to MACS, this refers to the fact that excited nuclear states are populated under stellar conditions due to interactions with the hot thermal photon bath. Because of the high photon intensity, all states with excitation energies E_i are in thermal equilibrium with population probabilities

$$p_i = \frac{(2J_i + 1)\exp(-E_i/kT)}{\sum_m (2J_m + 1)\exp(-E_m/kT)}, \quad (4)$$

where J denotes the level spin and the denominator represents the nuclear partition function.

The capture cross section of excited states can be modeled as done for ground states. However, in reactions on excited states an additional possibility for inelastic scattering must be considered, the so-called "superelastic" channel, in which the incident neutron gains in energy, leaving the target nucleus in a lower state. This particularly relevant process has to be taken into account in the HFSM equation [Eq. (2)] by adding the transmission coefficients $T_{n',ls}$ for the open superelastic channels.

Possibilities for testing the calculations of the stellar MACS are the comparison of measured and calculated inelastic scattering cross sections, which provides a good benchmark for the neutron-nucleus interaction needed to obtain the transmission functions in such calculations and the comparison with the experimental capture cross section for the ground state. Unfortunately, experimental data for

the inelastic channel in the astrophysically relevant energy range are rather scarce.

In practice, these effects are taken into account by the so-called stellar enhancement factor (SEF)

$$\mathrm{SEF} = \frac{\langle\sigma\rangle^{*}}{\langle\sigma\rangle^{\mathrm{lab}}},$$

where the MACS labeled by $*$ and lab indicate the stellar average over the thermally populated states and for the laboratory (ground state) cross section, respectively. On average, these factors are below 10% at the *s*-process temperatures in low-mass AGB stars, but can reach values of more than 40% during shell C burning in massive stars, especially for the heavy odd isotopes with low-lying excited states.

An important example for the role of SEFs is the Re/Os nuclear cosmochronology (Clayton, 1964), where the MACS of the *s*-only isotopes ^{186}Os and ^{187}Os are of key importance. The aspects related to the neutron physics of this clock have been studied by the n_TOF Collaboration in papers dealing with cross-section measurements in the astrophysically relevant energy range (Mosconi *et al.*, 2010a, 2010b) and the SEF calculations based on the HFSM approach with model parameters tuned to reproduce the experimental (n, γ) and (n, n') cross sections (Fujii *et al.*, 2010).

The SEF corrections are particularly relevant for ^{187}Os, where the ground state is populated by only about 30% at $kT = 30$ keV, while 70% of the nuclei exist in excited states, 47% alone in the first excited state at 9.75 keV, the state which strongly dominates the competition by inelastic and superelastic scattering. The comparison of the SEF values for ^{186}Os and ^{187}Os in Fig. 5 underlines the importance of this correction for ^{187}Os in the relevant range of thermal energies around $kT = 25$ keV. A relatively small uncertainty of $\pm 4\%$ could be estimated for the SEF of ^{187}Os from the difference between the results obtained with a spherical and deformed optical model potential for the neutron-nucleus interaction.

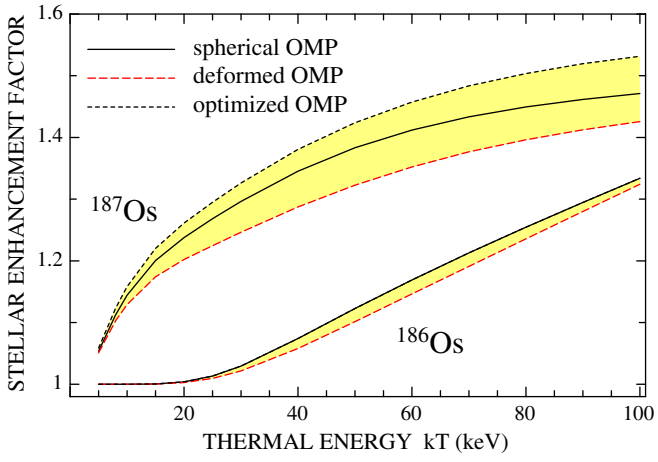

FIG. 5 (color online). Stellar enhancement factor (SEF) for the ^{187}Os$(n, \gamma)^{188}$Os reaction. The first ten excited states in ^{187}Os, up to an excitation energy of 260 keV, have been included in the calculation. The difference between the results obtained with a spherical and a deformed optical model potential for the neutron-nucleus interaction could be used for estimating the uncertainties of the SEF results.

The impact of the estimated SEF uncertainties and of other relevant nuclear physics input on the galactic age (or on the duration of nucleosynthesis) has been estimated by means of the simple model proposed by Fowler and Hoyle (1960) to be less than 1 Gyr (Fujii *et al.*, 2010). This means that uncertainties of the experimental data are no longer limiting a revision of the Re/Os chronometer. Further work can now concentrate on the related astrophysical issues, which are mostly due to the time dependence of the production rate of ^{187}Re and the related problem of astration, i.e., that ^{187}Re is partially destroyed in later stellar generations.

The example of ^{187}Re shows that uncertainties of $\approx 4\%$–5% can be obtained in SEF calculations, provided that the measured capture cross section for the ground state is known with sufficient accuracy and that the other parameters in HFSM calculations can be derived from measured quantities.

C. β decay under stellar conditions

A detailed evaluation of β-decay rates for *s*-process analyses has been given by Takahashi and Yokoi (1987) on the basis of a thorough classification of possible contributions from thermally excited states and by considering the relevant effects related to the high degree of ionization in the stellar plasma. The most spectacular consequence of ionization is the enormous enhancement of decays with small Q_β values, where the decay electrons can be emitted into unoccupied atomic orbits. This bound β decay was eventually confirmed in storage ring experiments with fully stripped ^{163}Ho and ^{187}Re atoms at GSI Darmstadt (Jung *et al.*, 1992; Bosch *et al.*, 1996).

The quantitative assessment of the temperature dependent decay rates of the key branch-point isotopes requires more experimental information on $\log_{10} ft$ values for the decay of excited states as well as more storage ring experiments to expand our knowledge of bound β-decay rates. Experimental possibilities have been discussed (Käppeler, 1999), but must be extended by the successful recent application of $(d, {}^2\mathrm{He})$ reactions (Frekers, 2005).

D. Status and prospects

1. Compilations of stellar (n, γ) cross sections and further requirements

Stellar neutron-capture cross sections were compiled in 1971 by Allen *et al.* (1971), who presented a set of recommended (n, γ) cross sections averaged over a Maxwell-Boltzmann distribution for a thermal energy of $kT = 30$ keV. This first collection of MACS comprised 130 experimental cross sections with typical uncertainties between 10% and 25%. These data were complemented by 109 semiempirical values estimated from the cross-section trends with a neutron number of neighboring nuclei to provide a full set of nuclear data for quantitative studies of the *s* process.

The next compilation of experimental and theoretical stellar neutron cross sections for *s*-process studies, which was published 16 years later by Bao and Käppeler (1987), included cross sections for (n, γ) reactions between ^{12}C and

^{209}Bi, some (n, p) and (n, α) reactions (from ^{33}Se to ^{59}Ni), and also (n, γ) and (n, f) reactions for long-lived actinides. Also in this version MACS were given at a single thermal energy of $kT = 30$ keV, sufficient for studies with the canonical *s* process formulated by Seeger *et al.* (1965) for a constant temperature and neutron density scenario. A major achievement, however, was the significant improvement of the accuracy, which was reaching the 1% –2% level for a number of important *s*-process isotopes.

Meanwhile, the canonical or "classical" approach had been challenged by refined stellar models, which indicated different sites for the *s* process, from He shell burning in thermally pulsing low-mass AGB stars (Gallino, Busso *et al.*, 1988; Hollowell and Iben, 1988) to shell C burning in massive stars (Raiteri *et al.*, 1991a, 1991b), where (α, n) reactions on ^{13}C and ^{22}Ne were identified as the dominant neutron sources, respectively. The fact that the temperatures at the various sites require MACS data for thermal energies between 8 and 90 keV was taken into account in the compilation of Beer, Voß, and Winters (1992), which listed values in the range $5 \leq kT \leq 100$ keV.

The following compilation of Bao *et al.* (2000) was extended to cover a network of 364 (n, γ) reactions, including relevant partial cross sections. This work presents detailed information on previous MACS results, which were eventually condensed into recommended values. Again, data are given for thermal energies from 5 to 100 keV. For isotopes without experimental cross-section information, recommended values were derived from calculations with the Hauser-Feshbach statistical model code NON-SMOKER (Rauscher Thielemann, 2000), which were empirically corrected for known systematic deficiencies in the nuclear input of the calculation. For the first time, SEFs, which take the effect of thermally excited nuclear states into account, were included as well.

For easy access, the compilation of Bao *et al.* (2000) was published in electronic form via the KADONIS project[2] (Dillmann *et al.*, 2005). The current version KADONIS V0.3 (Dillmann *et al.*, 2009) is already the third update and includes [compared to the Bao *et al.* compilation (Bao *et al.*, 2000)] recommended values for 38 improved and 14 new cross sections. In total, data sets are available for 356 isotopes, including 77 radioactive nuclei on or close to the *s*-process path. For 13 of these radioactive nuclei, experimental data are available, i.e., for ^{14}C, ^{60}Fe, ^{93}Zr, ^{99}Tc, ^{107}Pd, ^{129}I, ^{135}Cs, ^{147}Pm, ^{151}Sm, ^{155}Eu, ^{163}Ho, ^{182}Hf, and ^{185}W. The remaining 64 radioactive nuclei are not (yet) measured in the stellar energy range and are represented only by empirically corrected Hauser-Feshbach rates with typical uncertainties of 25% to 30%. Almost all of the (n, γ) cross sections of the 277 stable isotopes have been measured. The few exceptions are ^{17}O, ^{36,38}Ar, ^{40}K, ^{50}V, ^{70}Zn, ^{72,73}Ge, ^{77,82}Se, ^{98,99}Ru, ^{131}Xe, ^{138}La, ^{158}Dy, and ^{195}Pt, which lie mostly outside the *s*-process path in the proton-rich *p*-process domain. These cross sections are difficult to determine because they are often not accessible by activation measurements or not available in sufficient amounts and/or enrichment for time-of-flight measurements.

[2]http://www.kadonis.org.

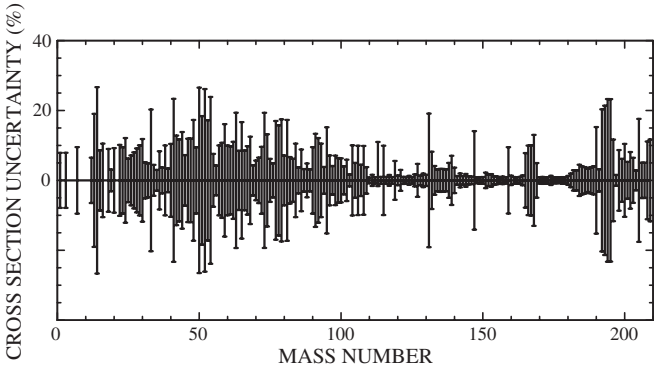

FIG. 6. Uncertainties of the stellar (n, γ) cross sections for *s*-process nucleosynthesis. These values refer to a thermal energy of $kT = 30$ keV, but may be considerably larger at lower and higher temperatures.

The actual status of the (n, γ) cross sections for *s*-process nucleosynthesis calculations is summarized in Fig. 6, which shows the respective uncertainties as a function of mass number. Though the necessary accuracy of 1% to 5% has been locally achieved, further improvements are clearly required, predominantly in the mass region below $A = 120$ and above $A = 180$.

Further efforts in this field are necessary as Fig. 6 reflects only the situation for a thermal energy of 30 keV. In most cases, however, extrapolation to lower and higher temperatures implies still larger uncertainties.

The lack of accurate data is particularly crucial for the weak *s* process in massive stars, which is responsible for most of the *s* abundances between Cu and Sr. Since the neutron exposure of the weak *s* process is not sufficient for achieving flow equilibrium, cross-section uncertainties may affect the abundances of a sequence of heavier isotopes (see Sec. III B).

The present version of KADONIS consists of two parts: the *s*-process library and a collection of available experimental *p*-process reactions. The *s*-process library will be complemented in the near future by some (n, p) and (n, α) cross sections measured at $kT = 30$ keV, as was already included by Bao and Käppeler (1987). The *p*-process database will be a collection of all available charged-particle reactions measured within or close to the Gamow window of the *p* process ($T_9 = 2$–3 GK).

In a further extension of KADONIS it is planned to include more radioactive isotopes, which are relevant for *s*-process nucleosynthesis at higher neutron densities (up to 10^{11} cm^{-3}) (Cristallo *et al.*, 2006). Since these isotopes are more than one atomic mass unit away from the "regular" *s*-process path on the neutron-rich side of stability, their stellar (n, γ) values have to be extrapolated from known cross sections by means of the statistical Hauser-Feshbach model. The present list covers 73 new isotopes and is available on the KADONIS home page.

2. Measurements on rare and unstable samples

The continuous development and optimization of techniques and facilities remains a most vital aspect of the field, especially with respect to unstable isotopes. This concerns the production of higher fluxes, i.e., by means of shorter flight

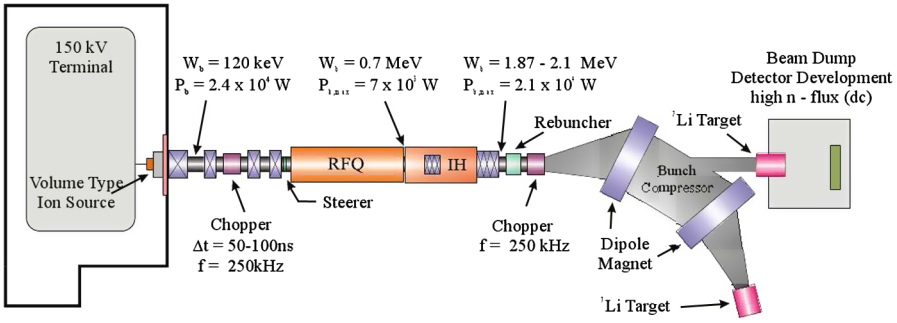

FIG. 7 (color online). Schematic layout and main parameters of the Frankfurt intense neutron source (see text).

paths at existing spallation sources, e.g., a 20 m station at n_TOF, or beam lines for keV neutrons at the new generation of high intensity accelerators such as the Japanese Proton Accelerator Complex J-PARC (Japan Proton Accelerator Complex, 2004).

A completely new approach is presently developed at the University of Frankfurt (Ratzinger *et al.*, 2007). The Frankfurt Neutron source at the Stern-Gerlach-Zentrum (FRANZ) will provide short neutron pulses by bombardment of a ^{7}Li target with an intense proton beam. The proton energy range is limited to 2.0 ± 0.2 MeV and the pulse rate will be typically 250 kHz.

The scheme of the accelerator is shown in Fig. 7, starting with a volume-type proton source on a 150 kV high voltage platform, followed by a 100 ns chopper in the low energy beam transport line to the acceleration stage consisting of a radio frequency quadrupole (RFQ) with an exit energy of 700 keV and a drift tube linac structure based on the interdigital H-mode principle (IH-DTL) with an effective energy gain of 1.4 MeV. The macropulses at the exit contain up to 10 rf bunches, which are compressed into 1 ns pulses for neutron production in the Li target. This is achieved by a second chopper, which deflects the bunches to traces of different path length in a Mobley-type buncher system (Chau *et al.*, 2006; Meusel *et al.*, 2006; Ratzinger *et al.*, 2007).

In this way, intense pulses of up to 5×10^{10} protons can be focused onto the Li target within 1 ns. The average beam current is expected to reach 2 mA, corresponding to a neutron flux of about 10^5 n/cm^2/s/keV at a distance of 80 cm from the target, more than an order of magnitude higher than is achieved at present spallation, sources. Since the amount of sample material can be reduced by the gain in flux, TOF measurements at FRANZ appear to be feasible with samples of 10^{14} to 10^{16} atoms. The use of such minute amounts represents a breakthrough with respect to the production of

TABLE III. Feasibility of future TOF measurements on unstable branch-point isotopes at the FRANZ facility.

Sample	Half-life (yr)	Q value (MeV)	Comment
^{63}Ni	100.1	β^-, 0.066	TOF work in progress (Couture, 2009), sample with low enrichment
^{79}Se	2.95×10^5	β^-, 0.159	Important branching, constrains *s*-process temperature in massive stars
^{81}Kr	2.29×10^5	EC, 0.322	Part of ^{79}Se branching
^{85}Kr	10.73	β^-, 0.687	Important branching, constrains neutron density in massive stars
^{95}Zr	64.02 d	β^-, 1.125	Not feasible in near future, but important for neutron density low-mass AGB stars
^{134}Cs	2.0652	β^-, 2.059	Important branching at $A = 134, 135$, sensitive to *s*-process temperature in low-mass AGB stars, measurement not feasible in near future
^{135}Cs	2.3×10^6	β^-, 0.269	So far only activation measurement at $kT = 25$ keV by Patronis *et al.* (2004)
^{147}Nd	10.981 d	β^-, 0.896	Important branching at $A = 147/148$, constrains neutron density in low-mass AGB stars
^{147}Pm	2.6234	β^-, 0.225	Part of branching at $A = 147/148$
^{148}Pm	5.368 d	β^-, 2.464	Not feasible in the near future
^{151}Sm	90	β^-, 0.076	Existing TOF measurements, full set of MACS data available (Abbondanno *et al.*, 2004a; Wisshak *et al.*, 2006c)
^{154}Eu	8.593	β^-, 1.978	Complex branching at $A = 154, 155$, sensitive to temperature and neutron density
^{155}Eu	4.753	β^-, 0.246	So far only activation measurement at $kT = 25$ keV by Jaag and Käppeler (1995)
^{153}Gd	0.658	EC, 0.244	Part of branching at $A = 154, 155$
^{160}Tb	0.198	β^-, 1.833	Weak temperature-sensitive branching, very challenging experiment
^{163}Ho	4570	EC, 0.0026	Branching at $A = 163$ sensitive to mass density during *s* process, so far only activation measurement at $kT = 25$ keV by Jaag and Käppeler (1996b)
^{170}Tm	0.352	β^-, 0.968	Important branching, constrains neutron density in low-mass AGB stars
^{171}Tm	1.921	β^-, 0.098	Part of branching at $A = 170, 171$
^{179}Ta	1.82	EC, 0.115	Crucial for *s*-process contribution to ^{180}Ta, nature's rarest stable isotope
^{185}W	0.206	β^-, 0.432	Important branching, sensitive to neutron density and *s*-process temperature in low-mass AGB stars
^{204}Tl	3.78	β^-, 0.763	Determines ^{205}Pb/^{205}Tl clock for dating of early Solar System

unstable samples, because beam intensities of the order of 10^{10} to 10^{12} s^{-1} are expected at future rare isotope facilities such as RIKEN (Tanihata, 1998; FAIR, 2007; FRIB, 2010).

The gain in beam intensity and the related reduction in sample mass implies that TOF measurements can be carried out on unstable nuclei with correspondingly higher specific activities, including a number of branch-point isotopes, which are not accessible by activation techniques. The concise list of important branch-point isotopes in Table III shows that most of these samples are accessible to TOF measurements at FRANZ thanks to the excellent sensitivity of that facility. It should be noted, however, that Table III includes a number of cases, which could, in principle, be studied at existing facilities. Such measurements are impeded, however, because isotopically enriched samples are not available in sufficient amounts. Among the 20 listed unstable isotopes in Table III there are only three cases where the specific γ activities seem to be too high for a promising experiment in the foreseeable future.

In addition to the gain in TOF sensitivity, FRANZ is also perfectly suited for the simulation of stellar neutron spectra via the ^{7}Li$(p, n)^7$Be reaction (see Sec. II.A.4). In fact the larger dispersion in proton energy will result in a closer approximation of the stellar spectrum as was pointed out by Mastinu *et al.* (2009). Similar to the situation sketched for TOF measurements, the higher flux will enable one to apply the activation method to a largely extended set of shorter-lived unstable nuclei, an important aspect for investigating the *s*-process during shell C burning in massive stars, where the reaction path is shifted by a few mass units from the valley of stability due to neutron densities in excess of 10^{12} cm^{-3} [see, e.g., Pignatari *et al.* (2010)]. In combination with AMS it will even be possible to use the double neutron-capture method to obtain the MACS for such crucial cases as ^{59}Fe, ^{125}Sn, and ^{181}Hf.

Apart from their importance for specific problems and their direct use in *s*-process networks, MACS of unstable isotopes represent valuable information in a wider sense, particularly for testing and improving statistical model calculations in areas which are not accessible to experiments in the near future.

III. *s*-Process MODELS

Stellar models for the He-burning stage of stellar evolution have been worked out in great detail over the past decade, both for low-mass stars in the AGB phase while suffering recurrent thermal pulses in the He shell and for massive stars. There, besides central He burning in the convective core, neutrons are released in the subsequent convective shell C-burning phase, which involves a large fraction of the final ejected mass in the supernova event. Accounting for a continuous updated network of neutron captures and charged-particle reaction rates, the *s* process taking place in both low-mass stars and massive stars will be discussed.

A. Classical approach

Shortly after stellar spectroscopy of the unstable element Tc provided evidence for active neutron-capture nucleosynthesis in red-giant stars (Merrill, 1952), the canonical or classical model of the *s* process was suggested by B^2FH (Burbidge *et al.*, 1957). Although it was argued that the He-burning zones of red giants were the most promising site of the *s* process, the lack of detailed stellar models led to a phenomenological solution. Within this approach it is empirically assumed that a certain fraction G of the observed ^{56}Fe abundance was irradiated by an exponential distribution of neutron exposures (Seeger *et al.*, 1965). In this case, an analytical solution can be obtained if a possible time dependence of the neutron-capture rates, $\lambda_n = n_n\langle\sigma\rangle v_T$, is neglected. In other words, it is assumed that temperature and neutron density n_n are constant. Then the product of the stellar cross section and resulting *s* abundance, which characterizes the reaction flow, can be given by

$$\langle\sigma\rangle_{(A)}N_{s(A)} = \frac{GN_{56}^{\odot}}{\tau_0}\prod_{i=56}^{A}\left(1+\frac{1}{\tau_0\langle\sigma\rangle_i}\right)^{-1}. \quad (5)$$

Apart from the two parameters G and τ_0 (which are adjusted by fitting the abundances of the *s*-only nuclei), the only remaining input for this expression are the stellar (n, γ) cross sections $\langle\sigma\rangle$ (Käppeler *et al.*, 1989; Wallerstein *et al.*, 1997).

Given the schematic nature of this classical approach, it surprisingly provided an excellent description of the *s*-process abundances in the solar system (see Fig. 2). One finds that equilibrium in the neutron-capture flow was obtained between magic neutron numbers, where the $\langle\sigma\rangle N_s$ curve is almost constant. The small cross sections of the neutron-magic nuclei around $A \sim 88$, 140, and 208 act as bottlenecks for the capture flow, resulting in distinct steps in the $\langle\sigma\rangle N_s$ curve.

The global parameters G and τ_0 that determine the overall shape of this curve represent a first constraint for the stellar *s*-process site with respect to the required seed abundance and total neutron exposure. It is found that 0.04% of the ^{56}Fe abundance observed in solar system material is a sufficient seed, and that on average about 15 neutrons are captured by each seed nucleus (Käppeler, Gallino *et al.*, 1990). These numbers refer to the *main* *s*-process component, which dominates the *s* abundances for $A > 90$. The rather steep increase of the $\langle\sigma\rangle N_s$ curve below $A = 90$ requires an additional component, the *weak* component.

The weak component is not firmly described by the classical analysis, because there are only six *s*-only isotopes below $A = 90$ (^{70}Ge, ^{76}Se, ^{80,82}Kr, ^{86,87}Sr), which are also partly produced by the main component and possibly even by the *p* process. Moreover, ^{80}Kr and ^{86,87}Sr are affected by branchings in the *s*-process path. The temperature and neutron density determining these branchings are to be treated as free parameters. Accordingly, it is difficult within the classical approach to distinguish between a single component or an exponential distribution of neutron exposures (Beer, 1986; Beer and Macklin, 1989; Käppeler *et al.*, 1989).

For about 40 years the classical model was quite successful in describing the solar *s*-process abundances (Käppeler *et al.*, 1982; Käppeler, Gallino *et al.*, 1990). In fact, the empirical $\langle\sigma\rangle N_s$ values of the *s*-only isotopes that are not affected by branchings are reproduced with a mean square deviation of only 3% (Käppeler, Gallino *et al.*, 1990) as shown in Fig. 2. About 20 years ago the development of new experimental techniques led to a set of accurate neutron-capture cross sections, which ultimately revealed that the classical

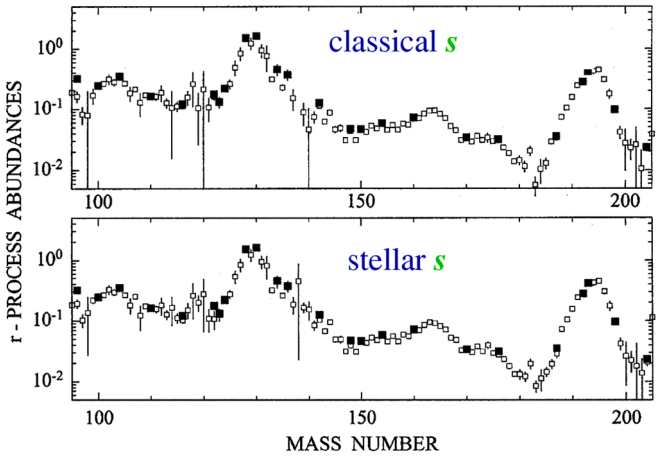

FIG. 8 (color online). The *r*-process abundances (open squares) obtained via the *r*-process residual method, $N_r = N_\odot - N_s$, using the classical and stellar *s*-process model. The *r*-only nuclei are represented by solid squares. (N_i relative to Si $\equiv 10^6$). From Arlandini *et al.*, 1999.

s process suffered from inherent inconsistencies. This was convincingly demonstrated at the example of the neutron-magic *s*-only isotope ^{142}Nd (Arlandini *et al.*, 1999). At this point, the classical approach was replaced by a first generation of stellar *s*-process models, where such problems could be successfully avoided (Gallino *et al.*, 1998; Arlandini *et al.*, 1999).

Nevertheless, the classical model still provides a useful tool for estimating the *s* abundances, in particular, in mass regions between magic numbers, where the cross sections are large enough that reaction flow equilibrium was actually reached. This is illustrated by the example of the solar *r*-process distribution obtained with the *r*-residual method,

$$N_r = N_\odot - N_s,$$

which represents the difference between the solar abundances and the corresponding *s*-process yields. The *r* distributions obtained via the classical approach or via stellar models are quite similar and match very well with the abundances of the *r*-only isotopes as shown in Fig. 8.

The separation of the solar abundance distribution into the *s* and *r* components also became important for the interpretation of abundance patterns of ultra-metal-poor stars (Westin *et al.*, 2000; Cowan *et al.*, 2002; Hill *et al.*, 2002; Sneden *et al.*, 2003), which turned out to agree very well with the scaled solar *r* component for the elements heavier than Ba.

B. Massive stars

As discussed at the end of Sec. III. A, the classical analysis of the *s* process fails to reproduce the cosmic abundances of the *s* isopotes below $A = 90$. The same problem is found for stellar models of low-mass AGB stars, as described in detail in Sec. III C. Actually, a complementary weak *s* process occurs in massive stars ($M > 8M_\odot$), which explode as supernovae of type II. Slow neutron captures are driven by the reaction ^{22}Ne$(\alpha, n)^{25}$Mg during convective core He burning at temperatures around 3×10^8 K as well as in the subsequent convective shell C burning at 1×10^9 K (Couch *et al.*, 1974; Lamb *et al.*, 1977; Käppeler *et al.*, 1989; Prantzos *et al.*, 1990; Beer, Walter, and Käppeler, 1992; Raiteri *et al.*, 1993). The available ^{22}Ne is produced via the reaction sequence ^{14}N$(\alpha, \gamma)^{18}$F$(\beta^+\nu)^{18}$O$(\alpha, \gamma)^{22}$Ne, where ^{14}N derives from the CNO cycle in the previous H-burning phase. Consequently, this weak *s*-process component produced in massive stars is secondarylike, decreasing with metallicity. At He exhaustion, not all the ^{22}Ne is consumed (see, e.g., Prantzos *et al.*, 1990), and neutron production via ^{22}Ne$(\alpha, n)^{25}$Mg continues during shell C burning by means of the α particles provided by the reaction channel ^{12}C$(^{12}$C, $\alpha)^{20}$Ne (Arnett and Truran, 1969).

In the ejecta of type II supernovae (SN II), the chemical composition of the core up to a mass of $3.5M_\odot$ (for a star of $25M_\odot$) is modified by explosive nucleosynthesis, which destroys any previous *s*-process signature. However, the ejecta still contain also an important mass fraction of $2.5M_\odot$, which preserves the original *s*-process abundances produced by the hydrostatic nucleosynthesis phases of the presupernova evolution.

This scenario was confirmed by postprocess models and full stellar models describing the evolution of massive stars up to the final burning phases and the SN explosion (Raiteri *et al.*, 1993; Woosley and Weaver, 1995; Limongi *et al.*, 2000; Woosley *et al.*, 2002; The *et al.*, 2007; El Eid *et al.*, 2009; Pignatari *et al.*, 2010).

In contrast to the main *s*-process component, the neutron fluence in the weak *s* process is too low for achieving reaction flow equilibrium. This has the important consequence that a particular MACS not only determines the abundance of the respective isotope, but also affects the abundances of all heavier isotopes as well (Pignatari *et al.*, 2010). This propagation effect is particularly critical for the abundant isotopes near the iron seed. A prominent example is the case of the ^{62}Ni$(n, \gamma)^{63}$Ni cross section, where the effect was discussed first (Rauscher and Guber, 2002, Rauscher *et al.*, 2002; Rauscher and Guber, 2005). This problem has triggered a series of experimental studies on that isotope (Nassar *et al.*, 2005; Tomyo *et al.*, 2005; Alpizar-Vicente *et al.*, 2008; Lederer *et al.*, 2010) and on other key reactions of the weak *s* process between Fe and Sr, which could be considerably improved (see, e.g., Heil *et al.*, 2008a, 2008b). For a full account, see the recent update of the KADONIS library (Dillmann *et al.*, 2009).

The cumulated uncertainties of the propagation effect are significant even for the heavier isotopes of the weak *s* process, up to Kr and Sr, with a possible, minor contribution to the Y and Zr abundances (Pignatari *et al.*, 2010). The corresponding uncertainties will be partly solved once the neutron-capture cross sections of the isotopes between Fe up to Sr are measured with an accuracy of 5% (see Fig. 6).

Apart from these problems with the neutron-capture cross sections, it was pointed out that the weak *s* process is also still affected by large uncertainties of several charged-particle reactions during He and C burning [see, e.g., Bennett *et al.* (2010) and The *et al.* (2007)].

C. AGB stars

During the AGB phase, the H- and He-burning shells are activated alternately on top of the degenerate C-O core. These

two shells are separated by a thin zone in radiative equilibrium, the so-called He intershell, enriched in He and C. The H-burning shell erodes the bottom layers of the envelope and produces He. The He intershell grows in mass and is progressively compressed and heated until He burning is triggered in a quasiexplosive way (thermal pulse, TP; Schwarzschild and Härm, 1965; Weigert, 1966). For a general discussion, see Iben and Renzini (1983), Busso *et al.* (1999), Herwig (2004), Straniero *et al.* (2006), and Sneden *et al.* (2008).

The sudden release of energy due to a TP drives convection in the whole intershell for a short period of time. During a TP, partial He burning occurs producing a large amount of ^{12}C. The envelope expands and the H shell is temporarily extinguished. He-shell burning continues radiatively for another few thousand years, and then H-shell burning starts again. After a limited number of TPs, when the mass of the H-exhausted core reaches $\sim 0.6 M_\odot$ and the H shell is inactive, the convective envelope penetrates into the top region of the He intershell and mixes newly synthesized material to the surface (third dredge-up, TDU).

The star undergoes recurrent TDU episodes, whose occurrence and efficiency depend on the physical and numerical treatment of the convective borders. The TDU is influenced by the parameters affecting the H-burning rate, such as the metallicity, the mass of the H-exhausted core, and the mass of the envelope, which in turn depends on the choice of the mass loss rate by stellar winds [see the discussion in Straniero *et al.* (2006)]. The upper panel of Fig. 9 shows the changes of the structural characteristics of a given AGB model with time (Cristallo, Piersanti *et al.*, 2009; Cristallo, Straniero *et al.*, 2009), the position in mass coordinates of the inner border of the convective envelope, the maximum energy production of the H-burning shell, and the maximum energy production within the H-depleted core. During each interpulse period, the flat segment of the lowest line corresponds to the radiative burning of the ^{13}C$(\alpha, n)^{16}$O reaction. The lower panel shows the H-burning and He-burning contributions to the luminosity.

During the TP-AGB phase, the envelope becomes progressively enriched in primary ^{12}C and in *s*-process elements. TDU drives a chemical discontinuity between the H-rich envelope and the He intershell, where a few protons likely penetrate into the top layers of the He intershell. At hydrogen reignition, these protons are captured by the abundant ^{12}C forming ^{13}C via ^{12}C$(p, \gamma)^{13}$N$(\beta^+ \nu)^{13}$C in a thin region of the He intershell (^{13}C pocket). Neutrons are released in the pocket under radiative conditions by the ^{13}C$(\alpha, n)^{16}$O reaction at $T \sim 0.9 \times 10^8$ K. This neutron exposure lasts for about 10 000 years with a relatively low neutron density of 10^6 to 10^8 cm^{-3}. The pocket, strongly enriched in *s*-process elements, is then engulfed by the subsequent convective TP. Models including rotation (Langer *et al.*, 1999) or gravity waves (Denissenkov and Tout, 2003) have obtained a partial mixing zone at the base of the convective envelope during the TDU episodes, which leads to the formation of a ^{13}C-rich layer of limited mass extension. Herwig *et al.* (1997) and Herwig (2000), (2004), guided by dynamical simulations of Freytag *et al.* (1996), introduced an exponential diffusive overshoot at the borders of all convective zones. A formally

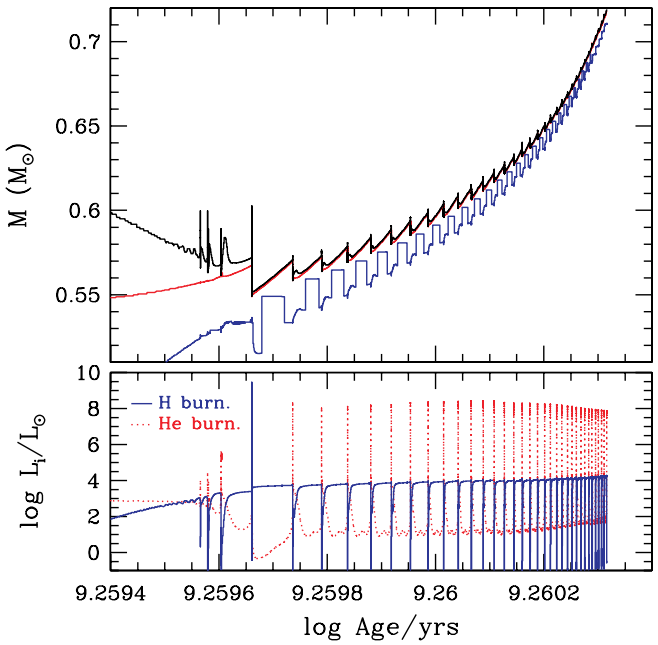

FIG. 9 (color online). Structural characteristics vs the age of an AGB model with initial mass $M_{\rm ini}^{\rm AGB} = 2\ M_\odot$ and solar metallicity. Upper panel, top to bottom: Temporal evolution of the mass coordinates of the inner border of the convective envelope, the mass location of maximum energy production in the H-burning shell, and the maximum energy production within the H-depleted core. During each interpulse period, the flat segment of the lowest line corresponds to the location of the radiative burning of the ^{13}C$(\alpha, n)^{16}$O reaction in the pocket. Lower panel: Temporal evolution of the H-burning and He-burning contributions to luminosity. From Cristallo, Piersanti *et al.*, 2009.

similar algorithm based on a nondiffusive mixing scheme has been proposed by Straniero *et al.* (2006). Applying the Schwarzschild criterion to determine the border of the H-rich convective envelope and the inner He-rich and C-rich intershells, a thermodynamical instability would ensue. In order to handle this instability, Straniero *et al.* (2006) assumed an exponentially decaying profile of the convective velocity

$$v = v_{\rm bce} \exp(-d/\beta H_P),$$

where d is the distance from the convective boundary, $v_{\rm bce}$ is the average element velocity at the convective boundary (as derived by means of the mixing length theory), H_P is the pressure scale height at the convective boundary, and β is a free parameter [for a proper choice, see Cristallo, Straniero *et al.* (2009)]. Figure 10 shows the formation of the ^{13}C pocket according to the full evolutionary model described by Straniero *et al.* (2009). The hydrogen profile adopted in the pocket and the consequent amount of ^{13}C (and of ^{14}N) determines the final *s*-abundance distribution.

At the maximum extension of the convective TP, when the temperature at the base of the convective zone exceeds 2.5×10^8 K, a second neutron burst is powered for a few years by the marginal activation of the ^{22}Ne$(\alpha, n)^{25}$Mg reaction. This neutron burst is characterized by a low neutron exposure and a high neutron density up to 10^{10} cm^{-3}, depending on the maximum temperature reached at the bottom of the TP. The dynamical conditions in which the two neutron

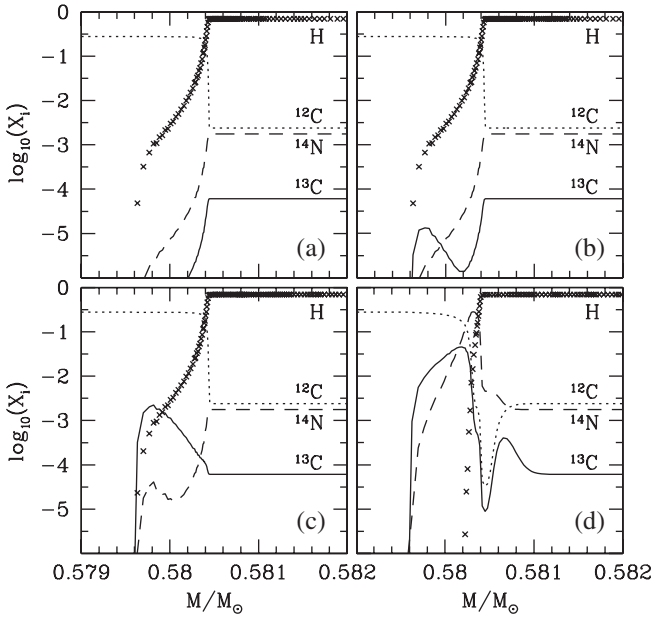

FIG. 10. The formation of the ^{13}C pocket according to Straniero *et al.* (2009). The sequence of the panels shows the evolution of the chemical composition in the transition zone between the H-rich envelope and the H-exhausted core. The various lines represent the abundances of H (crosses), ^{12}C (dotted), ^{13}C (solid), and ^{14}N (dashed). (a) The TDU just occurred and the convective envelope is receding. (b) Production of ^{13}C by proton capture on the abundant ^{12}C starts in the hotter region. (c) Some ^{14}N is also produced, and (d) the ^{13}C (and ^{14}N) pocket is fully developed.

sources operate define the final abundances of nuclei involved in branchings along the *s*-process path. A comparison of low-mass AGB models computed with different evolutionary codes has been discussed by Lugaro *et al.* (2003).

In AGB stars of intermediate mass ($4 < M/M_\odot < 8$), the maximum temperature during a TP reaches about 3.5×10^8 K, leading to a substantial neutron production via the ^{22}Ne$(\alpha, n)^{25}$Mg reaction. However, both the mass of the He intershell and the TDU efficiency are much smaller in these stars than in low-mass AGBs. Consequently, the predicted *s*-process abundances in the envelope are fairly low.

The production of the *s* elements at very low metallicity ($[\mathrm{Fe/H}] < -2.5$) may be affected by a new phenomenon, which is limited to AGB stars of the lowest mass leading to TDU and takes place only during the first fully developed TP. There the reduction of CNO catalysts is compensated by an increase of the temperature in the H shell and, consequently, the entropy in the H shell decreases. Under these conditions, the first convective He instability may expand over the H shell, thus engulfing protons from the envelope, which are instantly captured by the abundant ^{12}C in the convective region. The ^{13}C$(\alpha, n)^{16}$O reaction now occurs during the TP, in competition with the ^{22}Ne$(\alpha, n)^{25}$Mg reaction at the bottom of the TP.

This complex feature was found by many authors despite the different physics adopted in the various works (Hollowell *et al.*, 1990; Fujimoto *et al.*, 2000; Iwamoto *et al.*, 2004; Straniero *et al.*, 2004; Cristallo *et al.*, 2007; Campbell and Lattanzio, 2008; Suda *et al.*, 2008; Woodward *et al.*, 2008; Lau *et al.*, 2009). First calculations of the consequences of this mechanism for the *s* process have been made by Cristallo, Piersanti *et al.* (2009) for an AGB model of an initial mass $M = 1.5M_\odot$, a metallicity of $[\mathrm{Fe/H}] = -2.6$, and no enhancement of the α elements. The convective shell was found to split into two subshells: the lower one boosted by the ^{13}C$(\alpha, n)^{16}$O reactions and the upper one by the CNO cycle. Once the splitting has occurred, the nucleosynthesis in the two shells exhibits a completely different behavior. In the upper shell, the very large ^{13}C abundance is marginally consumed via ^{13}C$(\alpha, n)^{16}$O, leading to the production of a corresponding amount of light *s*-process elements (ls) elements. This peculiar phase is followed by a deep third dredge-up episode, which mixes freshly synthesized ^{13}C, ^{14}N, and ls elements into the envelope. The second TDU carries a large amount of heavy *s*-process elements (hs) elements and Pb to the surface, which was previously synthesized by ^{13}C$(\alpha, n)^{16}$O reactions in the lower splitted shell. After this initial event, the subsequent series of TPs and TDUs follow the standard pattern. The whole problem and its consequences on the surface abundances are currently a matter of intense study. This phenomenon may be of interest for the analysis of some carbon-enhanced metal-poor (CEMP) stars showing *s*-process enhancement (CEMP-*s* stars); see Secs. III.D and IV.B.2.

D. Theoretical AGB results

The *s* process in AGB stars is not a unique process, but depends on the initial mass, metallicity, the strength of the ^{13}C pocket, and the choice of the mass loss rate. Important observational constraints can be derived from the abundances of elements belonging to the three *s*-process peaks located at the magic neutron numbers $N = 50$, 82, and 126. The peaks occur because the low neutron-capture cross sections of Sr, Y, Zr (light *s*-process elements, ls), Ba, La, Ce, Nd, Sm (heavy *s*-process elements, hs), and Pb act as bottlenecks for the *s*-process reaction path. For a given metallicity, a spread in the three *s*-process peaks is observed in stars of spectral type MS, S, C(N) and Ba stars of the galactic disk [see Busso *et al.* (1995), Abia *et al.*, (2001), Busso *et al.* (2001), Abia *et al.* (2002), and Gallino *et al.* (2005)]. At low metallicities, high-resolution spectroscopic measurements of CEMP-*s* stars showed an even larger spread (Ivans *et al.*, 2005; Aoki *et al.*, 2006a; Roederer, Frebel *et al.*, 2008; Sneden *et al.*, 2008; Thompson *et al.*, 2008). The observed spread can be interpreted by assuming different *s*-process efficiencies of these stars, corresponding to a change in the amount of ^{13}C in the pocket.

We discuss here theoretical results from models based on the FRANEC code (Frascati Raphson-Newton evolutionary code (Chieffi and Straniero, 1989), coupled with a postprocess code that includes a full *s*-process network up to Bi (Bisterzo *et al.*, 2010). In the postprocess code, the prescriptions for the amount of the dredged-up mass, the number of TDUs, the choice of the mass loss rate, as well as for the temporal history of the temperature and density during the TPs were adopted from Straniero *et al.* (2003, 2006). The ^{13}C pocket is artificially introduced starting from the standard (ST) pocket adopted by Gallino *et al.* (1998) and Arlandini *et al.* (1999), which was shown to reproduce the solar main

s-process component as the average of the 1.5 and $3.0M_\odot$ models at half solar metallicity (Sec. III.E). The ^{13}C (and ^{14}N) abundances in the pocket were then multiplied by different factors. A minimum ^{13}C pocket may be defined as the one that affects the final *s*-process distribution. Higher ^{13}C-pocket efficiencies than the case ST × 2 would not produce a correspondingly higher abundance of ^{13}C, because of the increasing competition by ^{13}C$(p,\gamma)^{14}$N reactions. For any given model, the efficiency of the ^{13}C pocket is assumed to be constant for all TPs.

The theoretical predictions in the envelope for elements from C to Bi ([El/Fe]) versus atomic number Z are shown in Fig. 11 for an AGB star with an initial mass $M = 1.5M_\odot$ and for a range of ^{13}C pockets (from the case ST down to ST/12) at solar metallicity (top panel) and at [Fe/H] = −0.5 (bottom panel) [see Husti *et al.* (2009) and Bisterzo *et al.* (2010)]. With decreasing metallicity, the *s*-process distribution is shifted toward heavier elements. This is the consequence of the primary nature of the ^{13}C neutron source: While ^{56}Fe (the seed of the *s* process) decreases with metallicity, the number of neutrons available per iron seed increases (Clayton, 1988). Hence, at halo metallicities, the neutron fluence overcomes the first two peaks, directly feeding ^{208}Pb (Gallino *et al.*, 1998; Goriely and Mowlavi, 2000; Travaglio *et al.*, 2001; see Sec. III.E).

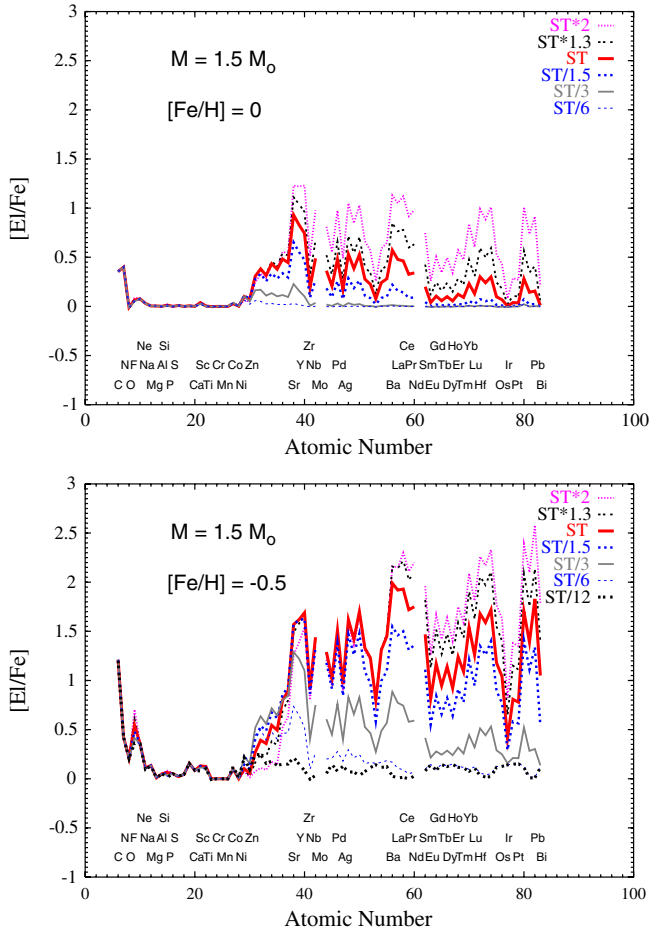

FIG. 11 (color online). Top panel: Theoretical results of [El/Fe] vs atomic number at the last TDU episode in the envelope of an AGB star with initial mass $M = 1.5M_\odot$ and [Fe/H] = 0. Bottom panel: The same as the top panel but [Fe/H] = −0.5. Adapted from Husti *et al.*, 2009 and Bisterzo *et al.*, 2010.

In Fig. 12, the relative behaviors of the three *s*-process peaks ls, hs, and Pb are analyzed using the definitions $[ls/Fe] = \frac{1}{2}([Y/Fe] + [Zr/Fe])$ and $[hs/Fe] = \frac{1}{3}([La/Fe] + [Nd/Fe] + [Sm/Fe])$. In general, the choice of the specific elements considered in the average ls and hs abundances varies and depends on the quality of the spectra available. Our choice is made because, at disk metallicity, Sr and Ba have few and saturated lines [see Busso *et al.* (1995, 2001)] and may be affected by nonlocal thermodynamical

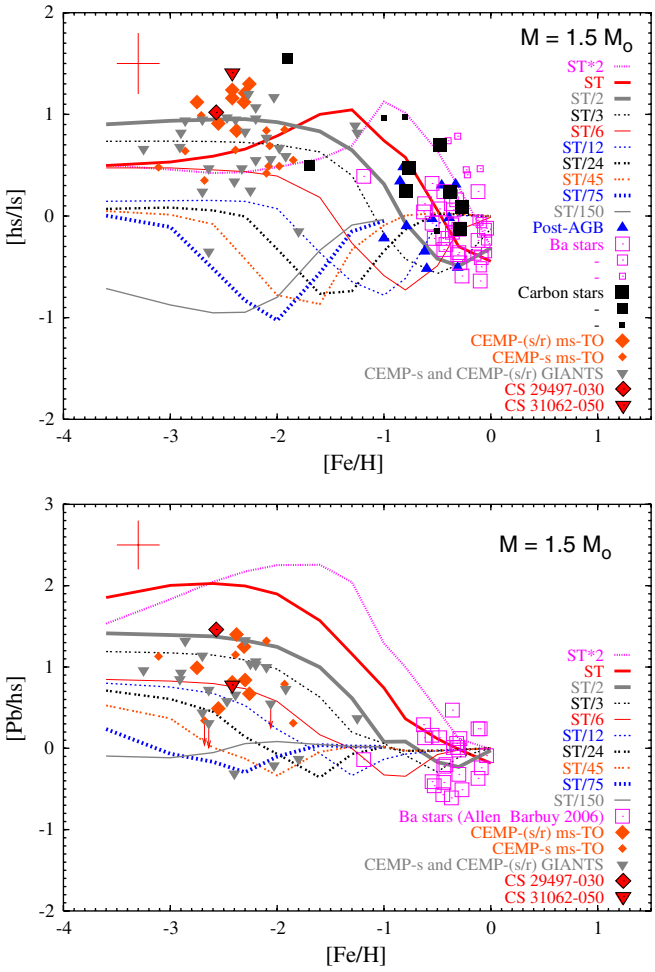

FIG. 12 (color online). Top panel: Theoretical results of the *s*-process index [hs/ls] as a function of [Fe/H] for AGB models of initial mass $M = 1.5M_\odot$ and a wide range of ^{13}C-pocket efficiencies. Spectroscopic observations are plotted for post-AGB stars (solid triangles, Van Winckel and Reyniers, 2000; Reddy *et al.*, 2002; Reyniers *et al.*, 2004, 2007), Ba stars (large open squares, Allen and Barbuy, 2006; medium open squares, Smiljanic *et al.*, 2007; small open squares, Liu *et al.*, 2009), carbon stars (large solid squares, Zamora *et al.*, 2009; medium solid squares Abia *et al.*, 2008; small solid squares de Laverny *et al.*, 2006), CEMP-*s* and CEMP-s/r stars (solid diamonds are main-sequence turn-off stars; solid triangles are giants stars, see text for references). Bottom panel: Theoretical results of the *s*-process index [Pb/hs] vs [Fe/H]. Spectroscopic observations: CEMP-*s*, CEMP-s/r, and galactic Ba stars for which Pb abundances have been reported. Symbols are the same as in the top panel. Typical error bars are indicated in the top left corner of the panels.

equilibrium corrections, in particular, at low metallicities [Andrievsky *et al.* (2009), and references therein].

The [hs/ls] and [Pb/hs] ratios are indexes of the whole *s*-process distribution. They remain unchanged both in the envelope of the AGB companion (now a white dwarf) and in the envelope of the observed star after accretion of AGB winds. The top panel of Fig. 12 shows [hs/ls] predictions for AGB stars of an initial mass of $1.5M_\odot$ as a function of [Fe/H] for different ^{13}C-pocket efficiencies. The figure also contains representative abundance data discussed in Sec. IV.

Considering the ST case as a function of metallicity in the top panel of Fig. 12, one finds that the [hs/ls] ratio first increases with decreasing [Fe/H], reaching a maximum at [Fe/H] $= -1.3$ and then decreases again. This behavior is due to the progressive buildup of hs elements and, subsequently, of the third *s* peak at ^{208}Pb. Note that ^{208}Pb becomes dominant over the ls and hs components already at a metallicity of [Fe/H] $= -1$. In the bottom panel of Fig. 12 theoretical predictions for [Pb/hs] vs [Fe/H] are compared with spectroscopic observations of Ba stars, CEMP-*s* and CEMP-s/r stars. For halo metallicities, the spread in [Pb/hs] is found to be about 2 dex.

A sample of 100 CEMP-*s* stars has been observed [see Sneden *et al.* (2008) and references therein] including main-sequence stars, subgiants, or giants, far from the AGB phase where the *s* process takes place. Moreover, to be observed today, these stars have long lifetimes and correspondingly low initial masses ($M \leq 0.9M_\odot$). Therefore, the hypothesis of mass accretion of *s*-rich material from a more massive AGB companion becomes essential to explain the overabundances detected in their spectra. The spectroscopic *s*-process abundances in CEMP-*s* stars depend on the fraction of the AGB mass transferred by stellar winds, whereas the *s*-process indexes [hs/ls] and [Pb/hs] remain unchanged. The mass transfer can be simulated by introducing a dilution factor between the accreted AGB mass and the original envelope of the observed star. The dilution factor dil can be defined as the logarithmic ratio between the mass of the convective envelope of the observed star before the mixing and the total transferred AGB mass.

About half of the known CEMP-*s* stars are also *r*-process rich with [Eu/Fe] comparable to [La/Fe]. Among the sample of stars reported in the literature with Eu measurements, six stars show an *r*-process enrichment of ~2 dex, among which are HE 2148-1247, the first CEMP-s/r star discovered (Cohen *et al.*, 2003), CS 29497-030 (Ivans *et al.*, 2005), HE 0338-3945 (Jonsell *et al.*, 2006), and CS 22898-027 (Aoki *et al.*, 2007). The *s* and *r* processes occur in completely different astrophysical scenarios: the *s* process in low-mass AGB stars and the *r* process during explosive nucleosynthesis in massive stars. While Eu is a typical *r*-process element (about 94% of solar Eu is of *r* origin), the elements of the hs peak, as Ba and La, are mainly synthesized by the *s* process. In particular, 70% of solar La is produced by the *s* process. AGB *s*-process predictions give $[\mathrm{La/Eu}]_s \sim 1$. Consequently, spectroscopic observations of enhanced [La/Fe] and comparable [Eu/Fe] cannot be explained by *s*-process AGB models alone. Cameron *et al.* (1997) and Vanhala and Cameron (1998) showed through numerical simulations how the supernova ejecta at high velocities interact with a nearby molecular cloud inducing Rayleigh-Taylor instabilities in the cloud, polluting it with freshly synthesized material, and at the same time triggering the condensation of a low-mass binary system. This scenario may explain the high fraction of CEMP-s/r stars. Other explanations for these peculiar CEMP-s/r stars have also been advanced, e.g., by Cohen *et al.* (2003) and Wanajo *et al.* (2006). On the other hand, 13 CEMP-*s* stars do not show any *r*-process enhancement, i.e., CS 22880-074 (Aoki *et al.*, 2007), HE 0024-2523 (Lucatello *et al.*, 2003), HE 2158-0348 (Cohen *et al.*, 2006), and HE 0202-2203 (Barklem *et al.*, 2005).

In Fig. 13 we show theoretical predictions of [hs/ls] vs [Fe/H] for AGB models with initial mass $M = 1.3M_\odot$, different ^{13}C-pocket efficiencies, and an initial *r*-process enrichment $[r/\mathrm{Fe}]^{\mathrm{ini}} = 2.0$. The label "n5" indicates the number of TDU episodes suffered by the $1.3M_\odot$ model. For a given element, the initial *r* enrichment is determined via the solar *r*-process contribution per isotope using the *r*-residual method (Arlandini *et al.*, 1999). Figure 13 also shows an abundance of data of all main-sequence–turnoff CEMP-s/r stars (solid diamonds). The two CEMP-s/r stars CS 29497-030 and CS 31062-050, which will be discussed in detail in Sec. IV.B, are indicated by a solid diamond and a solid rotated triangle, respectively. Because of the small number of TDUs in the $1.3M_\odot$ AGB model, the final surface distribution is affected by the initial *r* enrichment. In particular, at low metallicities, the predicted [hs/ls] ratios reach values as high as 1.3 dex. In the top panel of Fig. 12, however, the predictions reach a maximum value [hs/ls] $= 1$, independent of whether an *r* enhancement of 2 dex is included or not. Therefore, the most important message is that theoretical predictions given in Fig. 13 match the observations of main-sequence–turnoff CEMP-s/r stars quite well.

As an example, we show in Fig. 14 the two CEMP-s/r stars CS 29497-030 (Ivans *et al.*, 2005) and CS 31062-050 (Aoki, Norris *et al.*, 2002; Aoki, Ryan *et al.*, 2002; Johnson and Bolte, 2004; Aoki *et al.*, 2006a, 2007), which are

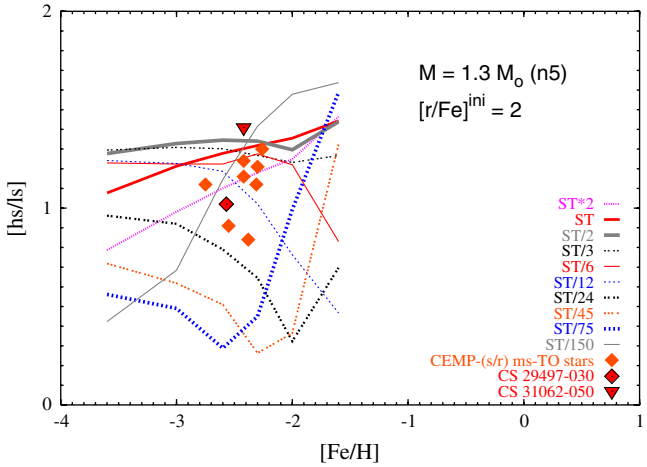

FIG. 13 (color online). Theoretical predictions of the *s*-process index [hs/ls] vs [Fe/H] for AGB models with initial mass $M = 1.3M_\odot$, a range of ^{13}C-pocket efficiencies, and an initial *r*-process enrichment $[r/\mathrm{Fe}]^{\mathrm{ini}} = 2.0$. The symbols of the spectroscopic observations are as in Fig. 12.

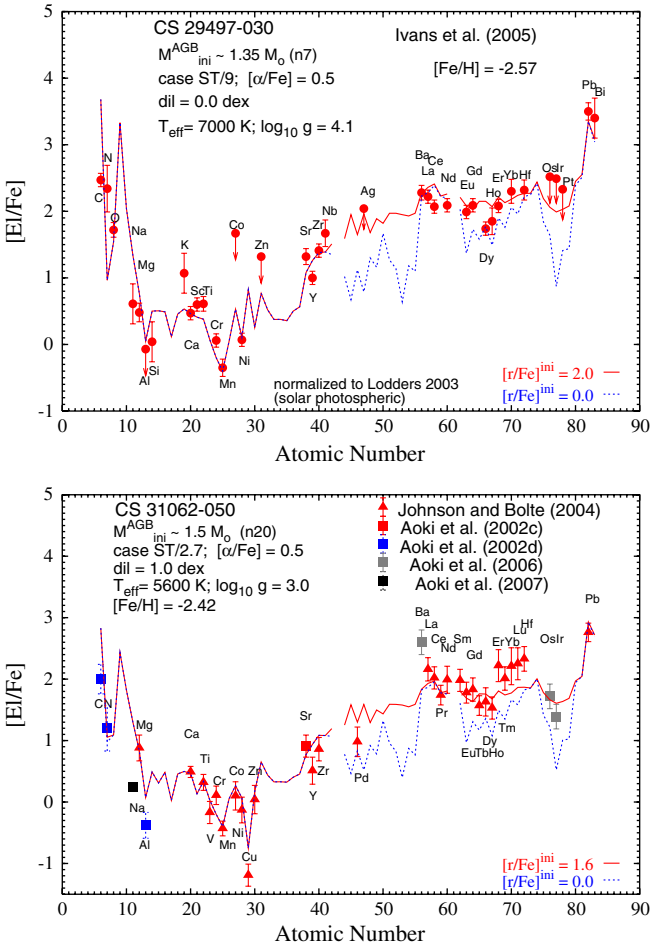

FIG. 14 (color online). Abundance patterns of the CEMP-s/r stars CS 31062-050 and CS 29497-030 compared with AGB models. Both stars show large excesses of heavy neutron-capture elements. The data and the theoretical expectations are normalized to the solar photospheric abundances of Lodders (2003). Top panel: CS 29497-030 compared with AGB models of $1.35M_{\odot}$ case ST/9 and no dilution. In this case an initial r-process enrichment of $[r/\mathrm{Fe}]^{\mathrm{ini}} = 2.0$ was adopted. Bottom panel: CS 31062-050 compared with AGB models of $1.5M_{\odot}$ case ST/2.7 and dil = 1.0 dex, with and without initial r-process enrichment ($[r/\mathrm{Fe}]^{\mathrm{ini}} = 1.6$ and 0.0, respectively).

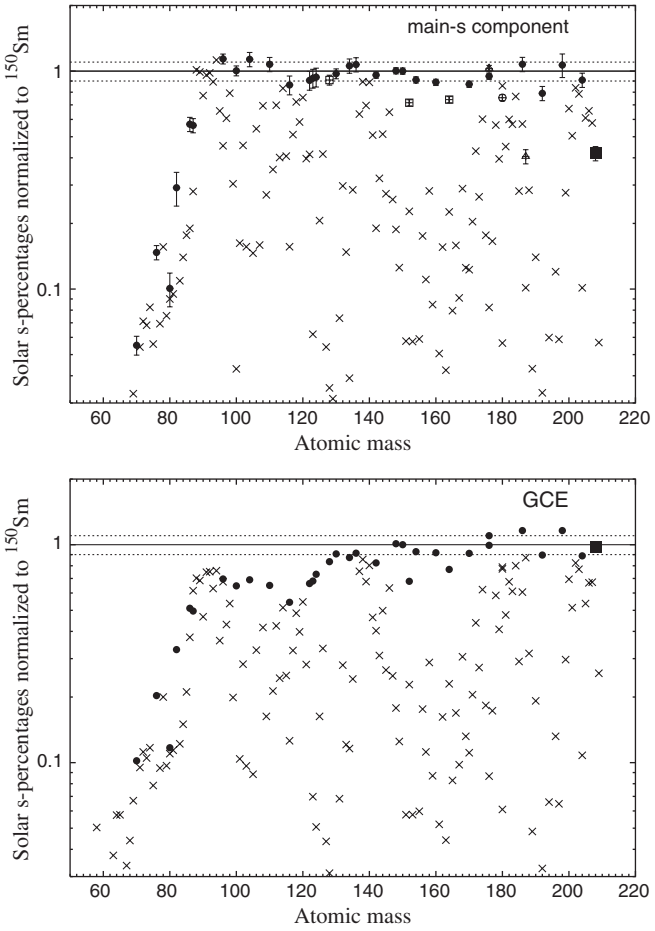

FIG. 15. Top panel: Solar s abundances normalized to ^{150}Sm vs atomic mass for the solar main component as in Arlandini *et al.* (1999), but updated by Bisterzo *et al.* (2010). Bottom panel: The predicted s-process distribution at the epoch of the Solar System formation obtained with a galactic chemical evolution code (Travaglio *et al.*, 2004) and AGB s-process yields at various metallicities. Note that ^{208}Pb is boosted to about 95% of its solar abundance by the contribution from low-metallicity AGB stars. Note also the 20%–30% deficit in the GCE distribution below magic neutron number $N = 82$. These are the two major changes compared to the Arlandini *et al.* (1999) stellar model with the ST pocket and $[\mathrm{Fe/H}] = -0.3$, which are AGB models reproducing the main s-process component but only about 34% of solar ^{208}Pb.

spectroscopically well studied. A more detailed discussion is presented in Sec. IV.B.

While the AGB model calculations are admittedly quite complex and subject to a number of free and model-dependent parameters, they have been successful in reproducing the abundance patterns of the CEMP-s stars.

E. The main *s* component and the role of a galactic chemical evolution model

The s-process abundance distribution of the heavy isotopes beyond $A \sim 90$ must be considered as the result of all previous generations of AGB stars that were polluting the interstellar medium before the formation of the Solar System. Therefore, the cosmic s-process abundances have to be explained by means of a general galactic chemical evolution (GCE) model.

It was shown by Gallino *et al.* (1998) and Arlandini *et al.* (1999) that the solar main component can be reproduced by assuming a standard ^{13}C pocket, a metallicity of $[\mathrm{Fe/H}] = -0.3$, and by averaging between stellar models of $M = 1.5M_{\odot}$ and $3M_{\odot}$. The distribution obtained with this prescription and updated nuclear input by Bisterzo *et al.* (2010) is plotted in the top panel of Fig. 15 normalized to the s-only isotope ^{150}Sm. The set of s-only isotopes indicated by solid circles is well reproduced. Open symbols have been used for ^{128}Xe, ^{152}Gd, and ^{164}Er, which have a non-negligible p contribution (10% for Xe), for ^{176}Lu, a long-lived isotope (3.8×10^{10} yr), which decays into ^{176}Hf, for ^{187}Os, which is affected by the long-lived decay of ^{187}Re (4.1×10^{10} yr), and for ^{180}Ta, which also receives contributions from the p process and from ν-nucleus interactions in massive stars. The solid square corresponds to ^{208}Pb, the only heavy isotope, which is clearly underproduced by the main s component (Clayton and Rassbach, 1967).

Employing a GCE code, in which the Galaxy is subdivided into three zones (halo, thick, and thin disks), adopting the *s*-process yields from AGB stars of different mass and metallicity, and accounting for their respective lifetimes Travaglio *et al.* (2004) determined the temporal variation of the *s*-process abundances in the interstellar medium. Their results were recently updated by Serminato *et al.* (2009). The resulting *s*-process distribution at the epoch of the Solar System formation is plotted in the bottom panel of Fig. 15. One finds that the GCE calculation (Travaglio *et al.*, 2004; Serminato *et al.*, 2009) yields good agreement with the solar abundance values of the *s*-only isotopes between ^{134,136}Ba and ^{204}Pb. Moreover, the solar abundance of ^{208}Pb is also well reproduced by the contributions from low-metallicity AGB stars, thus solving the long-standing problem of the origin of the strong *s* component in a natural way. Below the magic neutron number $N = 82$, however, there is a significant discrepancy between the abundance distribution obtained by the GCE approach and the Solar System values. It turned out that GCE models underproduce the *s*-process component of the Solar System abundances of Sr-Y-Zr by about 20%–30% (Travaglio *et al.*, 2004). A similar deficit holds for the *s*-only isotopes from ^{96}Mo up to ^{130}Xe. This finding prompted Travaglio *et al.* (2004) to postulate another source of neutron-capture nucleosynthesis in the Galaxy defined as the light element primary process (LEPP). The LEPP process is different from the *s* process in AGB stars and also different from the weak *s*-process component occurring in massive stars. Travaglio *et al.* (2004) suggested that 8% of solar Sr and 18% of solar Y and Zr must come from the LEPP. There is a general consensus for the need of an additional LEPP source of yet unknown origin for the light isotopes, including Sr, Y, and Zr, an issue that is still highly debated (Qian and Wasserburg, 2007; Farouqi *et al.*, 2010; Pignatari *et al.*, 2010). Montes *et al.* (2007) surveyed the possible ranges of parameters (e.g., for the neutron density) that reproduce the abundance patterns of HD 122563, a very metal-poor star representing the yields of the LEPP (Honda *et al.*, 2006).

Comparisons of the GCE models with observations of Galactic stars are discussed in Sec. IV.E.

IV. OBSERVATIONAL CONSTRAINTS

Models of nuclear reactions and enrichment of elements in the Universe are examined by astronomical observations as well as by the analysis of solar system material. The mechanisms and astronomical sites of the *s* process are constrained by the comparison of chemical abundance patterns with model predictions. Some key observational studies obtained before the mid-1990s have been outlined by Wallerstein *et al.* (1997). In the following sections a summary of the observational studies on the *s* process obtained in the past 15 years is presented.

Detailed chemical abundances have been determined for solar system material. As described, the classical model of the *s* process has been constructed by fitting the σN curve to those nuclei, which are only produced by the *s* process (Käppeler *et al.*, 1989). A more physical approach is to fit the abundances predicted by AGB models to the solar *s*-process component (Arlandini *et al.*, 1999).

The chemical abundances of the Solar System reflect the composition of a particular site of the Galaxy at 4.6×10^9 years ago, to which numerous nuclear processes in a variety of stars have contributed. Therefore, the abundance pattern of the *s*-process nuclei represents an average over the products from a variety of objects. In addition, information on individual nucleosynthesis events is provided by the rapid progress in the measurements on presolar grains, which provide accurate isotope ratios of important elements (Zinner, 1998; Clayton and Nittler, 2004; Nittler, 2009).

A. Stellar abundances

Useful information on chemical *s*-process yields by individual objects is obtained by observations of stars and planetary nebulae. Stellar abundances are derived from high-resolution spectra of the ultraviolet, optical, and infrared ranges. In general, only elemental abundances can be determined in analyses of stellar spectral lines and the measurable elements are limited compared with the analyses of solar system material. However, observations for appropriately selected targets (e.g., AGB stars) enable one to directly investigate the products of individual processes, and to identify the respective astrophysical sites. Moreover, measurements of isotope abundance ratios have been made for a few exceptional elements from detailed analyses of spectral line profiles (see Sec. IV.C).

Measurable elements are dependent on objects. Stellar abundances are usually derived from the absorption features formed at the surface of stars in the so-called photosphere. In cool stars, neutral species of alkali metals (e.g., Na, K, and Rb) and singly ionized species of alkaline earth metals (e.g., Mg and Ca) show strong resonance doublet lines. Singly ionized Sr and Ba atoms, which belong to elements of the *s*-process abundance peaks at neutron-magic numbers 50 and 82, exhibit strong absorption features in the optical range, which makes it possible to determine their abundances even in very metal-poor stars. Molecular absorption dominates in very cool stars. In such cases, molecular bands, e.g., for ZrO, can be used to estimate the elemental and isotopic abundances of heavy neutron-capture elements.

The abundances of noble gases (e.g., Ne and Ar) are difficult to determine in cool stars as well as in the Sun because of the lack of useful spectral lines. Such elements are observable from emission lines in planetary nebulae, where these elements are ionized and excited by the ultraviolet photons from the hot central star. Hence, observations of planetary nebulae provide complementary information to the chemical yields obtained from stellar observations.

Considerable progress has been achieved in the past few decades in stellar spectroscopy related to the *s* process. They are promoted by high-resolution spectrographs mounted on large telescopes, the application of a spectrum synthesis technique to the high-resolution spectra of cool stars, and surveys of metal-poor stars that provide useful samples of binary stars (see Sec. IV.A.2).

The main targets of *s*-process observations are (i) AGB stars, post-AGB stars, and planetary nebulae evolving to white dwarfs, and (ii) binary companions accreting the products of primary AGB stars. AGB stars are objects where the *s* process

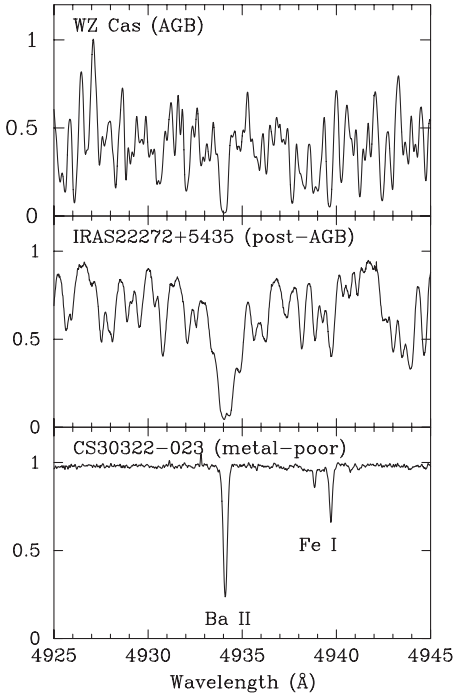

FIG. 16. Comparison of spectra around the Ba II 4934 Å line for AGB, post-AGB, and CEMP stars. Spectral data were obtained with the high dispersion spectrograph of the Subaru telescope with a resolving power of 60 000 or higher. The spectrum of the metal-poor star is normalized to the continuum level (bottom panel). The atomic absorption lines are clearly seen in the spectrum and are useful for abundance analyses. In contrast, molecular absorption (mostly of C_2) is dominant in the AGB star (top panel), and the continuum level is very uncertain. Molecular absorption of the post-AGB star is not as severe as in the AGB star, depending on stellar temperature.

currently takes place (or recently took place), giving direct information on the *s*-process nucleosynthesis in such stars. However, the surface of AGB stars is very cool and the spectra are crowded by numerous molecular lines (see Fig. 16). Accordingly, abundance analyses from such spectra are difficult and the number of measurable elements is limited.

In binary systems with appropriate separation, on the other hand, material from the surface of the primary star starts to accrete onto the secondary companion when the primary evolves to an AGB star. Such mass transfer across a binary system is expected by stellar winds from the AGB primary or by forming a common envelope when the separation is sufficiently small. The secondary is usually an unevolved main-sequence star with a much longer time scale of stellar evolution compared to the AGB primary. After the primary evolves to a faint white dwarf, only the companion, which preserves the material provided by the AGB primary, is observable. In such cases, the *s*-process yields are easily measurable at the surface of the secondary, because the object is still relatively warm and molecular absorption is not severe (see Fig. 16).

1. AGB, post-AGB, and planetary nebulae

As described in Sec. III, heavy *s*-process elements are enriched on the surface of AGB stars as the result of repeated TPs and TDU episodes. In such objects, the initial CNO abundances at the surface are significantly changed. In particular, carbon is enhanced and might become comparable or more abundant than oxygen. These stars are classified as spectroscopic types S or N. In massive AGB stars, which are affected by the hot bottom burning (HBB) process (Herwig, 2005, and references therein), the surface composition changes toward the equilibrium values of the CNO cycle with a reduced C/O ratio. Some *s*-process elements might also be enriched in such stars.

The surface of AGB stars is cool (~ 3000 K) and the optical and near-infrared spectra are dominated by molecular absorption lines, e.g., from CO, TiO, and C_2, depending on chemical composition and temperature. While the abundances of C, N, O, and some other elements can be determined via molecular lines [see, e.g., Lambert *et al.* (1986)], analyses of atomic spectra are difficult. However, recent analyses based on the spectrum synthesis technique provided important results on the surface abundances of heavy elements in cool AGB stars (see Sec. IV.D). Molecular absorption features such as ZrO are also useful to determine abundances of neutron-capture elements and their isotope ratios (Peery and Beebe, 1970; Zook, 1985; Lambert *et al.*, 1995).

Excesses of heavy *s*-process elements are also found in post-AGB stars, which are quickly losing their residual envelopes while evolving from AGB stars to planetary nebulae. The surface of such objects becomes warmer and molecular absorption becomes weaker as this transition proceeds, but the atmospheric structure is unstable and quite complicated compared to that of supergiants, making spectral analyses difficult (see Fig. 16). The duration of this evolutionary stage is very short, indicating that one must observe apparently faint objects to increase the sample, even though the luminosity of such objects is high. Useful results have been obtained by recent observations with large telescopes and detailed analyses of high-resolution spectra.

Planetary nebulae are formed by the material ejected from evolved low- and intermediate-mass stars and ionized by the central star that is evolving to a hot white dwarf. Hence, the spectra of nebulae provide direct information on the yields that these stars contribute to the chemical enrichment of the Galaxy. The light elements (e.g., C and O) in planetary nebulae are accessible by x-ray observations [see, e.g., Murashima *et al.* (2006)], while neutron-capture elements can be studied by optical spectroscopy (see Sec. IV.D).

2. Binary systems affected by mass transfer

Detailed information on the abundance patterns of heavy elements produced by AGB stars can be obtained by analyses of a binary companion that is affected by mass accretion from the primary AGB star. In these cases, the target objects are main-sequence or red giant stars, but they are distinguished from normal stars by excesses of carbon and heavy *s*-process elements such as Ba.

Such stars with high metallicity similar to the Sun are known as Ba stars (Bidelman and Keenan, 1951). Since the CNO abundances and, in particular, the oxygen abundance in stars with solar metallicity are already high, mass accretion from carbon-enriched AGB stars does not significantly change the molecular features of their spectra. Instead, strong

absorption features of Ba can be a signature for the stellar classification. Periodic variations of the radial velocity have been found for many Ba stars, supporting the scenario that these stars experienced accretion of *s*-process enhanced material from a primary AGB star in a binary system (McClure, 1984; McClure and Woodsworth, 1990).

Mass accretion from AGB stars has stronger impacts on the spectra of metal-poor stars. Such objects are classified into CH stars (Keenan, 1942) or subgiant CH stars (Bond, 1974). Excesses of heavy elements have also been detected in such objects, and the binarity has been confirmed by radial velocity monitoring (McClure, 1984; McClure and Woodsworth, 1990; Preston and Sneden, 2001). Recent surveys of metal-poor stars based on the weakness of calcium absorption lines have detected a number of carbon-enhanced objects, e.g., the HK survey (Beers *et al.*, 1992; 2007), the Hamburg/ESO Survey (Christlieb, 2003), the Sloan Digital Sky Survey (SDSS) (York *et al.*, 2000), including the subprogram SEGUE (Sloan Extension for Galactic Understanding and Exploration), and the SEGUE Stellar Parameter Pipeline (SSPP) (Lee *et al.*, 2008a; 2008b). Follow-up high-resolution spectroscopy has been made by the ESO Large Programme First Stars with VLT/UVES [see, e.g., Sivarani *et al.* (2006)], the Chemical Abundances of Stars in the Halo (CASH) Project (Roederer *et al.*, 2008), and others [see, e.g., Aoki *et al.* (2007)]. Enhancements of heavy elements are found for most of these stars, indicating that their peculiar abundances originate from AGB nucleosynthesis and mass transfer in binary systems, as in the case of CH stars. The sample of such objects contains stars with a variety of metallicities, and enables one to investigate the metallicity dependence of the *s* process.

B. Abundance patterns of heavy elements

1. Overall abundance patterns covering three magic neutron numbers

Measurements of abundance patterns of heavy elements in AGB stars or objects affected by AGB nucleosynthesis and comparisons with model predictions are important for understanding the *s*-process mechanisms. The *s*-process abundance pattern exhibits three peaks at ^{88}Sr, ^{138}Ba, and ^{208}Pb, corresponding to the magic neutron numbers 50, 82, and 126, respectively. The singly ionized Sr and Ba have strong resonance lines in the optical range, making such elements detectable even in spectra of very metal-poor stars. There are also many useful lines in the near UV and blue spectral range for the determination of, e.g., Y, Zr, La, Nd, and Eu abundances. For this reason, measurements of light (ls, comprising Sr, Y, and Zr) and heavy (hs, with Ba, La, etc.) neutron-capture elements have been performed for many CH and Ba stars in order to estimate the neutron exposure from the ls/hs ratios.

Abundance studies of cool AGB stars are difficult due to the dominant molecular absorption features. Important progress has been, however, obtained by recent work. Abia *et al.* (2002) determined chemical abundances of N-type AGB stars. By means of the spectrum synthesis technique abundances of neutron-capture elements were determined for a large sample of AGB stars with excesses of such elements. The abundance ratios could be explained by *s*-process nucleosynthesis in AGB stars with $M \leq 3M_{\odot}$. However, the large scatter in the abundance ratios (e.g., [hs/ls]) suggests that the efficiency of the *s* process is affected by yet uncertain model parameters (see Figs. 12 and 13).

The *s*-process products of AGB stars are also recorded in Ba stars. Allen and Barbuy (2006) studied neutron-capture elements for 26 Ba stars, separating the contribution of the main *s* process by the progenitor (i.e., the former primary star in the binary system that provided the *s*-enhanced material) from other original components of the observed Ba stars and compared the observational results with the model predictions by Malaney (1987a, 1987b) for single and exponential neutron exposures of the *s* process. Also Smiljanic *et al.* (2007) determined abundances of neutron-capture elements in Ba stars. Excesses of heavy neutron-capture elements and the hs/ls ratios are discussed in their work, while no significant *s*-process effects were found for Cu, Mn, V, and Sc.

Recent important progress is that measurements have been extended to Pb, the stable element at the third abundance peak of the *s* process. The lack of strong spectral features in the optical range makes the abundance measurements of Pb from stellar spectra difficult. The detection of Pb was reported for the post-AGB star FG Sge by Gonzalez *et al.* (1998). Measurements of Pb abundances have been made by Aoki *et al.* (2000), (2001) for CEMP stars, by Van Eck *et al.* (2001) for CH stars, and by Allen and Barbuy (2006) for Ba stars using the absorption line of neutral Pb at 4058 Å. These observations made it possible to investigate the overall *s*-process abundance pattern more consistently. To date abundance studies for Pb have been made for more than 20 carbon-enhanced objects (Aoki, Ryan *et al.*, 2002; Cohen *et al.*, 2003; Lucatello *et al.*, 2003; Van Eck *et al.*, 2003; Sivarani *et al.*, 2004, 2006; Aoki, Beers *et al.*, 2008). Moreover, Ivans *et al.* (2005) reported the detection of Bi as well as Pb for the carbon-enhanced metal-poor star CS 29497-030. Figure 14 shows the abundance pattern of this and another well-studied carbon-enhanced star (see Fig. 17).

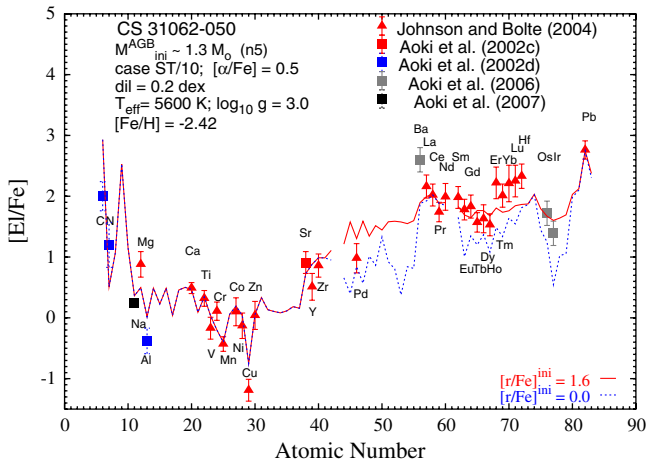

FIG. 17 (color online). The same as in the bottom panel of Fig. 14, but for AGB models with initial mass $M = 1.3M_{\odot}$, case ST/10, and dil = 0.2 dex. This solution is obtained under the hypothesis of a turn-off star before the first dredge-up.

The Pb abundances determined for carbon-enhanced metal-poor stars revealed that the abundance ratios of elements between the second and third abundance peaks (e.g., [Pb/hs]) show large star-to-star scatter (see Fig. 12) as discussed in Sec. III. A similar scatter is also found in the abundance ratios of elements between the first and second abundance peaks. This scatter can be interpreted as due to a dispersion of the hydrogen mixing into the ^{13}C pocket that determines the efficiency of the *s* process in AGB stars [see, e.g., Busso *et al.* (1999)]. The efficiency is expected to depend on the metallicity, which determines the ratio of neutrons to seed nuclei at the *s*-process site. However, Fig. 12 shows no clear correlation between the metallicity or iron abundance and the [Pb/hs] or [hs/ls] abundance ratios. Thus, the reason for the scatter of the abundance ratios is still unclear.

Using the technique described in Sec. III.D and AGB stellar models of disk metallicity, Husti *et al.* (2009) were able to fit the Ba stars in a range of ^{13}C-pocket efficiencies ST $\times 2$ down to ST/3 and initial AGB masses between $1.5M_\odot$ and $3M_\odot$. The results are plotted in Fig. 12 for [hs/ls] and for the somewhat more uncertain [Pb/hs].

2. Detailed abundance patterns: CEMP-*s* and -*s*/*r* stars

In addition to the overall abundance patterns, which are represented by the abundance ratios between the three *s*-process peaks, detailed abundance measurements for CEMP stars with [C/Fe] > 1 provide useful constraints on the origin of the heavy elements and the role of the *s* process.

An illustrative case are the high Eu abundances, relative to Ba and other *s*-process elements, in some CEMP stars, which cannot be explained by standard *s*-process models (Hill *et al.*, 2000; Aoki, Ryan *et al.*, 2002; Cohen *et al.*, 2003). Although the *r* process is the dominant source of Eu in solar system material (Eu is sometimes called an *r*-process element), this element is also produced by the *s* process. Therefore, large enhancements of heavy elements in carbon-enhanced objects can also provide some excess Eu. However, the measured abundance ratios of Eu with respect to Ba, La, and other elements around Eu are significantly higher than in model predictions as well as in the *s*-process component of solar system material. For this reason, the Eu excess suggests a large *r*-process contribution in addition to the *s*-process component, and such stars are sometimes called CEMP-*s*/*r* stars (Beers and Christlieb, 2005). As discussed in Sec. III.D, a preliminary comparison of CEMP-*s* with the theoretical models by Bisterzo *et al.* (2006) has provided reasonable interpretations for all CEMP-*s* and CEMP-*s*/*r* stars published so far as shown for the *s*-process indexes [hs/ls] and [Pb/hs] in Fig. 12. A full analysis with updated AGB models is underway (Bisterzo *et al.*, 2010).

Examples of the detailed elemental abundance patterns of two CEMP-*s*/*r* stars have been shown in Fig. 14, where the top panel shows the situation for the blue metal-poor star CS 29497-030 with [Fe/H] $= -2.57$ (Ivans *et al.*, 2005). A large number of elements have been detected in that star besides the usual ls and hs elements and Pb, including Nb, Bi, some of the heaviest rare-earth elements, and a few useful upper limits. The abundance ratios with respect to Fe are normalized to the solar values, and compared to an AGB model of the same metallicity, for an inferred initial mass of $1.3M_\odot$, and a rather small ^{13}C pocket (case ST/9). Note that no dilution is required to fit this CEMP-*s* star, suggesting that the material from the AGB companion dominates at the surface of this object. The very low ratio [hs/Eu] ~ 0 indicates that the original composition of the binary system had a large *r*-process enhancement of [Eu/Fe] ~ 2 dex, even higher than the known *r*-II stars.[3]

CS 31062-050 is a subgiant CH star with a large enhancement in *s*- and *r*-process elements. Lines of interesting elements such as Os and Ir (Aoki *et al.*, 2006a) and Na (Aoki *et al.*, 2007) have been detected due to its relatively cool temperature and low gravity ($T_{\rm eff} = 5600 \pm 150$ K and $\log_{10} g = 3.0 \pm 0.3$). This star has probably undergone the first dredge-up episode, where the convective envelope extends over about 80% of the stellar mass. This implies that the *s*-process-rich material accreted from the AGB star by stellar winds needs to be diluted by a large extent with the original material of the observed star. In the bottom panel of Fig. 14 the observed abundances are compared with AGB yields from models of $1.5M_\odot$ (case ST/2.7) and dil $= 1.0$ dex, which corresponds to ten parts of original material mixed with one part of accreted material from the AGB star. This star appears to be particularly highly enhanced in both *s*- and *r*-process elements. [Eu/Fe] observed is about 1 dex higher than expected for a pure *s*-process AGB prediction (dashed line), indicating an important initial *r*-process contribution corresponding to $[r/{\rm Fe}]^{\rm ini} = 1.6$. Ba is possibly overestimated with respect to the other heavy-*s* elements (Aoki *et al.*, 2006a).

Detailed abundance ratios provide other constraints on AGB models. For instance, the observation of Zr and Nb permits the immediate confirmation of the extrinsic AGB nature of CS 29497-030. In AGB stars Nb is produced by the radiogenic decay of the long-lived ^{93}Zr ($\tau_{1/2} = 1.5 \times 10^6$ yr), which will mostly decay later in the interstellar medium to ^{93}Nb. In the envelope of an intrinsic AGB one would expect [Zr/Nb] $= 1$, but in an extrinsic (mass receiving) star such as CS 29497-030 all ^{93}Zr should have already decayed to ^{93}Nb, and thus one expects [Zr/Nb] $= 0$. This ratio is potentially a powerful tool for determining the state of *s*-process enhanced stars, but, unfortunately, Nb has only a single, easily observable transition. The Nb II 3215.6 Å line falls in the crowded near-UV spectral region, and no systematic survey of Nb abundances in CEMP-*s* stars has been undertaken so far.

Na in CS 31062-050, for which a single line has been detected Aoki *et al.* (2007), is lower by approximately 1 dex than the model predictions for the $M = 1.5M_\odot$ case (Fig. 14). A lower Na yield is obtained with models of lower mass AGB

[3]Such stars are labeled *r*-II by Christlieb *et al.* (2004), defined as those very metal-poor ([Fe/H] < -2.5) stars with [Eu/Fe] > 1.0 and [Eu/Ba] < 0.0 [e.g., CS 31082-001 by Hill *et al.* (2002), CS 22183-031 by Honda *et al.* (2004), HE 1523-0901 by Frebel *et al.* (2007), and CS 29497-004 by Christlieb *et al.* (2004)]. A few other stars, such as BD + 17 3248 Cowan *et al.* (2002) and CS 30306-132 Honda *et al.* (2004), would formally be classified in this system as *r*-II stars ($+0.3 \leq$ [Eu/Fe] $\leq +1.0$ and [Eu/Ba] < 0.0).

stars and would agree with an AGB model of $M = 1.3M_\odot$ (case ST/10 and $[r/\mathrm{Fe}]^{\mathrm{ini}} = 1.6$, and a negligible dilution of 0.2 dex, Fig. 17). This solution would only be compatible with a subgiant star before the first dredge-up. Note that the exact evaluation of the effective temperature at which the first dredge-up occurs may be affected by the treatment of gravitational settling in binary systems with mass transfer as is the case in CEMP stars. Another possibility is to consider low-mass AGB models at *very* low metallicities. As discussed, low-metallicity AGBs with initial mass $M < 1.5M_\odot$ may undergo a deep first TDU episode (Sec. III C).

C. Branchings

Detailed abundance measurements, in particular, determinations of isotope ratios, are useful for the analysis of the branching points of the *s* process to derive observational constraints on the temperature and neutron density of the *s*-process sites as illustrated in the following examples.

1. ^{85}Kr branch

The ground state of the unstable isotope ^{85}Kr has a half-life of 10.7 yr. At low neutron density, e.g., $n_n < 10^7$ cm^{-3}, the β decay of ^{85}Kr dominates over the neutron-capture rate and the *s*-process path runs from ^{84}Kr to ^{85}Rb to ^{86}Sr. At high neutron density the neutron-capture chain runs from ^{84}Kr to ^{86}Kr and on to ^{87}Rb [see Käppeler *et al.* (1989)]. These main paths are somewhat affected by the minor branching at ^{86}Rb as well. As a result, a high Rb abundance ratio with respect to Sr, Y, or Zr signifies an *s* process at high neutron density ($> 10^8$ cm^{-3}), because of the small neutron-capture cross section of the neutron-magic isotope ^{87}Rb. In thermally pulsing AGB stars low neutron densities are expected during the interpulse phase, where the neutron source is the ^{13}C$(\alpha, n)^{16}$O reaction, while high neutron densities are obtained during the He shell flashes, when the ^{22}Ne$(\alpha, n)^{25}$Mg reaction is activated at the higher temperatures at the bottom of the reaction zone.

In very cool stars Rb abundances are measurable via resonance lines of neutral Rb at 7800 and 7947 Å. This is not the case for warmer stars because the ionization potential of this element is very low, and ionized species have no measurable lines in the optical and the near-infrared ranges.

Rb abundance ratios were obtained for AGB stars of spectral type M, MS, and S by Lambert *et al.* (1995), who derived values of Rb/Sr ~ 0.05 for *s*-processed material from stellar surface abundances and taking the dilution by envelope material into consideration. The low Rb/Sr ratio is consistent with the predicted low neutron density during the interpulse phase in low-mass AGB stars. They also measured the Zr isotope ratios from ZrO molecular bands and investigated the branching at ^{95}Zr, an isotope with a β-decay half-life of 65 days. No evidence of existence of ^{96}Zr was found, supporting the low neutron density estimated from the Rb abundances. A similar conclusion was obtained for carbon stars by Abia *et al.* (2001), who measured the abundances of Rb and other elements for 21 N-type carbon stars and found that the [Rb/Sr, Y, Zr] abundances are better explained by AGB models for low-mass ($M \lesssim 3M_\odot$) than for intermediate-mass stars, although the determination of Rb is uncertain for carbon stars and some calibration of abundance ratios to a non-*s*-process-enhanced AGB star (the J-type carbon star WZ Cas) was required.

García-Hernández *et al.* (2007) investigated OH/IR stars, oxygen-rich AGB stars that are believed to have high masses [(4–8)$M_\odot$]. They found large enhancements of Rb in these objects over a wide range ($-1.0 < [\mathrm{Rb/Fe}] < 2.6$). Given the only mild excesses of *s* material ($[\mathrm{Zr/Fe}] < 0.5$), the Rb/Zr ratios are significantly higher than in low-mass AGB stars (S-type and carbon stars) investigated in the above studies. Accordingly, the high Rb/Zr ratios were interpreted as evidence for the ^{22}Ne$(\alpha, n)^{25}$Mg reaction during thermal pulses in massive AGB stars.

Measurements of Rb abundances were extended to metal-deficient ($-2.0 < [\mathrm{Fe/H}] < 0.0$) stars in the galactic disk and halo by Tomkin and Lambert (1999). Excluding CH stars, the Y, Zr, and Ba in their sample with $[\mathrm{Fe/H}] < -0.5$ are underabundant, while Rb is overabundant ($[\mathrm{Rb/Fe}] = 0.21$) on average. The high Rb abundance ratios with respect to Y and Zr are at least partially attributable to the larger component of the *r* process in metal-deficient stars than in solar system material. However, an alternative possibility is that the *s*-process neutron density is higher in metal-deficient AGB stars than that in stars with solarlike composition.

Rb abundances in globular cluster stars with $-1.7 < [\mathrm{Fe/H}] < -1.2$ have been studied by Yong *et al.* (2006, 2008). While Rb, as well as other *s*-process elements, is overabundant in M4 (see Sec. IV.E), the [Rb/Fe] ratios in NGC 6752 and M13 are similar to the solar value. The [Rb/Y] and [Rb/Zr] ratios are constant within the uncertainty of the measurement, suggesting that the nature of the *s* process which has contributed to these clusters is similar (although the *s* contribution is significantly larger in M4 than in the other two cases). The discussion might be, however, more complicated if the contribution of the *r* process is fully taken into consideration. Such measurements are also important for the understanding of the abundance variation of light elements (e.g., O, Na, and Mg) found in some globular clusters (Yong *et al.*, 2006).

2. ^{151}Sm branch

The branching at ^{151}Sm is of particular interest because the 93 yr half-life of ^{151}Sm decreases by about a factor of 30 at *s*-process temperatures (Takahashi and Yokoi, 1987). This branch has been studied using the solar system abundance ratios of Gd isotopes [see, e.g., Wisshak *et al.* (1995)]. However, the physical conditions of the *s* process in an individual site (object) are not obtained from the analysis of solar system abundances. Moreover, the Gd isotopes are also affected by contamination of the *p* process.

The effect of the ^{151}Sm branching also appears in the abundance ratio of the two stable europium isotopes ^{151}Eu and ^{153}Eu. Although measurements of isotope ratios from stellar spectra are difficult in general, Eu lines show relatively large hyperfine splitting, which is characteristic of the two isotopes (see Fig. 18). Thus, detailed analyses of Eu absorption line profiles enable one to estimate the Eu isotope ratios (Lawler *et al.*, 2001). Aoki, Honda *et al.* (2003) and Sneden *et al.* (2002) determined the Eu isotope ratios for *r*-process-enhanced, metal-poor stars. The results agree well

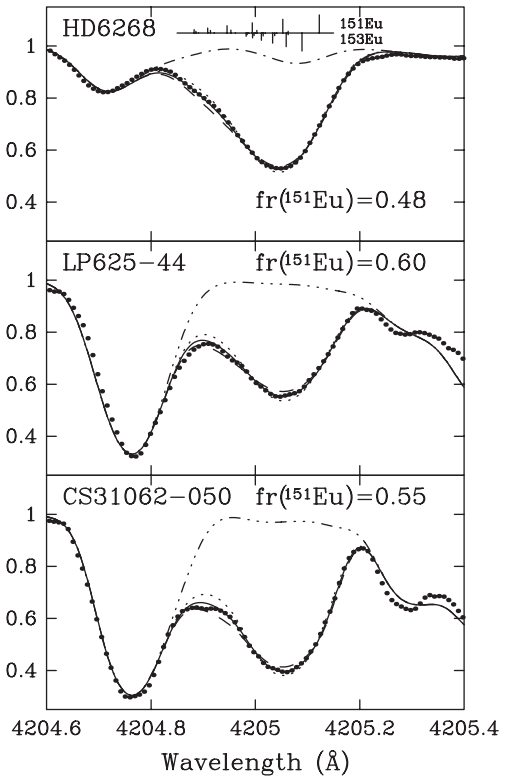

FIG. 18. Measurements of Eu isotope ratios from the Eu II absorption line profile for an *r*-process-enhanced star (top panel) and CEMP-*s* and CEMP-*s*/*r* stars. Adapted from Aoki, Ryan *et al.* (2003).

with the Eu isotope ratio of the *r*-process component of solar system material (with a 48% fraction of ^{151}Eu), confirming the usefulness of the line profile analysis.

Aoki, Ryan *et al.* (2003) applied such an analysis to two CEMP stars that show large excesses of *s*-process elements. The fractions of ^{151}Eu derived are 55% and 60%, slightly higher than was found for *r*-process-enhanced stars. These results are consistent with the predictions of *s*-process models for wide ranges of neutron density and temperature, given the uncertainties of the measurements (3%). However, the high neutron density case might be preferable for explaining the results if recent measurements of the ^{151}Sm neutron-capture cross section are adopted (Marrone *et al.*, 2006a; Wisshak *et al.*, 2006c). Further detailed analyses for a larger sample will give stronger constraints on neutron density and temperature at *s*-process sites of low metallicity.

D. Stellar evolution

Observations of characteristic *s*-process elements are important for probing the evolution of AGB stars (see Sec. III C). Tc has no stable isotope, and the first isotope was artificially produced in 1937. While ^{98}Tc has the longest half-life ($t_{1/2} = 4 \times 10^6$ yr), ^{99}Tc ($t_{1/2} = 2 \times 10^5$ yr) is expected to be the most abundant isotope produced by the *s* process in AGB stars. The discovery of Tc in the spectrum of an AGB star of spectral type S by Merrill (1952) provided firm evidence for the synthesis of heavy elements in such evolved stars and for stellar nucleosynthesis in general.

Abundance studies for Tc in AGB stars have been made by Little *et al.* (1987) and Smith and Lambert (1988), for example. Recently, Vanture *et al.* (2007) compiled the observational results for S stars and investigated the correlation of the spectral features between Tc and Li, because a strong Li line indicates the contribution of HBB in massive AGB stars. Tc line absorption is detected in 28 stars of their sample, and nine of these stars also show a strong Li line. Tc is expected to be observed in low-mass AGB stars, which are actively producing the *s* abundances. The simultaneous detection of Tc and Li suggests the existence of a concomitant production mechanism for Li, although HBB is not expected in AGB stars.

García-Hernández *et al.* (2007) studied Zr as well as Li in galactic OH/IR stars, which are oxygen-rich AGB stars with relatively high masses (3–4$M_\odot$). These stars are expected to show HBB, the CNO cycle at the bottom of a hydrogen-rich envelope that makes the C/O ratio lower than unity and produces high Li abundances. Although the effect of HBB is confirmed by the Li overabundances in one-half of their sample, no excess Zr was found in these cases. This led to the conclusion that the high mass AGB stars in our Galaxy do not show any significant *s*-process enrichments, in contrast to the results derived for AGB stars in the Magellanic clouds, which are lower in metallicity by a factor of 2 or 3 than galactic objects. Plez *et al.* (1993) and Smith *et al.* (1995) found effects of HBB for luminous (massive) AGB stars in the Magellanic clouds that show *s*-process enhancement as well. These observations confirmed that the *s* process in massive AGB stars depends strongly on metallicity.

The heavy neutron-capture elements in planetary nebulae have recently been studied by optical and near-infrared spectroscopy. Sharpee *et al.* (2007) measured weak emission lines in the optical range for five planetary nebulae. These observations included neutron-capture elements, for which the required atomic data for a reliable abundance determination became available recently. The discovered excesses of Kr and Xe in three objects can be assigned to the first and second *s*-process abundance peaks, although a large correction for the *r*-process contribution is required for Xe. These two elements are enhanced by a similar factor in three planetary nebulae ([Xe/Kr] $\sim$ 0), suggesting the effect of an *s* process with a significant neutron exposure.

Sterling and Dinerstein (2008) measured abundances of the light neutron-capture elements Kr and Se for a large number of planetary nebulae (81 objects for Kr and 120 for Se). The abundances were determined from emission features in near infrared (2.2 μm) and showed that 44% of the sample, which corresponds to 20% of all planetary nebulae in the Galaxy, are *s* process enriched ([Kr, Se/Ar] $>$ 0.3).

E. Contribution to the Galactic chemical evolution

The stars in the substructures of the Milky Way, the thin and thick disks, the bulge, and the halo, differ with respect to metallicity and kinematical properties, i.e., their orbital motion around the Galactic center. The formation time scale of the Galactic structure is usually estimated by the abundance ratios between the α elements, e.g., Mg, and iron (McWilliam, 1997).

The thin disk is the relatively new component of the Galaxy, and the Sun is involved in this structure. The metallicity is similar to the solar one, while the ages of stars range between 0 and 10×10^9 yr. The thick disk consists of old stars of lower metallicity. The formation of this component is still debated, a possible scenario being the burstlike star formation when a small galaxy merged with the Milky Way at some early epoch of the Galactic history [see, e.g., Freeman and Bland-Hawthorn (2002)].

The bulge consists mostly of old stars with a broad metallicity distribution, including stars of solar metallicity. It has been suggested that the bulge was formed at very early times of the Universe and its evolution during Galactic history has been discussed. To date, abundance measurements of neutron-capture elements for the bulge are still quite limited because of its long distance and severe interstellar extinction. Therefore, future studies with larger telescopes are required.

The halo structure consists of old, metal-deficient stars and extends to distances of 100 kpc around the disks. The formation time scale is estimated to be 1 or at most a few billion years after the big bang. About 150 globular clusters have been found in the Galaxy, which also belong to the old population of the Galaxy and are believed to be related to the formation of the halo and bulge structures.

There are tens of satellite dwarf galaxies around the Milky Way, which probably formed and evolved by interactions with the Galaxy. Spectroscopy for individual stars in such dwarf galaxies has revealed significant *s*-process contributions in some cases, providing observational constraints on the *s* process at different metallicities and their roles in chemical enrichment (Tolstoy *et al.*, 2009).

1. *s*-process contributions to Galactic field stars

Because the lifetimes of low- to intermediate-mass stars, the progenitors of AGB stars that are responsible for the main component of the *s* process, are longer than for massive stars [$M \gtrsim (8\text{–}10)M_\odot$], it is not expected that the main *s* process deriving from AGB stars of all masses and metallicities contributed to the chemical evolution of the early Galaxy for $[\mathrm{Fe/H}] < -1.5$ (Travaglio *et al.*, 2004).

As for the weak *s* process, which is to be ascribed to the presupernova evolution of massive stars, we point out that, besides the present MACS uncertainties in the region below $A = 90$ (see Sec. III B), neutron capture in massive stars is driven by the $^{22}\mathrm{Ne}(\alpha, n)^{25}\mathrm{Mg}$ reaction, where ^{22}Ne acts as a secondarylike source. In fact ^{22}Ne comes from the original CNO abundances, which are transmuted into ^{14}N during H burning and then converted to ^{22}Ne by the chain $^{14}\mathrm{N}(\alpha, \gamma)^{18}\mathrm{F}(\beta^+\nu)^{18}\mathrm{O}(\alpha, \gamma)^{22}\mathrm{Ne}$ in the early phase of core He burning [Raiteri *et al.* (1993), and references therein]. Consequently, the weak *s* process is not expected to play any role in galactic halo stars. The weak *s* process is also believed to occur in massive stars (see Sec. III C). However, the process requires high metallicities and is, therefore, effective only in young, metal-rich stars. Although the abundance patterns produced by the weak *s* process are not clearly found in stellar atmospheres, some constraints have been obtained from Cu, Zn, Ga, and Ge abundances in galactic stars (Pignatari *et al.*, 2010).

With respect to Zn, the most abundant isotope ^{64}Zn (48.6% of solar Zn) derives from SNe of type II in the α-rich freeze-out of neutrino winds (Woosley and Hoffman, 1992) or in hypernovae (Umeda and Nomoto, 2002), while the other 50% of solar Zn are almost fully ascribable to the weak *s* process (Bisterzo *et al.*, 2004). Assuming that SN II produce about 1/3 of solar Fe, this means that the ratio [Zn/Fe] in the halo should be a bit positive, about 0.2 dex on average, consistent with spectroscopic observations [see, e.g., Cayrel *et al.* (2004)].

Concerning Cu, the weak *s* process accounts for 90% and the main *s* component for 5% of the solar abundance, whereas SN Ia are not predicted to contribute any Cu (Thielemann *et al.*, 1986). This implies that [Cu/Fe] in the halo should be constant and strongly negative, around −0.8 dex. The origin of this small primary Cu contribution may be ascribable to the explosive nucleosynthesis in massive stars. These expectations have been confirmed by the theoretical expectations of Woosley and Weaver (1995) for a range of massive stars with metallicities from 0 to solar. A large number of spectroscopic observations of [Cu/Fe] vs [Fe/H] exist in the literature, again confirming the above expectations [see, e.g., Bisterzo *et al.* (2004), Pignatari *et al.* (2010), and Romano and Matteucci (2007)].

The nucleosynthetic origin of primary Zn and Cu is still a subject of debate. This may imply different processes, e.g., the so-called νp process (Fröhlich *et al.*, 2006). Other light elements beyond the Fe group, such as Ga and Ge, should behave like Cu, that is with a major weak and secondarylike *s*-process contribution (Pignatari *et al.*, 2010). For the few spectroscopic observations available in halo stars, see Cowan *et al.* (2005).

Although the astrophysical sites of the *r* process are not well identified, massive stars that terminate their lives by core-collapse supernovae would be promising candidates for the progenitor. Because of the short lifetimes of massive stars it appears plausible that the *r* process contributed significantly to the enrichment of the early Galaxy. Apart from the *r* process and weak *s* process, recent studies on light neutron-capture elements suggest a LEPP as an additional source of these elements in the very early Galaxy (Truran *et al.*, 2002; Travaglio *et al.*, 2004; Aoki *et al.*, 2005) as discussed in Sec. III.

The abundances of Ba (or La) and Eu are used as indicators of the *s*- and *r*-process contributions to the origin of the heavy elements. Analyses of the abundances in the Solar System showed that about 80% of Ba (Travaglio *et al.*, 1999; Serminato *et al.*, 2009) and 70% of La (Winckler *et al.*, 2006) originate from the *s* process, while about 95% of Eu comes from the *r* process (Käppeler *et al.*, 1989; Arlandini *et al.*, 1999).

Heavy neutron-capture elements of metal-poor stars in the halo have recently been studied with high-resolution spectroscopy (McWilliam *et al.*, 1995; Ryan *et al.*, 1996; Burris *et al.*, 2000; Honda *et al.*, 2004; Simmerer *et al.*, 2004; Aoki *et al.*, 2005; François *et al.*, 2007; Sneden *et al.*, 2008). On the other hand, the chemical composition of a large sample of disk stars has been studied in the past two decades [see, e.g., Edvardsson *et al.* (1993)]. Recently, Reddy *et al.* (2003, 2006) determined abundances of many elements including Y,

Ba, and Eu for 181 thin disk stars and 95 thick disk stars based on high quality spectra.

The elemental abundance ratios for Ba and Eu, as a function of metallicity, are shown in Fig. 19, which includes also examples for theoretical GCE expectations. The distributions were obtained by considering the *s* and *r* components separately. The Galactic abundances of these elements were computed from the sum of both processes by comparing model results (Travaglio *et al.*, 2004; Serminato *et al.*, 2009) with the available spectroscopic observations of field stars at different metallicities. For the *s* component of each isotope at the epoch of the formation of the Solar System, only the contributions of AGB stars are considered. Subsequently, the *r*-process residual method ($r = 1 - s$) was used to determine the respective solar system *r*-process fractions, assuming that the production of *r* nuclei is a primary process occurring in type II supernovae, independent of metallicity. Given the present theoretical uncertainties of the *r*-process modeling, the *r*-process residual method is to be considered as an approximation of the fractional *r* abundances in solar system material. It does not exclude, however, that some spread in the *r*-process ratios, e.g., $[Ba/La]_r$, $[Ba/Eu]_r$, $[Eu/Pb]_r$, and $[Eu/Th]_r$, may exist in low-metallicity stars, indicating a multiplicity of *r*-process components. Significant examples concerning $[Eu/Th]_r$ are already reported from spectroscopic observations (Plez *et al.*, 2004; Roederer *et al.*, 2009). Concerning the ratio $[Ba/Eu]_r$, a certain spread is apparent in Fig. 19, but a more detailed analysis of the spectroscopic data and the related uncertainties reported by different authors might be necessary. From a theoretical point of view, a range of *r*-process predictions has recently been advanced by Kratz *et al.* (2007) and Farouqi *et al.* (2010).

The top and middle panels of Fig. 19 refer to the typical *s*- and *r*-process elements [Ba/Fe] and [Eu/Fe], whereas the bottom panel shows their ratio [Ba/Eu]. Theoretical GCE expectations using only the *s*-process products from AGB stars in the galactic halo as well as in the thick and thin disks are separately indicated by dashed lines. Theoretical predictions of the total ($s + r$) yields are shown as solid lines. We recall that the elemental composition of the *r* process has been obtained via the *r*-residual method described before. Below $[Fe/H] < -1.5$ the *r* process dominates the theoretical expectations. According to our prescriptions the *r* process is to be considered of primary origin, i.e., to originate from reactions starting from H and He. However, as discussed by Travaglio *et al.* (2004), calculations of the GCE trend versus metallicity have been made assuming that only a small range of massive stars, with initial masses of $(8–10)M_\odot$ are involved in the *r*-process production. This implies that [Ba/Fe] as well as [Eu/Fe] decrease below $[Fe/H] < -2.3$, but other choices also may be invoked to explain the general decrease of spectroscopic observations. As to the large observed spread of [Ba, Eu/Fe], an easy explanation could be that at those metallicities the interstellar medium in the halo was not fully homogenized (Ishimaru and Wanajo, 1999; Raiteri *et al.*, 1999; Travaglio, Galli *et al.*, 2001; Ishimaru *et al.*, 2004). Notice that the observed ratio [Ba/Eu] stays almost flat (bottom panel of Fig. 19). In conclusion, the [Eu/Fe] shown in Fig. 19 is basically explained by the *r* process. In the metal-rich range, a decreasing trend of [Eu/Fe] with increasing metallicity is found as in the case of $[\alpha/Fe]$ [see, e.g., McWilliam (1997)]. Actually, the decreasing trend of [Eu/Fe] in the disk versus higher metallicities is not due to a decreasing efficiency of the *r* process, but to an increasing apport of Fe in the interstellar medium from the long-lived SNe of type Ia. By contrast, the model curves for [Ba/Fe] (top panel of Fig. 19) indicate that the main *s* process is the dominant contributor to Ba in the metal-rich range ($[Fe/H] > -1$). Indeed, there is no decreasing trend of [Ba/Fe] with increasing metallicity. The models also indicate that the Ba in metal-poor stars is provided by the *r* process as in the case of Eu.

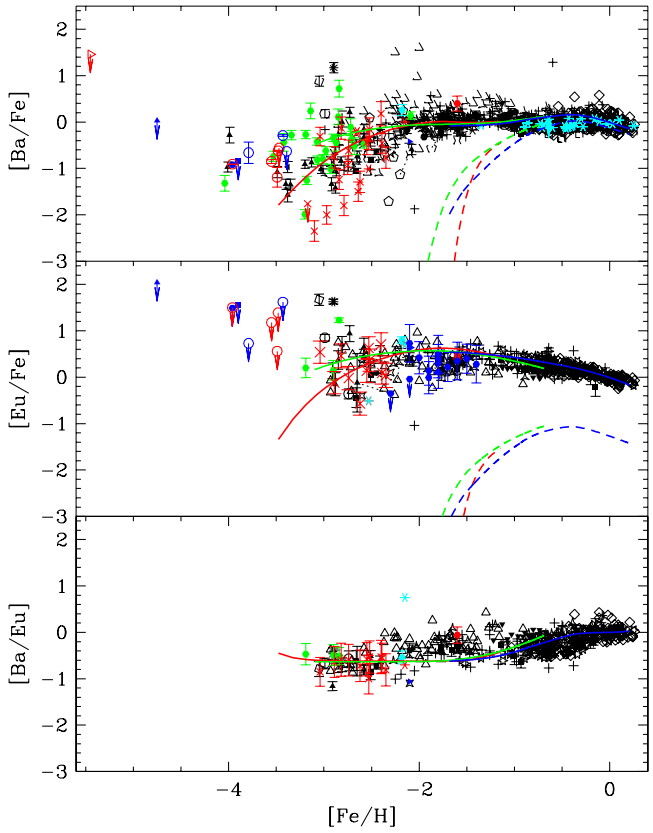

FIG. 19 (color online). Top panel: The evolution of the *s*-process fractions of [Ba/Fe] vs [Fe/H] in the galactic halo as well as in the thick and thin disk (dashed lines) and theoretical predictions of the total s/r abundances (solid lines) from Travaglio *et al.* (2004) and Serminato *et al.* (2009). The spectroscopic data from observations of galactic disk and halo stars are collected from the literature (Edvardsson *et al.*, 1993; Gratton and Sneden, 1994; McWilliam *et al.*, 1995; McWilliam, 1998; Jehin *et al.*, 1999; Tomkin and Lambert, 1999; Burris *et al.*, 2000; Fulbright, 2000; Mashonkina and Gehren, 2001; Mishenina and Kovtyukh, 2001; Norris *et al.*, 2001; Cowan *et al.*, 2002; Van Eck *et al.*, 2003; Aoki *et al.*, 2005; Yushchenko *et al.*, 2005; Aoki *et al.*, 2006b; Ivans *et al.*, 2006; Mashonkina and Zhao, 2006; Cohen *et al.*, 2007; François *et al.*, 2007; Frebel *et al.*, 2007; Norris *et al.*, 2007; Aoki and Honda, 2008; Aoki *et al.*, 2008; Cohen *et al.*, 2008; Lai *et al.*, 2008; Mashonkina *et al.*, 2008; Roederer, Lawler *et al.*, 2008). Error bars are plotted only when reported for individual objects by the authors. The dotted line connects a star observed by different authors. Analogous plots are shown for [Eu/Fe] (middle panel) and [Ba/Eu] (bottom panel).

[La/Eu] is another indicator for the relative contributions of the two processes. Simmerer *et al.* (2004) suggested a correlation with kinematical properties, because it was found that stars with high [La/Eu] show low velocities with respect to the galactic plane. Therefore, these stars possibly indicate the existence of a substructure in the halo to which the *s* process has contributed. In view of the long time scale of the *s*-process effects, such a substructure has an impact on the formation history of the halo.

On average, stars in the thick disk have lower metallicity than thin disk stars. Low-metallicity thick disk stars have 0.3–0.5 dex higher [Eu/Fe] than the solar value, while [Ba/Fe] is slightly lower. The overabundance of Eu implies that the formation time scale of the thick disk is shorter than that of type Ia supernovae (approximately a few billion years), which is also supported by the abundance ratios between α elements and iron. The [Ba/Eu] ratios of -0.5 to -0.7 agree with the *r*-process composition, indicating that the dominant source of heavy neutron-capture elements in thick disk stars is indeed the *r* process. The absence or minor contribution of the *s* process supports the rapid formation of the thick disk. However, there are several thick disk stars with higher metallicity than thin disk stars which have similar [Ba/Fe] to solar. Their existence indicates that star formation continued longer in the thick disk, although the fraction of such stars is quite small.

Figure 20 shows the light and heavy *s*-process elements [Y/Fe] and [Pb/Fe] as a function of metallicity. Pb, which is formally produced by the *s* process in low-metallicity AGB stars (see Sec. III.E), represents a good *s*-process indicator. Travaglio *et al.* (2001) provided model predictions of Pb enrichments in the Galaxy compared to observations in several metal-poor stars, but the observational constraint was rather weak due to the small sample size. Recently, Pb abundances of 12 giants in the halo were determined by

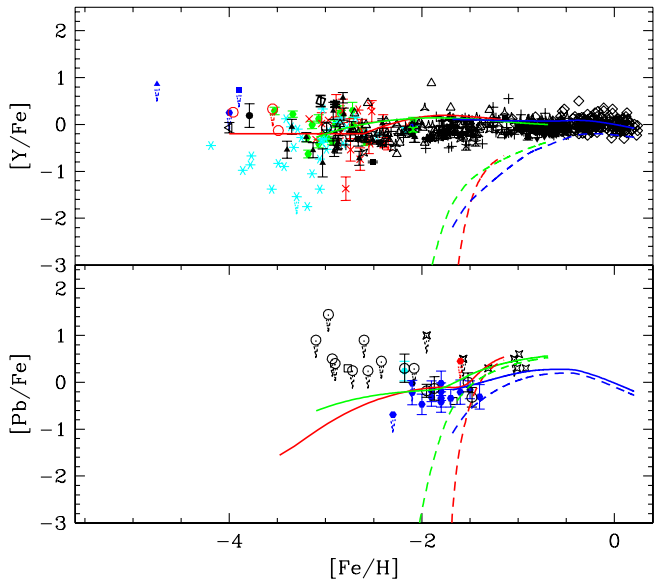

FIG. 20 (color online). Same as Fig. 19, but for [Y/Fe] (top panel) and [Pb/Fe] (bottom panel). The observational data of Y are from the references given in Fig. 19. The Pb data are from Sneden *et al.* (1998), Travaglio *et al.* (2001), Ivans *et al.* (2006), Aoki and Honda (2008), Roederer, Lawler *et al.* (2008), and Roederer *et al.* (2009).

Aoki *et al.* (2008). The [Pb/Fe] and [Pb/Eu] ratios of these stars are constant within the observational uncertainties, and the [Pb/Eu] values agree with the inferred *r*-process component in the Solar System, clearly indicating that there is no significant *s*-process contribution in these stars [see also Roederer *et al.* (2009) for the latest compilation]. However, the sample for [Fe/H] > -1.5, where the *s* process is expected to become significant, is still scarce. Further measurements of Pb abundances for halo stars, particularly in those stars with high [La/Eu], will be useful for understanding the formation time scale of the halo.

The situation is more complicated in the enrichment of the light neutron-capture elements. Figure 20 (top panel) shows [Y/Fe] as an example. As discussed in Sec. III.E, the galactic chemical enrichment of Y by the apport of all previous generations of AGB stars at the epoch of the solar system formation explains only 67% of the solar Y abundance (Travaglio *et al.*, 2004; Serminato *et al.*, 2009). According to that discussion, the solid line in the plot includes contributions of 67%, 5%–10%, about 8%, and 15%–20% from the main and weak *s* process, from the *r* process, and from the LEPP, respectively. The flat theoretical GCE prediction of [Y/Fe] $= -0.2$ dex in the halo is based upon the assumption that the primary LEPP component is obtained in all massive stars, which are exploding as SN II. We recall instead that the primary *r* process was assumed to derive from a small range of massive stars, between $8M_\odot$ and $10M_\odot$ (see discussion for the [Eu/Fe] trend and Fig. 19). The [Y/Fe] in extremely metal-poor stars ([Fe/H] < -3) shows very large scatter, indicating a diversity of the relative contributions by the LEPP and the *r* process, as well as incomplete mixing in the gas cloud from which these stars have formed.

The Y abundances of thick disk stars are similar to the stars in the thin disk. However, the origin of Y would be significantly different, given the different [Y/Eu] ratios of the two structures. The dominant source of this element in thin disk stars, as in the Solar System, is the (main) *s* process (Travaglio *et al.*, 2004). On the other hand, the *r* process and the LEPP should be significant sources of Y in thick disk stars. The thick disk is currently assumed to have suffered a rapid evolution and a high star formation rate, such that contributions from SN Ia or from the main *s* process by AGB stars should be absent. Because of the high star formation rate, however, higher [Fe/H] values are observed compared to the halo. Indeed, [Eu/Fe] is almost flat with an average of 0.5 dex, the same as observed in the halo. A similar behavior is found for the so-called α enhancement. Therefore, we may expect [Y/Fe] $= -0.2$ dex, as discussed before in the analysis of Fig. 20 (top panel). Consequently, the small variation of [Y/Fe] in thick disk stars with respect to the thin disk is not surprising.

2. Globular clusters and galaxies in the local group

The Ba and Eu abundances measured in globular clusters have been summarized by Gratton *et al.* (2004). Figure 6 of their paper indicates that there are no significant variations in the abundances of Ba and Eu compared to the observational uncertainties. One remarkable exception is the metal-poor cluster M15, which shows significant star-to-star scatter of Ba and Eu abundances (Sneden *et al.*, 1997), presumably as the

result of ''local'' massive star nucleosynthesis. In general, however, globular clusters are modestly *r* process rich compared with solar system material.

There are several exceptional clusters that exhibit significant *s*-process contributions. A few clusters show variations in metallicity and abundance ratios. Among those, ω Cen represents a remarkable case. This cluster has a metallicity distribution between $[Fe/H] = -1.8$ and -0.8, implying chemical evolution inside the cluster. Studies of neutron-capture elements for a significant sample of cluster stars by Norris and Da Costa (1995) and Smith *et al.* (2000) showed that the [Ba/Fe] and [La/Fe] ratios increase with increasing metallicity. This behavior can be explained by the contributions of the *s* process in $(1–3)M_\odot$ AGB stars. Accordingly, star formation in this cluster continues over a period, which is longer than the lifetime of these stars, i.e., longer than 1×10^9 yr.

Other exceptions are clusters without significant variation of chemical abundances but with an enhancement in *s*-process elements. A well-known example is M4 ($[Fe/H] = -1.2$), where [Ba/Fe] is 0.6 dex higher than in other clusters with similar metallicity (Ivans *et al.*, 1999). The fact that no variations of metallicity and chemical abundance ratios are observed suggests that the origin of these heavy elements is primordial. In other words, the cluster forming cloud was already polluted by the ejecta of previous generations of stars. This is a strong constraint for the formation time scale of the cluster.

A few other clusters are also suggested to have excesses of *s*-process elements, though they are not as clear as in M4. A good probe of the *s*-process contribution is Pb. Abundances of this element have been measured in four clusters including M4 by Yong *et al.* (2006, 2008). In M4, Pb was found to be enhanced as expected from other *s*-process elements, but no such excess was found for three other clusters, which showed Pb abundances compatible with that in halo stars (Aoki *et al.*, 2008).

Heavy element abundances have been measured for bright stars (supergiants and stars at the red-giant branch tip) in the Magellanic clouds, the irregular satellite galaxies of the Milky Way. Recently, Pompéia *et al.* (2008) reported chemical abundances of a large sample of disk stars in the large Magellanic cloud. Y, Zr, Ba, and La abundances were determined for 30–50 red-giant stars covering a metallicity range of $-1.3 < [Fe/H] < -0.3$. The heavy neutron-capture elements Ba and La turned out to be overabundant, while the ls elements Y and Zr are underabundant. Although the measurement of Eu was not available for the sample, Ba and La are likely of *s*-process origin. The high abundance ratios between the hs and ls elements are compatible with the model prediction for the *s* process in metal-deficient AGB stars.

Measurements of heavy elements in stars of dwarf spheroidal galaxies around the Milky Way have been made in the past decade [see, e.g., Shetrone *et al.* (2001, 2003), and Sadakane *et al.* (2004)]. Although the sample size is still small, in particular, for the measurement of Eu abundances, the neutron-capture elements in metal-deficient ($[Fe/H] < -1.0$) stars in dwarf galaxies can be explained by the *r* process, while *s*-process contributions are seen in metal-rich stars of some galaxies, e.g., in Fornax and Carina (Shetrone *et al.*, 2003; Tolstoy *et al.*, 2009). The *s*-process contributions from low- and intermediate-mass AGB stars are an important probe for the star formation history of galaxies. The α/Fe abundance ratios of stars in dwarf galaxies are lower than those of halo stars in general, indicating the possible role of type Ia supernovae. This is unlikely the case in galaxies without significant *s*-process contribution, because the time scales for type Ia supernovae are longer than the evolution of intermediate-mass stars.

V. SUMMARY

The *s* process, which is ascribed to low-mass stars during the TP-AGB phase (main and the strong components) and to massive stars (the weak component), has been discussed with respect to the underlying nuclear physics, current stellar models, and the rapidly growing observational evidence.

From the nuclear physics side, there is an increasingly complete set of neutron-capture measurements that provide the necessary Maxwellian averaged cross sections for detailed network calculation of the *s*-abundance patterns of the various scenarios. Over the last two decades considerable experimental progress has been achieved on the basis of new and improved neutron facilities and detector developments. Although the productive facilities at Oak Ridge and Karlsruhe have recently been closed, replacement became available through intense pulsed neutron sources using spallation reactions (n_TOF at CERN, J-PARC in Japan, and LANSCE at Los Alamos) or the ^{7}Li(p, n) reaction (FRANZ at Frankfurt, Germany and SARAF at the Weizmann Institute in Jerusalem, both under construction). Apart from the high fluxes, which these facilities have in common, they exhibit widely complementary characteristics, thus providing promising solutions for a variety of improved TOF measurements. Such measurements also benefit from developments in detector technology, aiming at higher efficiency (total absorption calorimeters) or minimized neutron sensitivity. Combined with new data acquisition systems and rapidly growing computing power, a new generation of experiments has already provided a number of accurate cross sections at astrophysically relevant energies. In parallel, the activation method proved to play an important role because of the superior sensitivity, which enabled first measurements on unstable branch-point nuclei along the *s*-process path.

Future efforts in *s*-process experiments would be most useful in the following areas: Improvements in the accuracy of (n, γ) cross sections are needed in mass regions where present uncertainties are still exceeding the 3%–5% level, i.e., around magic neutron numbers, in the Fe-Sr region, and for the lighter elements. The persisting problem of the cross sections for the neutron source reactions ^{13}C$(\alpha, n)^{16}$O and ^{22}Ne$(\alpha, n)^{25}$Mg in the respective Gamow windows is still unsolved. Together with the abundant light elements, which act as neutron poisons, the source reactions determine the *s*-process neutron balance and represent, therefore, important constraints for stellar models, i.e., for the role of the ^{13}C pocket in thermally pulsing low-mass AGB stars. The scarce information for (n, γ) cross sections of unstable isotopes, which are crucial for the analysis of *s*-process branchings, needs to be completed. The feasibility of such measurements

will benefit from progress in neutron facilities and advanced experimental techniques. Ultimately, they will also be needed to treat the extended reaction paths into the neutron-rich region, which follow from the high neutron densities during C shell burning in massive stars and during the first, strong pulse in low-metallicity AGB stars.

Theory remains indispensable for complementing the experimental (n, γ) information, either by closing gaps in the data, where measured cross sections are not (yet) available, or by providing stellar enhancement factors to correct the laboratory results for the effect of thermally populated excited nuclear states in the hot stellar plasma. Correspondingly, the even more pronounced enhancement of the weak interaction rates as a function of neutron and electron density at the *s*-process sites remains an important domain of theoretical studies, especially because experimental work in this field had long been neglected.

The weak *s* process, which produces a large fraction of the *s* isotopes between Fe and Sr during convective core He burning and subsequent convective shell C burning, is of secondary nature. The neutron source is driven by (α, n) reactions on ^{22}Ne deriving from the conversion of initial CNO nuclei to ^{14}N during core H burning via the sequence $^{14}\mathrm{N}(\alpha, \gamma)^{18}\mathrm{F}(\beta^+\nu)^{18}\mathrm{O}$, and subsequently by $^{18}\mathrm{O}(\alpha, \gamma)^{22}\mathrm{Ne}$ reactions at the beginning of convective core He burning, when the central temperature rises above 2.5×10^8 K. The weak *s* contribution to the solar abundances is not easy to estimate in a quantitative way due to the present uncertainties of the stellar cross sections in the range from Fe to Se and to the physical uncertainties in the treatment of the preexplosive and explosive nucleosynthesis in supernovae. However, one-half of solar Zn and about 70%–80% of solar Cu, Ga, Ge, and As are to be ascribed to the weak *s* process. The interplay between theory and spectroscopic observations has been briefly discussed.

All *s* isotopes beyond $A = 90$ and about one-half of solar Pb are contributed by the main *s* process. The second half of solar Pb is produced by low-mass AGB stars at low metallicities (strong component). Below $A = 90$ the contribution of the main component to the *s*-process abundances decreases rapidly. The main *s* process is not a unique process, but depends on the initial mass, metallicity, the strength of the ^{13}C pocket, the efficiency of the TDU, and the choice of the mass loss rate. Stellar models could be verified by comparison with a large body of data obtained from analyses of presolar material in the form of circumstellar dust grains and by the conspicuous number of observations of MS, S, C(N), and Ba stars of the galactic disk as well as of CH stars in the halo. The *s*-process contribution to the cosmic abundances in the interstellar medium in the mass range $A > 90$ is the result of all previous generations of AGB stars that polluted the interstellar medium before the formation of the Solar System.

The impact of the chemical evolution of the Galaxy has been analyzed for the representative elements Y, Ba, and Pb corresponding to the *s*-abundance peaks at magic neutron numbers 50, 82, and 126. The origin of the heavy neutron-capture elements is partly due to the main *s* process and partly due to the primary *r* process. Usually the *r*-process contribution to each isotope in the Solar System is estimated using the so-called *r*-residual method by subtracting the well-defined *s*-process components from the respective solar abundances. This approach provides a fair basis for comparison with the still uncertain predictions from current *r*-process models.

Progress in stellar modeling depends on a continuous interplay between theory and observation. This is particularly true for recent observations of the rare class of carbon-enhanced metal-poor stars with *s*-process enhancements, the CEMP-*s* stars, which are main sequence, turnoff, or giant stars of low mass ($M \sim 0.8 M_\odot$) in close binary systems. The primary more massive companion (now a white dwarf) evolved along the AGB and polluted the envelope of the observed star with C and *s*-process elements when it lost its entire envelope at the end of the AGB phase.

A strongly debated issue is the subclass of CEMP-s/r stars, showing *s*- and *r*-process contributions at the same time, although both processes are of completely different astrophysical origin. Some of them are highly enhanced in Ba, Ce, and La, which belong to the second *s*-process peak at $N = 82$, as well as in Eu, which is a typical *r*-process element. In fact, the *s* and *r* elements beyond Ba are enhanced at the same level in these very metal-poor stars. A plausible scenario considers the formation of binary systems in giant clouds that were locally polluted by the ejecta of type II supernovae.

Apart from the contributions from the weak and main *s* processes and from the *r* process, the light *s*-process elements Sr, Y, and Zr in the Solar System contain an additional component contributed by a primary source of still unknown origin, the LEPP. The different proposed hypotheses, all related to the most advanced phases of preexplosive and explosive nucleosynthesis in massive stars, represent a relevant issue of present nucleosynthesis research.

These intriguing problems have been recognized by the rapid increase of observational data in the past decade, using high-resolution and high signal-to-noise spectra. Further chemical abundance studies, in particular, isotope abundance measurements for key elements, will provide useful hints and constraints for understanding the physical processes behind these unsolved problems.

Further improvement of the models related to the weak, main, and strong *s*-process components coming from massive and intermediate-to-low-mass stars will have a strong impact on studies of the Milky Way and surrounding smaller galaxies. Great efforts have been made to understand the chemical evolution and formation history of these galaxies, which are traced by chemical abundance ratios as well as kinematic properties of individual stars. Abundance ratios of *s*-process elements provide useful constraints for the chemical evolution models, i.e., on the time scale of the star formation history and on the initial mass function.

ACKNOWLEDGMENTS

We are deeply indebted to O. Straniero and S. Cristallo for continuous clarifying discussions concerning the modeling of AGB stars. We also thank the referees for their suggestions, which led to a substantial improvement of the manuscript.

REFERENCES

Abbondanno, U., *et al.*, 2003, *CERN n_TOF Facility: Performance Report*, Technical Report, CERN, Geneva, Switzerland, Report No. CERN-SL-2002-053 ECT.

Abbondanno, U., *et al.*, 2004a, Phys. Rev. Lett. **93**, 161103.

Abbondanno, U., *et al.*, 2004b, Nucl. Instrum. Methods Phys. Res., Sect. A **521**, 454.

Abbondanno, U., *et al.*, 2005, Nucl. Instrum. Methods Phys. Res., Sect. A **538**, 692.

Abia, C., M. Busso, R. Gallino, I. Domínguez, O. Straniero, and J. Isern, 2001, Astrophys. J. **559**, 1117.

Abia, C., P. de Laverny, and R. Wahlin, 2008, Astron. Astrophys. **481**, 161.

Abia, C., I. Domínguez, R. Gallino, M. Busso, S. Masera, O. Straniero, P. de Laverny, and B. Plez, 2002, Astrophys. J. **579**, 817.

Agostinelli, S., *et al.*, 2003, Nucl. Instrum. Methods Phys. Res., Sect. A **506**, 250.

Allen, B., J. Gibbons, and R. Macklin, 1971, Adv. Nucl. Phys. **4**, 205.

Allen, D., and B. Barbuy, 2006, Astron. Astrophys. **454**, 917.

Alpizar-Vicente, A., *et al.*, 2008, Phys. Rev. C **77**, 015806.

Andrievsky, S. M., M. Spite, S. A. Korotin, F. Spite, P. François, P. Bonifacio, R. Cayrel, and V. Hill, 2009, Astron. Astrophys. **494**, 1083.

Angulo, C., *et al.*, 1999, Nucl. Phys. **A656**, 3.

Aoki, W., *et al.*, 2006b, Astrophys. J. **639**, 897.

Aoki, W., T. Beers, N. Christlieb, J. Norris, S. Ryan, and S. Tsangarides, 2007, Astrophys. J. **655**, 492.

Aoki, W., T. Beers, T. Sivarani, B. Marsteller, Y. Lee, S. Honda, J. Norris, S. Ryan, and D. Carollo, 2008, Astrophys. J. **678**, 1351.

Aoki, W., S. Bisterzo, R. Gallino, T. Beers, J. Norris, S. Ryan, and S. Tsangarides, 2006a, Astrophys. J. **650**, L127.

Aoki, W., and S. Honda, 2008, Publ. Astron. Soc. Jpn. **60**, L7.

Aoki, W., S. Honda, T. Beers, T. Kajino, H. Ando, J. Norris, S. Ryan, H. Izumiura, K. Sadakane, and M. Takada-Hidai, 2005, Astrophys. J. **632**, 611.

Aoki, W., S. Honda, T. Beers, and C. Sneden, 2003, Astrophys. J. **586**, 506.

Aoki, W., J. Norris, S. Ryan, T. Beers, and H. Ando, 2000, Astrophys. J. **536**, L97.

Aoki, W., J. Norris, S. Ryan, T. Beers, and H. Ando, 2002, Publ. Astron. Soc. Jpn. **54**, 933.

Aoki, W., S. Ryan, N. Iwamoto, T. Beers, J. Norris, H. Ando, T. Kajino, G. Mathews, and M. Fujimoto, 2003, Astrophys. J. **592**, L67.

Aoki, W., S. Ryan, J. Norris, T. Beers, H. Ando, N. Iwamoto, T. Kajino, G. Mathews, and M. Fujimoto, 2001, Astrophys. J. **561**, 346.

Aoki, W., S. Ryan, J. Norris, T. Beers, H. Ando, and S. Tsangarides, 2002, Astrophys. J. **580**, 1149.

Arlandini, C., F. Käppeler, K. Wisshak, R. Gallino, M. Lugaro, M. Busso, and O. Straniero, 1999, Astrophys. J. **525**, 886.

Arnett, W., and J. Truran, 1969, Astrophys. J. **157**, 339.

Arnould, M., and S. Goriely, 2003, Phys. Rep. **384**, 1.

Asplund, M., 2005, Annu. Rev. Astron. Astrophys. **43**, 481.

Asplund, M., N. Grevesse, A. Sauval, and P. Scott, 2009, Annu. Rev. Astron. Astrophys. **47**, 481.

Assunção, M., *et al.*, 2006, Phys. Rev. C **73**, 055801.

Bao, Z., H. Beer, F. Käppeler, F. Voss, K. Wisshak, and T. Rauscher, 2000, At. Data Nucl. Data Tables **76**, 70.

Bao, Z., and F. Käppeler, 1987, At. Data Nucl. Data Tables **36**, 411.

Barklem, P., N. Christlieb, T. Beers, V. Hill, M. Bessell, J. Holmberg, B. Marsteller, S. Rossi, F.-J. Zickgraf, and D. Reimers, 2005, Astron. Astrophys. **439**, 129.

Beer, H., 1986, in *Advances in Nuclear Astrophysics*, edited by E. Vangioni-Flam, J. Audouze, M. Cassé, J. Chièze, and J. Tran Thanh Van (Editions Frontières, Paris), p. 375.

Beer, H., and F. Käppeler, 1980, Phys. Rev. C **21**, 534.

Beer, H., F. Käppeler, and K. Wisshak, 1982, Astron. Astrophys. **105**, 270.

Beer, H., and R. Macklin, 1989, Astrophys. J. **339**, 962.

Beer, H., F. Voß, and R. Winters, 1992, Astrophys. J. Suppl. Ser. **80**, 403.

Beer, H., G. Walter, and F. Käppeler, 1992, Astrophys. J. **389**, 784.

Beers, T., and N. Christlieb, 2005, Annu. Rev. Astron. Astrophys. **43**, 531.

Beers, T., G. Preston, and S. Shectman, 1992, Astron. J. **103**, 1987.

Beers, T., T. Sivarani, B. Marsteller, Y. Lee, S. Rossi, and B. Plez, 2007, Astron. J. **133**, 1193.

Belgya, T., *et al.*, 2005, *Handbook for Calculations of Nuclear Reaction Data, RIPL-2*, Technical Report, International Atomic Energy Agency, Vienna, Austria, http://www-nds.iaea.org/RIPL-2/.

Belic, D., *et al.*, 1999, Phys. Rev. Lett. **83**, 5242.

Belic, D., *et al.*, 2002, Phys. Rev. C **65**, 35801.

Bennett, M., *et al.*, 2010, J. Phys. Conf. Ser. **202**, 012023.

Bidelman, W., and P. Keenan, 1951, Astrophys. J. **114**, 473.

Bisterzo, S., R. Gallino, M. Pignatari, L. Pompeia, K. Cunha, and V. V. Smith, 2004, Mem. Soc. Astron. Ital. **75**, 741.

Bisterzo, S., R. Gallino, O. Straniero, S. Cristallo, F. Käppeler, and W. Aoki, 2010, Mon. Not. R. Astron. Soc. **404**, 1529.

Bisterzo, S., R. Gallino, O. Straniero, I. Ivans, F. Käppeler, and W. Aoki, 2006, Mem. Soc. Astron. Ital. **77**, 985.

Bond, H., 1974, Astrophys. J. **194**, 95.

Borella, A., G. Aerts, F. Gunsing, A. Moens, R. Wynants, and P. Schillebeeckx, 2005, in *Nuclear Data for Science and Technology*, edited by R. Haight, M. Chadwick, T. Kawano, and P. Talou, AIP Conf. Proc. No. 769 (AIP, New York), pp. 652–655.

Bosch, F., *et al.*, 1996, Phys. Rev. Lett. **77**, 5190.

Boyer, S., *et al.*, 2006, Nucl. Phys. **A775**, 175.

Bradley, T., Z. Parsa, M. Stelts, and R. Chrien, 1979, in *Nuclear Cross Sections for Technology*, edited by J. L. Fowler, C. H. Johnson, and C. D. Bowman, NBS Special Publication—594 (U.S. GPO, Washington, DC), p. 344.

Brown, F., A. Kahler, G. McKinney, R. Mosteller, and M. White, 2007, in *Proceedings of the MCNP5+Data+MCNPX Workshop, ANS Mathematics & Computation Division Topical Meeting, Monterey, CA, 2007*, Technical Report, Los Alamos National Laboratory, NM, Report No. LA-UR-07-2035.

Burbidge, E., G. Burbidge, W. Fowler, and F. Hoyle, 1957, Rev. Mod. Phys. **29**, 547.

Burris, D., C. Pilachowski, T. Armandroff, C. Sneden, J. Cowan, and H. Roe, 2000, Astrophys. J. **544**, 302.

Busso, M., R. Gallino, D. Lambert, C. Travaglio, and V. Smith, 2001, Astrophys. J. **557**, 802.

Busso, M., R. Gallino, and G. Wasserburg, 1999, Annu. Rev. Astron. Astrophys. **37**, 239.

Busso, M., D. Lambert, L. Beglio, R. Gallino, C. Raiteri, and V. Smith, 1995, Astrophys. J. **446**, 775.

Cameron, A., 1957, A.E.C.L. Chalk River, Canada, Technical Report No. CRL–41.

Cameron, A., H. Vanhala, and P. Höflich, 1997, in *Astrophysical Implications of the Laboratory Study of Presolar Materials*, AIP Conf. Proc. No. 402 (AIP, New York), pp. 665–693.

Campbell, S., and J. Lattanzio, 2008, Astron. Astrophys. **490**, 769.

Cayrel, R., *et al.*, 2001, Nature (London) **409**, 691.
Cayrel, R., *et al.*, 2004, Astron. Astrophys. **416**, 1117.
Chau, L., O. Meusel, U. Ratzinger, A. Schempp, K. Volk, and M. Heil, 2006, in *Proceedings of EPAC Edinburgh 2006* (CERN, Geneva, Switzerland), p. 1690, http://accelconf.web.cern.ch/AccelConf/e06/PAPERS/TUPLS082.PDF.
Chieffi, A., and M. Limongi, 2006, Technical Report, http://www.iasf-roma.inaf.it/orfeo7.
Chieffi, A., and O. Straniero, 1989, Astrophys. J. Suppl. Ser. **71**, 47.
Christlieb, N., 2003, Rev. Mod. Astron. **16**, 191.
Christlieb, N., *et al.*, 2004, Astron. Astrophys. **428**, 1027.
Clayton, D., 1964, Astrophys. J. **139**, 637.
Clayton, D., 1988, Mon. Not. R. Astron. Soc. **234**, 1.
Clayton, D., W. Fowler, T. Hull, and B. Zimmerman, 1961, Ann. Phys. (Leipzig) **12**, 331.
Clayton, D., M. Leising, L.-S. The, W. Johnson, and J. Kurfess, 1992, Astrophys. J. **399**, L141.
Clayton, D., and L. Nittler, 2004, Annu. Rev. Astron. Astrophys. **42**, 39.
Clayton, D., and M. Rassbach, 1967, Astrophys. J. **148**, 69.
Clayton, D., and R. Ward, 1974, Astrophys. J. **193**, 397.
Cohen, J., N. Christlieb, A. McWilliam, S. Shectman, I. Thompson, J. Melendez, L. Wisotzki, and D. Reimers, 2008, Astrophys. J. **672**, 320.
Cohen, J., N. Christlieb, Y.-Z. Qian, and G. Wasserburg, 2003, Astrophys. J. **588**, 1082.
Cohen, J., A. McWilliam, N. Christlieb, S. Shectman, I. Thompson, J. Melendez, L. Wisotzki, and D. Reimers, 2007, Astrophys. J. **659**, L161.
Cohen, J., A. McWilliam, S. Shectman, I. Thompson, N. Christlieb, J. Melendez, S. Ramirez, A. Swensson, and F.-J. Zickgraf, 2006, Astron. J. **132**, 137.
Corvi, F., A. Prevignano, H. Liskien, and P. Smith, 1988, Nucl. Instrum. Methods Phys. Res., Sect. A **265**, 475.
Couch, R., A. Schmiedekamp, and W. Arnett, 1974, Astrophys. J. **190**, 95.
Couture, A., 2009, "Measurement of the $N^{63}i(n,\gamma)$ Cross Section with DANCE" (private communication).
Couture, A., and R. Reifarth, 2007, At. Data Nucl. Data Tables **93**, 807.
Cowan, J., and C. Sneden, 2006, Nature (London) **440**, 1151.
Cowan, J., C. Sneden, T. C. Beers, J. E. Lawler, J. Simmerer, J. W. Truran, F. Primas, J. Collier, and S. Burles, 2005, Astrophys. J. **627**, 238.
Cowan, J., *et al.*, 2002, Astrophys. J. **572**, 861.
Cristallo, S., R. Gallino, O. Straniero, L. Piersanti, and I. Domínguez, 2006, Mem. Soc. Astron. Ital. **77**, 774.
Cristallo, S., L. Piersanti, O. Straniero, R. Gallino, I. Domínguez, and F. Käppeler, 2009, Pub. Astron. Soc. Aust. **26**, 139.
Cristallo, S., O. Straniero, R. Gallino, L. Piersanti, I. Domínguez, and M. Lederer, 2009, Astrophys. J. **696**, 797.
Cristallo, S., O. Straniero, M. Lederer, and B. Aringer, 2007, Astrophys. J. **667**, 489.
de Laverny, P., C. Abia, I. Domínguez, B. Plez, O. Straniero, R. Wahlin, K. Eriksson, and U. Jørgensen, 2006, Astron. Astrophys. **446**, 1107.
de L. Musgrove, A., B. Allen, J. Boldeman, and R. Macklin, 1978, in *Neutron Physics and Nuclear Data for Reactors and other Applied Purposes* (OECD, Paris), p. 449.
Denissenkov, P., and C. Tout, 2003, Mon. Not. R. Astron. Soc. **340**, 722.
Diehl, R., 1998, in *Nuclear Astrophysics*, edited by M. Buballa, W. Nörenberg, J. Wambach, and A. Wirzba (GSI, Darmstadt), p. 234.
Dietrich, F., and J. Escher, 2007, Nucl. Phys. **A787**, 237.
Dillmann, I., 2009, revised ^{62}Ni value of Nassar *et al.*, 2005 (private communication).
Dillmann, I., *et al.*, 2010, Nucl. Instrum. Methods Phys. Res., Sect. B **268**, 1283.
Dillmann, I., M. Heil, F. Käppeler, R. Plag, T. Rauscher, and F.-K. Thielemann, 2005, in *Capture Gamma-Ray Spectroscopy and Related Topics*, edited by A. Woehr and A. Aprahamian, AIP Conference Series 819 (AIP, New York), p. 123, http://www.kadonis.org.
Dillmann, I., R. Plag, F. Käppeler, and T. Rauscher, 2009, in *Proceedings of EFNUDAT Fast Neutrons—Scientific Workshop on Neutron Measurements, Theory & Applications* (JRC-IRMM, Geel), http://www.kadonis.org.
Doll, C., H. Börner, S. Jaag, and F. Käppeler, 1999, Phys. Rev. C **59**, 492.
Domingo-Pardo, C., *et al.*, 2006a, Phys. Rev. C **74**, 025807.
Domingo-Pardo, C., *et al.*, 2006b, Phys. Rev. C **74**, 055802.
Domingo-Pardo, C., *et al.*, 2007a, Phys. Rev. C **76**, 045805.
Domingo-Pardo, C., *et al.*, 2007b, Phys. Rev. C **75**, 015806.
Dupraz, C., H. Bloemen, K. Benett, R. Diehl, W. Hermsen, A. Iyudin, J. Ryan, and V. Schönfelder, 1997, Astron. Astrophys. **324**, 683.
Edvardsson, B., J. Andersen, B. Gustafsson, D. Lambert, P. Nissen, and J. Tomkin, 1993, Astron. Astrophys. **275**, 101.
El Eid, M., L.-S. The, and B. Meyer, 2009, Space Sci. Rev. **147**, 1.
Esch, E.-I., *et al.*, 2008, Phys. Rev. C **77**, 034309.
Escher, J., L. Ahle, L. Bernstein, J. Church, F. Dietrich, C. Forssén, and R. Hoffman, 2005, Nucl. Phys. **A758**, 86.
FAIR, 2007, *An International Accelerator Facility for Beams of Ions and Antiprotons, Conceptual Design Report*, Technical Report, Facility for Antiproton and Ion Research, http://www.gsi.de/fair/.
Farouqi, K., K.-L. Kratz, B. Pfeiffer, T. Rauscher, F.-K. Thielemann, and J. Truran, 2010, Astrophys. J. **712**, 1359.
Forssén, C., L. Ahle, L. Bernstein, J. Church, F. Dietrich, J. Escher, and R. Hoffman, 2005, Nucl. Phys. **A758**, 130.
Fowler, W., and F. Hoyle, 1960, Ann. Phys. (Leipzig) **10**, 280.
François, P., *et al.*, 2007, Astron. Astrophys. **476**, 935.
Frebel, A., N. Christlieb, J. Norris, C. Thom, T. Beers, and J. Rhee, 2007, Astrophys. J. **660**, L117.
Freeman, K., and J. Bland-Hawthorn, 2002, Annu. Rev. Astron. Astrophys. **40**, 487.
Frekers, D., 2005, Nucl. Phys. **A752**, 580.
Freytag, B., H. Ludwig, and M. Steffen, 1996, Astron. Astrophys. **313**, 497.
FRIB, 2010, *Facility for Rare Isotope Beams*, Technical Report, Michigan State University, http://www.frib.msu.edu/.
Fröhlich, C., G. Martínez-Pinedo, M. Liebendörfer, F.-K. Thielemann, E. Bravo, W. Hix, K. Langanke, and N. Zinner, 2006, Phys. Rev. Lett. **96**, 142502.
Fujii, K., *et al.*, 2010, Phys. Rev. C, **82**, 015804.
Fujimoto, M., Y. Ikeda, and I. J. Iben, 2000, Astrophys. J. **529**, L25.
Fulbright, J., 2000, Astron. J. **120**, 1841.
Fürst, E., W. Reich, and B. Aschenbach, 1997, Astron. Astrophys. **319**, 655.
Gallino, R., C. Arlandini, M. Busso, M. Lugaro, C. Travaglio, O. Straniero, A. Chieffi, and M. Limongi, 1998, Astrophys. J. **497**, 388.
Gallino, R., M. Busso, G. Picchio, C. Raiteri, and A. Renzini, 1988, Astrophys. J. **334**, L45.
Gallino, R., G. Wasserburg, M. Busso, and O. Straniero, 2005, in *From Lithium to Uranium: Elemental Tracers of Early Cosmic Evolution*, edited by V. Hill, P. François, and F. Primas, IAU Symposium Proceedings of the International Astronomical

Union 228 (Cambridge University Press, Cambridge, UK), pp. 461–466.
García-Hernández, D., P. García-Lario, B. Plez, A. Manchado, F. D'Antona, J. Lub, and H. Habing, 2007, Astron. Astrophys. **462**, 711.
Gonzalez, G., D. Lambert, G. Wallerstein, N. Rao, V. Smith, and J. McCarthy, 1998, Astrophys. J. Suppl. Ser. **114**, 133.
Goriely, S., 1998, *MOST Statistical Model Code, Version 2005*, Technical Report, http://www-astro.ulb.ac.be.
Goriely, S., and N. Mowlavi, 2000, Astron. Astrophys. **362**, 599.
Gratton, R., and C. Sneden, 1994, Astron. Astrophys. **287**, 927.
Gratton, R., C. Sneden, and E. Carretta, 2004, Annu. Rev. Astron. Astrophys. **42**, 385.
Guber, K., L. Leal, R. Sayer, P. Koehler, T. Valentine, H. Derrien, and J. Harvey, 2005a, Nucl. Instrum. Methods Phys. Res., Sect. B **241**, 218.
Guber, K., L. Leal, R. Sayer, P. Koehler, T. Valentine, H. Derrien, and J. Harvey, 2005b, in *Nuclear Data for Science and Technology*, AIP Conference Series 769 (AIP, New York), pp. 1706–1711.
Guber, K., R. Spencer, P. Koehler, and R. Winters, 1997, Nucl. Phys. **A621**, 254.
Gustafsson, B., 1989, Annu. Rev. Astron. Astrophys. **27**, 701.
Habing, H., 1996, Astron. Astrophys. Rev. **7**, 97.
Harris, M., 1981, Astrophys. Space Sci. **77**, 357.
Heger, A., 2006, Technical Report http://www.ucolick.org/ alex/, PII: S0146-6410(99)00098-8.
Heil, M., S. Dababneh, A. Juseviciute, F. Käppeler, R. Plag, R. Reifarth, and S. O'Brien, 2005, Phys. Rev. C **71**, 025803.
Heil, M., F. Käppeler, P. Tischhauser, M. Wiescher, J. Görres, R. Detwiler, A. Couture, J. Daly, C. Ugalde, and R. Reifarth, 2008, Phys. Rev. C **78**, 025803.
Heil, M., F. Käppeler, E. Uberseder, R. Gallino, S. Bisterzo, and M. Pignatari, 2008a, Phys. Rev. C **78**, 025802.
Heil, M., F. Käppeler, E. Uberseder, R. Gallino, and M. Pignatari, 2008b, Phys. Rev. C **77**, 015808.
Heil, M., N. Winckler, S. Dababneh, F. Käppeler, K. Wisshak, S. Bisterzo, R. Gallino, A. Davis, and T. Rauscher, 2008c, Astrophys. J. **673**, 434.
Heil, M., *et al.*, 2001, Nucl. Instrum. Methods Phys. Res., Sect. A **459**, 229.
Herwig, F., 2000, Astron. Astrophys. **360**, 952.
Herwig, F., 2004, Astrophys. J. Suppl. Ser. **155**, 651.
Herwig, F., 2005, Annu. Rev. Astron. Astrophys. **43**, 435.
Herwig, F., T. Blöcker, D. Schönberner, and M. El Eid, 1997, Astron. Astrophys. **324**, L81.
Hill, V., B. Barbuy, M. Spite, F. Spite, R. Cayrel, B. Plez, T. Beers, B. Nordström, and P. Nissen, 2000, Astron. Astrophys. **353**, 557.
Hill, V., *et al.*, 2002, Astron. Astrophys. **387**, 560.
Hollowell, D., and I. Iben, 1988, Astrophys. J. **333**, L25.
Hollowell, D., I. J. Iben, and M. Fujimoto, 1990, Astrophys. J. **351**, 245.
Holmes, J., S. Woosley, W. Fowler, and B. Zimmerman, 1976, At. Data Nucl. Data Tables **18**, 305.
Honda, S., W. Aoki, Y. Ishimaru, S. Wanajo, and S. G. Ryan, 2006, Astrophys. J. **643**, 1180.
Honda, S., W. Aoki, T. Kajino, H. Ando, T. Beers, H. Izumiura, K. Sadakane, and M. Takada-Hidai, 2004, Astrophys. J. **607**, 474.
Husti, L., R. Gallino, S. Bisterzo, O. Straniero, and S. Cristallo, 2009, Pub. Astron. Soc. Aust. **26**, 176.
Iben, I. J., and A. Renzini, 1983, Annu. Rev. Astron. Astrophys. **21**, 271.
Igashira, M., Y. Nagai, K. Masuda, T. Ohsaki, and H. Kitazawa, 1995, Astrophys. J. **441**, L89.
Iliadis, C., J. D'Auria, S. Starrfield, W. Thompson, and M. Wiescher, 2001, Astrophys. J. Suppl. Ser. **134**, 151.
Ishimaru, Y., and Wanajo, S., 1999, Astrophys. J. **511**, L133.
Ishimaru, Y., S. Wanajo, W. Aoki, and S. G. Ryan, 2004, Astrophys. J. **600**, L47.
Ivans, I., J. Simmerer, C. Sneden, J. Lawler, J. Cowan, R. Gallino, and S. Bisterzo, 2006, Astrophys. J. **645**, 613.
Ivans, I., C. Sneden, R. Gallino, J. Cowan, and G. Preston, 2005, Astrophys. J. **627**, L145.
Ivans, I., C. Sneden, R. Kraft, N. Suntzeff, V. Smith, G. Langer, and J. Fulbright, 1999, Astron. J. **118**, 1273.
Iwamoto, N., T. Kajino, G. Mathews, M. Fujimoto, and W. Aoki, 2004, Astrophys. J. **602**, 377.
Jaag, S., and F. Käppeler, 1995, Phys. Rev. C **51**, 3465.
Jaag, S., and F. Käppeler, 1996a, Phys. Rev. C **53**, 2474.
Jaag, S., and F. Käppeler, 1996b, Astrophys. J. **464**, 874.
Jaeger, M., R. Kunz, A. Mayer, J. Hammer, G. Staudt, K.-L. Kratz, and B. Pfeiffer, 2001, Phys. Rev. Lett. **87**, 202501.
Jandel, M., *et al.*, 2008, Phys. Rev. C **78**, 034609.
Japan Proton Accelerator Complex, Technical Report, JAERI and KEK, 2004, http://j-parc.jp/.
Jehin, E., P. Magain, C. Neuforge, A. Noels, G. Parmentier, and A. Thoul, 1999, Astron. Astrophys. **341**, 241.
Johnson, J., and M. Bolte, 2004, Astrophys. J. **605**, 462.
Jonsell, K., P. Barklem, B. Gustafsson, N. Christlieb, V. Hill, T. Beers, and J. Holmberg, 2006, Astron. Astrophys. **451**, 651.
Jung, M., *et al.*, 1992, Phys. Rev. Lett. **69**, 2164.
Käppeler, F., 1999, Prog. Part. Nucl. Phys. **43**, 419.
Käppeler, F., C. Arlandini, M. Heil, F. Voss, K. Wisshak, R. Reifarth, O. Straniero, R. Gallino, S. Masera, and C. Travaglio, 2004, Phys. Rev. C **69**, 055802.
Käppeler, F., H. Beer, and K. Wisshak, 1989, Rep. Prog. Phys. **52**, 945.
Käppeler, F., H. Beer, K. Wisshak, D. Clayton, R. Macklin, and R. Ward, 1982, Astrophys. J. **257**, 821.
Käppeler, F., R. Gallino, M. Busso, G. Picchio, and C. Raiteri, 1990, Astrophys. J. **354**, 630.
Käppeler, F., A. Naqvi, and M. Al-Ohali, 1987, Phys. Rev. C **35**, 936.
Käppeler, F., K. Wisshak, and L. D. Hong, 1983, Nucl. Sci. Eng. **84**, 234.
Käppeler, F., W. Zhao, H. Beer, and U. Ratzel, 1990, Astrophys. J. **355**, 348.
Keenan, P., 1942, Astrophys. J. **96**, 101.
Klay, N., and F. Käppeler, 1988, Phys. Rev. C **38**, 295.
Klay, N., F. Käppeler, H. Beer, and G. Schatz, 1991, Phys. Rev. C **44**, 2839.
Klug, J., *et al.*, 2007, Nucl. Instrum. Methods Phys. Res., Sect. A **577**, 641.
Knoll, G., 1979, Ed., *Radiation Detection and Measurement* (Wiley, New York), p. 34.
Koehler, P., 2001, Nucl. Instrum. Methods Phys. Res., Sect. A **460**, 352.
Koehler, P., R. Spencer, R. Winters, K. Guber, J. Harvey, N. Hill, and M. Smith, 1996, Phys. Rev. C **54**, 1463.
Koehler, P., *et al.*, 2000, Phys. Rev. C **62**, 055803.
Koehler, P., *et al.*, 2001, Phys. Rev. C **63**, 049901.
Koning, A., S. Hilaire, and M. Duijvestijn, 2005, in *Nuclear Data for Science and Technology*, edited by R. Haight, M. Chadwick,

T. Kawano, and P. Talou, AIP Conference Series 769 (AIP, New York), pp. 1154–1157.
Kratz, K.-L., K. Farouqi, B. Pfeiffer, J. Truran, C. Sneden, and J. Cowan, 2007, Astrophys. J. **662**, 39.
Lai, D., M. Bolte, J. Johnson, S. Lucatello, A. Heger, and S. Woosley, 2008, Astrophys. J. **681**, 1524.
Lamb, S., W. Howard, J. Truran, and I. Iben, 1977, Astrophys. J. **217**, 213.
Lambert, D., 1991, in *Evolution of Stars: The Photospheric Abundance Connection*, edited by G. Michaud and A. Tutukov (Kluwer, Dordrecht), pp. 299–316.
Lambert, D., B. Gustafsson, K. Eriksson, and K. Hinkle, 1986, Astrophys. J. Suppl. Ser. **62**, 373.
Lambert, D., V. Smith, M. Busso, R. Gallino, and O. Straniero, 1995, Astrophys. J. **450**, 302.
Langer, N., A. Heger, S. Wellstein, and F. Herwig, 1999, Astron. Astrophys. **346**, L37.
Lau, H., R. Stancliffe, and C. Tout, 2009, Mon. Not. R. Astron. Soc. **396**, 1046.
Lawler, J., M. Wickliffe, E. den Hartog, and C. Sneden, 2001, Astrophys. J. **563**, 1075.
Lederer, C., *et al.*, 2010 (unpublished).
Lee, Y., *et al.*, 2008a, Astron. J. **136**, 2022.
Lee, Y., *et al.*, 2008b, Astron. J. **136**, 2050.
Limongi, M., O. Straniero, and A. Chieffi, 2000, Astrophys. J. Suppl. Ser. **129**, 625.
Lisowski, P., C. Bowman, G. Russell, and S. Wender, 1990, Nucl. Sci. Eng. **106**, 208.
Little, S., I. Little-Marenin, and W. Bauer, 1987, Astron. J. **94**, 981.
Liu, G., Y. Liang, and L. Deng, 2009, Res. Astron. Astrophys. **9**, 431.
Lodders, K., 2003, Astrophys. J. **591**, 1220.
Lucatello, S., R. Gratton, J. Cohen, T. Beers, N. Christlieb, E. Carretta, and S. Ramírez, 2003, Astron. J. **125**, 875.
Lugaro, M., F. Herwig, J. Lattanzio, R. Gallino, and O. Straniero, 2003, Astrophys. J. **586**, 1305.
Macklin, R., 1982a, 197au, private communication to S. F. Mughabghab (1982), see also www.nndc.bnl.gov/nndc/ EXFOR 12720.002.
Macklin, R., 1982b, Nucl. Sci. Eng. **81**, 520.
Macklin, R., 1983, Nucl. Sci. Eng. **85**, 350.
Macklin, R., 1985, Nucl. Sci. Eng. **89**, 79.
Macklin, R., 1987, Nucl. Sci. Eng. **95**, 200.
Macklin, R., and J. Gibbons, 1967, Phys. Rev. **159**, 1007, based on H. Maier-Leibnitz (private communication), and F. Rau, 1963, Nukleonika **5**, 191.
Macklin, R., J. Halperin, and R. Winters, 1975, Phys. Rev. C **11**, 1270.
Malaney, R., 1987a, Astrophys. Space Sci. **137**, 251.
Malaney, R., 1987b, Astrophys. J. **321**, 832.
Marganiec, J., I. Dillmann, C. Domingo Pardo, F. Käppeler, R. Gallino, M. Pignatari, and P. Grabmayr, 2009, Phys. Rev. C **79**, 065802.
Marrone, S., *et al.*, 2006a, Phys. Rev. C **73**, 034604.
Marrone, S., *et al.*, 2006b, Nucl. Instrum. Methods Phys. Res., Sect. A **568**, 904.
Mashonkina, L., and T. Gehren, 2001, Astron. Astrophys. **376**, 232.
Mashonkina, L., and G. Zhao, 2006, Astron. Astrophys. **456**, 313.
Mashonkina, L., G. Zhao, T. Gehren, W. Aoki, M. Bergemann, K. Noguchi, J. Shi, M. Takada-Hidai, and H. Zhang, 2008, Astron. Astrophys. **478**, 529.
Mastinu, P., G. Martín Hernández, and J. Praena, 2009, Nucl. Instrum. Methods Phys. Res., Sect. A **601**, 333.
McClure, R., 1984, Publ. Astron. Soc. Pac. **96**, 117.
McClure, R., and A. Woodsworth, 1990, Astrophys. J. **352**, 709.
McWilliam, A., 1997, Annu. Rev. Astron. Astrophys. **35**, 503.
McWilliam, A., 1998, Astron. J. **115**, 1640.
McWilliam, A., G. Preston, C. Sneden, and L. Searle, 1995, Astron. J. **109**, 2757.
Merrill, S., 1952, Astrophys. J. **116**, 21.
Meusel, O., L. Chau, I. Mueller, U. Ratzinger, A. Schempp, K. Volk, C. Zhang, and S. Minaev, 2006, in *Proceedings of Linac 2006, Knoxville, USA*, http://accelconf.web.cern.ch/AccelConf/l06/PAPERS/MOP051.pdf.
Mishenina, T., and V. Kovtyukh, 2001, Astron. Astrophys. **370**, 951.
Mohr, P., S. Bisterzo, R. Gallino, F. Käppeler, U. Kneissl, and N. Winckler, 2009, Phys. Rev. C **79**, 045804.
Mohr, P., T. Shizuma, H. Ueda, S. Goko, A. Makinaga, K.Y. Hara, T. Hayakawa, Y.-W. Lui, H. Ohgaki, and F. Utsunomiya, 2004, Phys. Rev. C **69**, 032801.
Moldauer, P., 1975, Phys. Rev. C **11**, 426.
Montes, F., *et al.*, 2007, Astrophys. J., **671**, 1685.
Mosconi, M., M. Heil, F. Käppeler, and A. Mengoni, 2010a, Phys. Rev. C, **82**, 015802.
Mosconi, M., *et al.*, 2010b, Phys. Rev. C, **82**, 015803.
Moxon, M., and E. Rae, 1963, Nucl. Instrum. Methods **24**, 445.
Murashima, M., M. Kokubun, K. Makishima, J. Kotoku, H. Murakami, K. Matsushita, K. Hayashida, K. Arnaud, K. Hamaguchi, and H. Matsumoto, 2006, Astrophys. J. **647**, L131.
Nagai, Y., M. Igashira, N. Mukai, T. Ohsaki, F. Uesawa, K. Takeda, T. Ando, H. Kitazawa, S. Kubono, and T. Fukuda, 1991, Astrophys. J. **381**, 444.
Nassar, H., *et al.*, 2005, Phys. Rev. Lett. **94**, 092504.
Nittler, L., 2009, Pub. Astron. Soc. Aust. **26**, 271.
Norris, J., N. Christlieb, A. Korn, K. Eriksson, M. S. Bessell, T. Beers, L. Wisotzki, and D. Reimers, 2007, Astrophys. J. **670**, 774.
Norris, J., and G. Da Costa, 1995, Astrophys. J. **447**, 680.
Norris, J., S. Ryan, and T. Beers, 2001, Astrophys. J. **561**, 1034.
O'Brien, S., S. Dababneh, M. Heil, F. Käppeler, R. Plag, R. Reifarth, R. Gallino, and M. Pignatari, 2003, Phys. Rev. C **68**, 035801.
Patronis, N., S. Dababneh, P. Assimakopoulos, R. Gallino, M. Heil, F. Käppeler, D. Karamanis, P. Koehler, A. Mengoni, and R. Plag, 2004, Phys. Rev. C **69**, 025803.
Peery, B., and R. Beebe, 1970, Astrophys. J. **160**, 619.
Péquignot, D., and J.-P. Baluteau, 1994, Astron. Astrophys. **283**, 593.
Perey, F., J. Johnson, T. Gabriel, R. Macklin, R. Winters, J. Todd, and N. Hill, 1988, in *Nuclear Data for Science and Technology*, edited by S. Igarasi (Saikon, Tokyo), Vol, 132, p. 379.
Pignatari, M., R. Gallino, M. Heil, M. Wiescher, F. Käppeler, F. Herwig, and S. Bisterzo, 2010, Astrophys. J. **710**, 1557.
Plag, R., 2009, Efnudat daq (private communication).
Plag, R., M. Heil, F. Käppeler, P. Pavlopoulos, R. Reifarth, and K. Wisshak, 2003, Nucl. Instrum. Methods Phys. Res., Sect. A **496**, 425.
Plag, R., M. Heil, F. Käppeler, R. Reifarth, and K. Wisshak, 2005, Nucl. Phys. **A758**, 415.
Plez, B., V. Hill, R. Cayrel, M. Spite, B. Barbuy, T. Beers, P. Bonifacio, F. Primas, and B. Nordström, 2004, Astron. Astrophys. **418**, L9.
Plez, B., V. Smith, and D. Lambert, 1993, Astrophys. J. **418**, 812.
Pompéia, L., V. Hill, M. Site, A. Cole, F. Primas, M. Romaniello, L. Pasquini, M.-R. Cioni, and T. Smecker Hane, 2008, Astron. Astrophys. **480**, 379.
Prantzos, N., M. Hashimoto, and K. Nomoto, 1990, Astron. Astrophys. **234**, 211.

Preston, G., and C. Sneden, 2001, Astron. J. **122**, 1545.
Qian, Y.-Z., and G. Wasserburg, 2007, Phys. Rep. **442**, 237.
Raiteri, C., M. Busso, R. Gallino, and G. Picchio, 1991a, Astrophys. J. **371**, 665.
Raiteri, C., M. Busso, R. Gallino, G. Picchio, and L. Pulone, 1991b, Astrophys. J. **367**, 228.
Raiteri, C., R. Gallino, M. Busso, D. Neuberger, and F. Käppeler, 1993, Astrophys. J. **419**, 207.
Raiteri, C. M., M. Villata, R. Gallino, M. Busso, and A. Cravanzola, 1999, Astrophys. J. **518**, L91.
Ratynski, W., and F. Käppeler, 1988, Phys. Rev. C **37**, 595.
Ratzinger, U., L. Chau, O. Meusel, A. Schempp, K. Volk, M. Heil, F. Käppeler, and R. Stieglitz, 2007, in *Proceedings of ICANS XVIII—Proceedings of the 18th International Collaboration on Advanced Neutron Sources*, edited by J. Wei, S. Wang, W. Huang, and J. Zhao (Institute of High Energy Physics, Chinese Academy of Science, Beijing, China), p. 210, http://www.ihep.ac.cn/english/conference/icans/proceedings/indexed/copyr/31.pdf.
Rau, F., 1963, Nukleonika **5**, 191.
Rauscher, T., 2001, *HTML Interface NON-SMOKER*, Technical Report, University of Basel, http://www.nucastrodata.org/datasets.html.
Rauscher, T., and F.-K. Thielemann, 2000, At. Data Nucl. Data Tables **75**, 1.
Rauscher, T., and K. Guber, 2002, Phys. Rev. C **66**, 028802.
Rauscher, T., and K. Guber, 2005, Phys. Rev. C **71**, 059903.
Rauscher, T., A. Heger, R. Hoffman, and S. Woosley, 2002, Astrophys. J. **576**, 323.
Reddy, B., D. Lambert, and C. Allende Prieto, 2006, Mon. Not. R. Astron. Soc. **367**, 1329.
Reddy, B., D. Lambert, G. Gonzalez, and D. Yong, 2002, Astrophys. J. **564**, 482.
Reddy, B., J. Tomkin, D. Lambert, and C. Allende Prieto, 2003, Mon. Not. R. Astron. Soc. **340**, 304.
Reifarth, R., C. Arlandini, M. Heil, F. Käppeler, P. Sedyshev, M. Herman, T. Rauscher, R. Gallino, and C. Travaglio, 2003, Astrophys. J. **582**, 1251.
Reifarth, R., F. Käppeler, F. Voss, K. Wisshak, R. Gallino, M. Pignatari, and O. Straniero, 2004a, Astrophys. J. **614**, 363.
Reifarth, R., *et al.*, 2004b, Nucl. Instrum. Methods Phys. Res., Sect. A **531**, 530.
Reifarth, R., *et al.*, 2008, Phys. Rev. C **77**, 015804.
Reyniers, M., C. Abia, H. Van Winckel, T. Lloyd Evans, L. Decin, K. Eriksson, and K. Pollard, 2007, Astron. Astrophys. **461**, 641.
Reyniers, M., H. Van Winckel, R. Gallino, and O. Straniero, 2004, Astron. Astrophys. **417**, 269.
Roederer, I., A. Frebel, M. Shetrone, C. Allende Prieto, J. Rhee, R. Gallino, S. Bisterzo, C. Sneden, T. Beers, and J. Cowan, 2008, Astrophys. J. **679**, 1549.
Roederer, I., K.-L. Kratz, A. Frebel, N. Christlieb, B. Pfeiffer, J. Cowan, and C. Sneden, 2009, Astrophys. J. **698**, 1963.
Roederer, I., J. Lawler, C. Sneden, J. Cowan, J. Sobeck, and C. Pilachowski, 2008, Astrophys. J. **675**, 723.
Romano, D., and F. Matteucci, 2007, Mon. Not. R. Astron. Soc. **378**, L59.
Rosman, K., and P. Taylor, 1998, Pure Appl. Chem. **70**, 217.
Rugel, G., I. Dillmann, T. Faestermann, M. Heil, F. Käppeler, K. Knie, G. Korschinek, W. Kutschera, M. Poutivtsev, and A. Wallner, 2007, Nucl. Instrum. Methods Phys. Res., Sect. B **259**, 683.
Rugel, G., T. Faestermann, K. Knie, G. Korschinek, D. Schumann, N. Kivel, I. Günther-Leopold, R. Weinreich, and M. Wohlmuther, 2009, Phys. Rev. Lett. **103**, 072502.
Ryan, S., J. Norris, and C. Beers, 1996, Astrophys. J. **471**, 254.
Sadakane, K., N. Arimoto, C. Ikuta, W. Aoki, P. Jablonka, and A. Tajitsu, 2004, Publ. Astron. Soc. Jpn. **56**, 1041.
Savage, B., and K. Sembach, 1996, Annu. Rev. Astron. Astrophys. **34**, 279.
Schumann, D., *et al.*, 2010, Nucl. Instrum. Methods Phys. Res., Sect. A **613**, 347.
Schwarzschild, M., and R. Härm, 1965, Astrophys. J. **142**, 855.
Seeger, P., W. Fowler, and D. Clayton, 1965, Astrophys. J. Suppl. Ser. **11**, 121.
Serminato, A., R. Gallino, C. Travaglio, S. Bisterzo, and O. Straniero, 2009, Pub. Astron. Soc. Aust. **26**, 153.
Sharpee, B., Y. Zhang, R. Williams, E. Pellegrini, K. Cavagnolo, J. Baldwin, M. Phillips, and X.-W. Lui, 2007, Astrophys. J. **659**, 1265.
Shetrone, M., P. Côté, and L. Sargent, 2001, Astrophys. J. **548**, 592.
Shetrone, M., K. Venn, E. Tolstoy, F. Primas, V. Hill, and A. Kaufer, 2003, Astron. J. **125**, 684.
Simmerer, J., C. Sneden, J. Cowan, J. Collier, V. Woolf, and J. Lawler, 2004, Astrophys. J. **617**, 1091.
Sivarani, T., *et al.*, 2004, Astron. Astrophys. **413**, 1073.
Sivarani, T., *et al.*, 2006, Astron. Astrophys. **459**, 125.
Smiljanic, R., G. Porto de Mello, and L. da Silva, 2007, Astron. Astrophys. **468**, 679.
Smith, V., and D. Lambert, 1988, Astrophys. J. **333**, 219.
Smith, V., B. Plez, D. Lambert, and D. Lubowitsch, 1995, Astrophys. J. **441**, 735.
Smith, V., K. Suntzeff, K. Cunha, R. Gallino, M. Busso, D. Lambert, and O. Straniero, 2000, Astron. J. **119**, 1239.
Sneden, C., J. Cowan, D. Burris, and J. Truran, 1998, Astrophys. J. **496**, 235.
Sneden, C., J. Cowan, and R. Gallino, 2008, Annu. Rev. Astron. Astrophys. **46**, 241.
Sneden, C., J. Cowan, J. Lawler, S. Burles, T. Beers, and G. Fuller, 2002, Astrophys. J. **566**, L25.
Sneden, C., R. Kraft, M. Shetrone, G. Smith, G. Langer, and C. Prosser, 1997, Astron. J. **114**, 1964.
Sneden, C., *et al.*, 2003, Astrophys. J. **591**, 936.
Sonnabend, K., P. Mohr, K. Vogt, A. Zilges, A. Mengoni, T. Rauscher, H. Beer, F. Käppeler, and R. Gallino, 2003, Astrophys. J. **583**, 506.
Sonnabend, K., D. Vogt, K. Galaviz, S. Müller, and A. Zilges, 2004, Phys. Rev. C **70**, 035802.
Sonnabend, K., D. Vogt, K. Galaviz, S. Müller, and A. Zilges, 2005, Phys. Rev. C **72**, 019901(E).
Spallation Neutron Source, Technical Report, Oak Ridge National Laboratory, 2004, http://www.sns.gov/.
Spencer, R., and R. Macklin, 1976, Nucl. Sci. Eng. **61**, 346.
Sterling, N., and H. Dinerstein, 2008, Astrophys. J. Suppl. Ser. **174**, 158.
Straniero, O., S. Cristallo, and R. Gallino, 2009, Pub. Astron. Soc. Aust. **26**, 133.
Straniero, O., S. Cristallo, R. Gallino, and I. Domínguez, 2004, Mem. Soc. Astron. Ital. **75**, 665.
Straniero, O., I. Domínguez, R. Cristallo, and R. Gallino, 2003, Pub. Astron. Soc. Aust. **20**, 389.
Straniero, O., R. Gallino, M. Busso, A. Chieffi, C. Raiteri, M. Limongi, and M. Salaris, 1995, Astrophys. J. **440**, L85.
Straniero, O., R. Gallino, and S. Cristallo, 2006, Nucl. Phys. **A777**, 311.
Suda, T., Y. Katsuta, S. Yamada, T. Suwa, C. Ishizuka, Y. Komiya, K. Sorai, M. Aikawa, and M. Fujimoto, 2008, Publ. Astron. Soc. Jpn. **60**, 1159.

Tagliente, G., *et al.*, 2008, Phys. Rev. C **77**, 035802.
Tain, J., F. Gunsing, D. Cano-Ott, and C. Domingo, 2002, J. Nucl. Sci. Tech. Suppl. **2**, 689.
Takahashi, K., and K. Yokoi, 1987, At. Data Nucl. Data Tables **36**, 375.
Tanihata, I., 1998, J. Phys. G **24**, 1311.
Terasawa, M., K. Sumiyoshi, T. Kajino, G. Mathews, and I. Tanihata, 2001, Astrophys. J. **562**, 470.
Terlizzi, R., *et al.*, 2007, Phys. Rev. C **75**, 035807.
The, L., M. El Eid, and B. Meyer, 2007, Astrophys. J. **655**, 1058.
Thielemann, F.-K., K. Nomoto, and K. Yokoi, 1986, Astron. Astrophys. **158**, 17.
Thompson, I., I. Ivans, S. Bisterzo, C. Sneden, R. Gallino, S. Vauclair, G. Burley, S. Shectman, and G. Preston, 2008, Astrophys. J. **677**, 556.
Timofeyuk, N., D. Baye, P. Descouvemont, R. Kamouni, and I. Thompson, 2006, Phys. Rev. Lett. **96**, 162501.
Tolstoy, E., V. Hill, and M. Tosi, 2009, Annu. Rev. Astron. Astrophys. **47**, 371.
Tomkin, J., and D. Lambert, 1999, Astrophys. J. **523**, 234.
Tomyo, A., Y. Temma, M. Segawa, Y. Nagai, H. Makii, T. Ohsaki, and M. Igashira, 2005, Astrophys. J. **623**, L153.
Toukan, K., K. Debus, F. Käppeler, and G. Reffo, 1995, Phys. Rev. C **51**, 1540.
Travaglio, C., D. Galli, and A. Burkert, 2001, Astrophys. J. **547**, 217.
Travaglio, C., D. Galli, R. Gallino, M. Busso, F. Ferrini, and O. Straniero, 1999, Astrophys. J. **521**, 691.
Travaglio, C., R. Gallino, E. Arnone, J. Cowan, F. Jordan, and C. Sneden, 2004, Astrophys. J. **601**, 864.
Travaglio, C., R. Gallino, M. Busso, and R. Gratton, 2001, Astrophys. J. **549**, 346.
Truran, J., J. Cowan, C. Pilachowski, and C. Sneden, 2002, Publ. Astron. Soc. Pac. **114**, 1293.
Uberseder, E., *et al.*, 2009, Phys. Rev. Lett. **102**, 151101.
Umeda, H., and K. Nomoto, 2002, Astrophys. J. **565**, 385.
Van Eck, S., S. Goriely, A. Jorissen, and B. Plez, 2001, Nature (London) **412**, 793.
Van Eck, S., S. Goriely, A. Jorissen, and B. Plez, 2003, Astron. Astrophys. **404**, 291.
Vanhala, H., and A. Cameron, 1998, Astrophys. J. **508**, 291.
Vanture, A., V. Smith, J. Lutz, G. Wallerstein, D. Lambert, and G. Gonzalez, 2007, Publ. Astron. Soc. Pac. **119**, 147.
Van Winckel, H., and M. Reyniers, 2000, Astron. Astrophys. **354**, 135.
Vockenhuber, C., I. Dillmann, M. Heil, F. Käppeler, A. Wallner, and N. Winckler, 2007, Phys. Rev. C **75**, 015804.
Vogt, K., P. Mohr, M. Babilon, J. Enders, T. Hartmann, C. Hutter, T. Rauscher, S. Volz, and A. Zilges, 2001, Phys. Rev. C **63**, 055802.
Voss, F., K. Wisshak, C. Arlandini, F. Käppeler, L. Kazakov, and T. Rauscher, 1999, Phys. Rev. C **59**, 1154.
Voss, F., K. Wisshak, K. Guber, F. Käppeler, and G. Reffo, 1994, Phys. Rev. C **50**, 2582.
Wallerstein, G., *et al.*, 1997, Rev. Mod. Phys. **69**, 995.
Wanajo, S., K. Nomoto, N. Iwamoto, Y. Ishimaru, and T. Beers, 2006, Astrophys. J. **636**, 842.
Ward, R., 1977, Astrophys. J. **216**, 540.
Ward, R., M. Newman, and D. Clayton, 1976, Astrophys. J. Suppl. Ser. **31**, 33.
Weigert, A., 1966, Z. Astrophys. **64**, 395.
Westin, J., C. Sneden, B. Gustafsson, and J. Cowan, 2000, Astrophys. J. **530**, 783.
Wiescher, M., J. Görres, and F.-K. Thielemann, 1990, Astrophys. J. **363**, 340.
Wiescher, M., J. Görres, and H. Schatz, 1999, J. Phys. G **25**, R133.
Winckler, N., S. Dababneh, M. Heil, F. Käppeler, R. Gallino, and M. Pignatari, 2006, Astrophys. J. **647**, 685.
Winters, R., and R. Macklin, 1987, Astrophys. J. **313**, 808.
Wisshak, K., K. Guber, F. Käppeler, and F. Voss, 1990, Nucl. Instrum. Methods Phys. Res., Sect. A **299**, 60.
Wisshak, K., K. Guber, F. Voss, F. Käppeler, and G. Reffo, 1993, Phys. Rev. C **48**, 1401.
Wisshak, K., and F. Käppeler, 1981, Nucl. Sci. Eng. **77**, 58.
Wisshak, K., F. Voss, C. Arlandini, M. Heil, F. Käppeler, R. Reifarth, F. Bečvář, and M. Krtička, 2004, Phys. Rev. C **69**, 055801.
Wisshak, K., F. Voss, F. Käppeler, K. Guber, L. Kazakov, N. Kornilov, M. Uhl, and G. Reffo, 1995, Phys. Rev. C **52**, 2762.
Wisshak, K., F. Voss, F. Käppeler, and L. Kazakov, 2002, Phys. Rev. C **66**, 025801.
Wisshak, K., F. Voss, F. Käppeler, and L. Kazakov, 2006a, Phys. Rev. C **73**, 045807.
Wisshak, K., F. Voss, F. Käppeler, and L. Kazakov, 2006b, Phys. Rev. C **73**, 015807.
Wisshak, K., F. Voss, F. Käppeler, L. Kazakov, and G. Reffo, 1998, Phys. Rev. C **57**, 391.
Wisshak, K., F. Voss, F. Käppeler, M. Krtička, S. Raman, A. Mengoni, and R. Gallino, 2006c, Phys. Rev. C **73**, 015802.
Wisshak, K., F. Voss, F. Käppeler, and G. Reffo, 1992, Phys. Rev. C **45**, 2470.
Wisshak, K., F. Voss, C. Theis, F. Käppeler, K. Guber, L. Kazakov, N. Kornilov, and G. Reffo, 1996, Phys. Rev. C **54**, 1451.
Wisshak, K., *et al.*, 2001, Phys. Rev. Lett. **87**, 251102.
Woodward, P., F. Herwig, D. Porter, T. Fuchs, A. Nowatzki, and M. Pignatari, 2008, in *First Stars III*, edited by B. W. O'Shea, A. Heger, and T. Abel, AIP Conference Series 990 (AIP, New York), p. 300.
Woosley, S., A. Heger, and T. Weaver, 2002, Rev. Mod. Phys. **74**, 1015.
Woosley, S., and R. Hoffman, 1992, Astrophys. J. **395**, 202.
Woosley, S., and T. Weaver, 1995, Astrophys. J. Suppl. Ser. **101**, 181.
Yong, D., W. Aoki, D. Lambert, and D. Paulson, 2006, Astrophys. J. **639**, 918.
Yong, D., D. Lambert, D. Paulson, and B. Carney, 2008, Astrophys. J. **673**, 854.
York, D., *et al.*, 2000, Astron. J. **120**, 1579.
Yushchenko, A., V. Gopka, S. Goriely, F. Musaev, A. Shavrina, C. Kim, Y. Woon Kang, J. Kuznietsova, and V. Yushchenko, 2005, Astron. Astrophys. **430**, 255.
Zamora, O., C. Abia, B. Plez, I. Domínguez, and S. Cristallo, 2009, Astron. Astrophys. **508**, 909.
Zinner, E., 1998, Annu. Rev. Earth Planet. Sci. **26**, 147.
Zook, A., 1985, Astrophys. J. **289**, 356.